2015

MEASUREMENTS AND MODELING OF HYDROCARBON MIXTURE FLUID PROPERTIES UNDER EXTREME TEMPERATURE AND PRESSURE CONDITIONS

Babatunde A. Bamgbade
Virginia Commonwealth University

Measurements and Modeling of Hydrocarbon Mixture Fluid Properties under Extreme Temperature and Pressure Conditions

A dissertation submitted in partial fulfillment of the requirements for the degree of Doctor of Philosophy at Virginia Commonwealth University.

by

Babatunde A Bamgbade
Doctor of Philosophy
Virginia Commonwealth University, 2015

Directors:
Dr. Frank B. Gupton
Professor, Department of Chemical and Life Science Engineering

And

Dr. Mark A. McHugh
Emeritus Professor, Department of Chemical and Life Science Engineering

Virginia Commonwealth University
Richmond, Virginia
August, 2015

Acknowledgment

All glory be to God the Alpha and Omega for seeing me through this journey.

I express my profound gratitude to my advisor, Professor Mark A. McHugh for supporting, encouraging, guiding, and where necessary showing me tough love throughout this research over the years. His devotion and passion to science, his great personality, and also a remarkable sense of humor causes me to marvel at the man behind the name and makes me feel that I have the best advisor ever. He also shows an express belief in me even when I doubt myself.

I appreciate my PhD committee members, Professor Frank Gupton, Professor Stephen Fong, Professor Vamsi Yadavalli, Professor, James McLeskey, Professor Worth Longest, and Dr. Isaac Gamwo for their time and efforts as well as valuable suggestions for my research.

I acknowledge Dr. Deepak Tapriyal, Professor Robert Enick, Dr. Ward Burgess, Dr. Hseen Baled and Dr. Yue Wu for their continual support, valuable remarks, and helpful technical discussions.

I also want to thank my colleagues in Dr. McHugh's research group, Mr. Matthew Newkirk, Mr., Mr. Sean Dudek, Dr. Rajendar R. Mallepally, Dr. Kun Liu, and Mr. Michael Marin for their helpful discussions and exchange of ideas.

I thank all my friends and colleagues who have contributed to this journey in one way or another

I especially thank my family for their continual support, prayers, and advice. I would like to take this time to remember my dad, who sadly passed on during this academic journey. RIP Dad!

I acknowledge National Energy Technology Laboratory for providing the financial support for this project.

Finally, I want to express my deep gratitude to my darling wife for her support and putting with my late night experiments and studies. All those times are remembered and well-appreciated.

I wish every one of them good health and happiness.

Table of Contents

List of Tables

viii

List of Figures

xv

List of Abbreviations

Latin Letters

$\tilde{a}^{res}$	residual molar Helmholtz free energy
$\tilde{a}^{hc}$	residual molar Helmholtz free energies for hard-chain interactions
$\tilde{a}^{hs}$	residual molar Helmholtz free energies for hard-sphere interactions
$\tilde{a}^{disp}$	residual molar Helmholtz free energies for dispersion interactions
$a_0 - a_2$	parameters to for calculating reference density in the Tait equation
$b_0 - b_2$	parameters to for calculating B parameter in the Tait equation
B	parameter used in the fit of the Tait equation to experimental data
c	volume translation term
C	carbon, parameter used in the fit of Tait equation
C_1	parameter in the PC-SAFT equation
C_3	propane
C_{10}	decane
C_{20}	eicosane
C_{30}	squalane
CH_4	methane
CN	carbon number
CN_p	carbon number if 100% paraffin
CN_{PNA}	carbon number if 100% polynuclear aromatic
DEHP	*bis* (2-ethylhexyl) phthalate
EoS	equation of state
GC	group contribution, gas chromatography
g^{hs}	radial distribution function for hard sphere
H	hydrogen

HTHP	high-temperature, high pressure
$k_0 - k_6$	parameter for HTHP volume translated cubic EoS
k_B	Boltzmann constant
k_{ij}	binary interaction parameter
Low-P	parameters from fit of vapor pressure and saturated liquid density
LVDT	linear variable differential transformer
m	number of segments
M_w	molecular weight
P	pressure
P_0	pressure at reference density in the Tait equation, usually 0.1 MPa
P_c	critical pressure
PC-SAFT	perturbed-chain associating fluid theory
PNA	polynuclear aromatic
PR	Peng-Robinson
P_r^{sat}	reduced vapor pressure
SAFT	statistical associating fluid theory
SARA	saturate aromatic resin and asphaltene
T	temperature
T_c	critical temperature
T_r	reduced temperature
V	volume
v_{EoS}	molar liquid volume predicted by cubic EoS
v_{exp}	experimental molar liquid volume
w	weight fraction
x_i	mole fraction of component i

xx

Greek Letters

β	isothermal compressibility
ε	interaction energy
δ	mean absolute percent deviation
γ	aromaticity
λ	standard deviation
ρ	density
ρ_0	reference density, usually at 0.1 MPa
$\rho_{i,corr}$	density calculated with the Tait equation
$\rho_{i,exp}$	experimental density reported in this study
$\rho_{i,lit}$	density reported in the literature
$\rho_{i,pred}$	density predicted with EoS
σ	temperature-independent segment diameter
σ_m	uncertainty in the reported mass
$\sigma_{intercept}$	uncertainty in the intercept
σ_P	uncertainty in the reported pressure
σ_ρ	uncertainty in the reported density
σ_{slope}	uncertainty in the slope
σ_T	uncertainty in the reported temperature
σ_m	uncertainty in the LVDT reading
σ_V	uncertainty in the volume
ω	acentric factor
η	reduced fluid density

Abstract

MEASUREMENTS AND MODELING OF HYDROCARBON MIXTURE FLUID
PROPERTIES UNDER EXTREME TEMPERATURE AND PRESSURE CONDITIONS

By Babatunde A. Bamgbade, Ph.D.

A dissertation submitted in partial fulfillment of the requirements for the degree of Doctor of
Philosophy at Virginia Commonwealth University.

Virginia Commonwealth University, 2015.

Major Director: Dr. B. Frank Gupton, Professor, Department of Chemical and Life Science
Engineering

Co-Advisor: Dr. Mark A. McHugh: Emeritus Professor, Department of Chemical and Life
Science Engineering

Knowledge of thermodynamic fluid properties, such as density and phase behavior, is important
for the design, operation, and safety of several processes including drilling, extraction,
transportation, and separation that are required in the petroleum. The knowledge is even more
critical at extreme temperature and pressure conditions as the search for more crude oil reserves
lead to harsher conditions. Currently, there is dearth of experimental data at these conditions and
as such, the predictive capability of the existing modeling tools are unproven. The objective of
this research is to develop a fundamental understanding of the impact of molecular architecture
on fluid phase behavior at temperatures to 523 K (250 °C) and pressures to 275 MPa (40,000
psi). These high-temperature and high-pressure (HTHP) conditions are typical of operating
conditions often encountered in petroleum exploration and recovery from ultra-deep wells that
are encountered in the Gulf of Mexico.

This PhD study focuses on the fluid phase behavior of a low molecular weight compound, two moderately high molecular weight compounds, three asymmetric binary mixtures of a light gas and a heavy hydrocarbon compound with varying molecular size. The compounds are selected to represent the family of saturated compounds found in typical crude oils. Furthermore, this study reports experimental data for two "dead" crude oil samples obtained from the Gulf of Mexico and their mixtures with methane from ambient to HTHP conditions. A variable-volume view cell coupled with a linear variable differential transformer is used to experimentally measure the high-pressure properties of these compounds and mixtures. The reported density data compare well to the limited available data in the literature with deviations that are less than 0.9%, which is the experimental uncertainty of the density data reported in this study.

The phase behavior and density data obtained in this study are modeled using the Peng-Robinson (PR), the volume-translated (VT) PR, and the Perturbed-Chain Statistical Associating Fluid Theory (PC-SAFT) equations of state (EoS). The EoS pure component parameters, typically obtained from the open literature, are derived from fitting the particular EoS to, critical point, or to vapor pressure and saturated liquid density data, or to HTHP density data. For the density data reported here, the PREoS provided the worst predictions, while the VT-PREoS gives an improved performance as compared to the PREoS. However, the PC-SAFT EoS provided the best HTHP density predictions especially when using HTHP pure component parameters. The situation is however reversed in the modeling performance for the phase behavior data whereby the PC-SAFT EoS with HTHP parameters provided the worst vapor-liquid equilibria predictions. Better predictions are obtained with the PC-SAFT EoS when using parameters obtained from fit of the vapor pressure data and is comparable to the PREoS predictions. This reversal in

performance is not surprising since the phase behavior data occur at moderately low pressures. The performance of the PC-SAFT EoS is extended to the experimental density data reported for the dead crude oil samples and their mixtures with methane. The PC-SAFT EoS with either set of pure component parameters yield similar predictions that are within 3% of the reported crude oil density data. However, when using the HTHP parameters, the PC-SAFT gives a good representation of the slope of experimental data, which is crucial in the calculation of second-derivative properties such has isothermal compressibility.

The PC-SAFT EoS is also employed to model the crude oil HTHP density data for both the dead crude oils and their mixtures with methane using correlations for both the Low-P parameters and the HTHP parameters. The Low-P parameters are derived from fitting the PC-SAFT EoS to pure compound vapor pressure and saturated liquid density data, while the HTHP parameters are obtained from fitting the PC-SAFT EoS to pure compound HTHP liquid density data. Interestingly, the PC-SAFT EoS with the Low-P parameters provided better HTHP density predictions that are within 1.5% of the experimental data for the dead oils than the HTHP parameters that are within 2 to 4% of the data. Density predictions for the dead oil mixtures with methane are however comparable for both sets of parameters and are within 1% on average. However, the PC-SAFT EoS with HTHP parameters clearly provided better representation of the isothermal property, a derivative property obtained from density data, within 10% while predictions with the Low-P parameters can be as high as 37%.

The successful completion of the thesis work expands the current knowledge base of fluid phase behavior at the extreme operating conditions encountered by engineers in the petroleum

industries. Furthermore, the reported HTHP experimental data also provide a means to scientists and researchers for the development, improvement, and validation of equations with improved modeling performance.

Chapter 1 Introduction

1.1. Importance of Hydrocarbon Fluid Properties at Extreme Conditions

The continued global reliance on fossil fuels for energy is posing a challenge to the petroleum industry and has led the industry to explore new and under-explored areas for oil reservoirs to meet the increased demand for oil and gas products. While the first oil well drilled in the United States had a depth of approximately 100 feet, prospectors today often must drill the ground further to tap oil reserves. The search for new oil reservoirs has led to drilling to greater depths, several miles below the surface, where harsher conditions are prevalent compared to those typically encountered in traditional surface oil reserves. In these ultra-deep wells, the hydrocarbons often exist at increasingly extreme temperatures beyond 420 K and pressures beyond 70 MPa [1]. From 1982 to 2012, there were 415 such wells that came into existence around the world [2]. This trend is expected to accelerate with the passage of time as existing oil reserves are depleted [3]. Further drilling has led to explorations in ultra-deep wells that can be 6 miles or more below the sea level, where the temperature and pressure conditions can be in excess of 500 K and 200 MPa [4]. Improvements on existing processes and methodologies are needed to ensure safe and responsible petroleum exploration at these conditions. Hence, information on volumetric properties of hydrocarbon and their mixtures in excess of 200 MPa and 500 K are crucial for the design and optimization of the processes related to the production of oil, condensate, and natural gas from ultra-deep reservoirs [5,6]. In addition, reliable estimate of the amount of hydrocarbons present in a reservoir is required to ascertain the rate of return of the potential well, for which the knowledge of the density is also important. Moreover, information on the volumetric properties at these conditions are also needed for calculations and

1

predictions of other thermophysical properties, such as viscosity [7-9] and isothermal compressibility [10,11]. Knowledge of the second derivative properties such as the isothermal compressibility are required to safely and efficiently liquefy, store, and transport condensable fluids [12,13]. Furthermore, the knowledge of phase behavior properties of hydrocarbons and their mixtures are important in the design of processes to maintain a steady flow of hydrocarbons. These phase behavior properties include such as bubble points in oil wells, dew points in gas wells, and solidification points during flow pipes.

There is a limited database for hydrocarbon gas-liquid binary mixture density on representative oil-reservoir compounds at extreme temperature and pressure conditions related to ultra-deep reservoir formations. Furthermore, there is even less data available for asymmetric binary hydrocarbon mixtures at these conditions. The present study reports high-temperature, high-pressure, (HTHP) density data for propane mixtures with *n*-decane, or *n*-eicosane, and squalane at several compositions and are described in chapter 4. Prior to the mixture study, this work also extended the literature database for three compounds including propane, squalane, and *bis* (2-ethlyhexyl) phthalate to HTHP conditions, which are described in chapter 3. Furthermore, in an earlier collaborative study, the density database for decane and eicosane, along with several other alkane compounds, were reported from ambient to HTHP conditions [4,14]. In addition, the experimental data of crude oil samples are measured from ambient to HTHP conditions and are described in chapter 5. The HTHP conditions in this study are defined as temperatures to 525 K and pressures to 275 MPa. Data on propane mixtures with *n*-octane [15] and *n*-decane [16] have recently been reported but only at maximum pressures to 40 MPa and temperatures to 448 K, which are well below HTHP conditions. However, the propane-*n*-decane (C_3-C_{10}) model system was studied in some broader detail by Reamer and Sage in 1966 [17] for nine mixture

2

compositions, at temperatures to 513 K, but only at pressures to 70 MPa. In the study, Reamer and Sage [17] reported both the phase behavior and mixture densities for this binary system. For the propane-squalane (C_3-C_{30}) system, Nanu *et al*. [18] reported the vapor-liquid equilibrium properties for the mixtures at temperatures to 473 K for 14 different mixture compositions. Aalto *et al*. [19] reported the volumetric properties of the mixture but only in the vicinity of the critical point of propane and at a single mixture composition, which is in excess of 0.996 mole fraction of propane. One of the objectives of this study is to expand the database of asymmetric hydrocarbon mixtures and crude oil samples to high-temperature, high-pressure conditions.

1.2. Correlations and Models for Representing Hydrocarbon Fluid Properties

It is desirable to determine the properties of hydrocarbon and their mixtures experimentally, however, it is impractical to experimentally measure all the required properties for all the hydrocarbons and possible mixture combinations that are encountered in each oil well at all the temperature and pressure conditions that are of interest. Therefore, several correlational and modeling methods have been proposed to describe the physical properties of hydrocarbon and crude oils in the petroleum industry. The modified Tait equation [20] is a popular correlation equation that is used to represent the volumetric properties of hydrocarbon compounds [21-23]. Often times, the petroleum industry use empirically derived "black oil" correlations that are based on reservoir fluid samples. The drawback to these empirical approaches is that the correlations thus obtained are unreliable when extrapolated to conditions beyond the temperature and pressure conditions at which the correlations were derived. In addition, these correlations cannot be reliably extended to crude oils from different region than which the correlation was obtained. This particular shortcoming can be addressed to an extent by equation of state (EoS)

3

models. Although the EoS models are more complex, they are equally more robust and versatile in their applications. The most widely used EoS models can be divided in two main classes, which are either cubic-based or SAFT-based. The second objective of this study is to investigate the performance of these two classes of EoS models to represent the HTHP thermophysical properties of hydrocarbons and their mixtures.

1.2.1. Cubic-Based Equation of State Models

The first class are the semi-empirical cubic-based EoS models, such as the Peng-Robinson (PR) [24] and Soave-Redlich-Kwong (SRK) [25] EoS. The cubic-based EoS models are so called because they can be expressed as third-degree polynomials in the volume term. This class of EoS models is often used in the petrochemical industry due to their relative simplicity and reliability (as compared to other EoS model class) when predicting phase equilibrium of nonpolar hydrocarbon systems. The general form of this class of EoS models is given in equation 1.1, where P is the pressure, T is the absolute temperature, and v is the molar volume.

$$P = \frac{RT}{v-b} - \frac{a_c\alpha}{v^2 + ubv + wb^2} \tag{1.1}$$

For PR equation, $u = 2$ and $w = -1$, while for SRK equation, $u = 1$ and $w = 0$. The attractive term contains a function, α, which is a correlation of temperature, critical temperature and the acentric term, ω. Parameter b is the co-volume, which is the effective molecular volume in the hard sphere repulsive term. Parameters a_c and b depends only on the critical temperature, T_c and the critical pressure, P_c. For instance the parameters for the PREoS are given in equations 1.2 to 1.5.

4

$$a_c = 0.45724 \frac{(RT_c)^2}{P_c} \qquad (1.2)$$

$$b = 0.07780 \frac{RT_c}{P_c} \qquad (1.3)$$

$$a = \left[1 + m \left(1 - \sqrt{\frac{T}{T_c}} \right) \right]^2 \qquad (1.4)$$

$$m = 0.37464 + 1.54226 w - 0.26992 w^2 \qquad (1.5)$$

The major drawbacks for the cubic EoS is their inability to reliably predict the high-pressure liquid density data [4,14] and they also have difficulty in modeling the properties of moderate to high molecular weight hydrocarbons with acentric factors greater than 0.4 [24,26]. The error associated with the high-pressure predictions obtained by cubic EoS can be as high as 50% [27]. The concept of the volume translation of the cubic EoS was introduced in other to improve the performance of the cubic EoS in high-pressure applications, while preserving the simplicity of calculations obtained with the traditional cubic EoS. In essence another fitted parameter, c, is incorporated into the cubic EoS that accounts for the systematic deviation observed between the predicted and the experimental liquid molar volume. The effect of the volume translation on the vapor molar volume is insignificant due to the large values of the vapor volume as compared to the liquid volume. Furthermore the calculation of the pure component vapor pressure is not affected by the volume translation when c is constant or only a function of temperature. Thus, the volume translation term c is defined in equation 1.6 as the difference between the predicted and experimental molar volumes. The volume translated PREoS is given in equation 1.7.

5

$$c = v_{EoS} - v_{exp} \tag{1.6}$$

$$P = \frac{RT}{v + c - b} - \frac{a_c a}{(v + c)(v + c + b) + b(v + c - b)} \tag{1.7}$$

Over the last three decades, the concept of volume translation has garnered a lot of attention in the literature as demonstrated by the numerous correlation schemes that have been suggested. The difference between these correlation schemes is the choice of combinations of the pure component physical properties to correlate the volume translation term [28-39]. For this study, the method proposed by Baled *et al*. is used correlate the volume translation term for the PREoS. In their work, Baled *et al*. [27] first obtain the value of *c* for each pure component by applying equation 1.6 to pure component HTHP liquid density data of *n*-alkanes, isoalkanes, cycloalkanes, and aromatic compounds. Then, they correlated the *c* values as a function of the reduced temperature, T_r as shown in equation 1.8, where the constants *A* and *B* are expressions in terms of molecular weight, M_w, and acentric factor, ω, as given by equation 1.9. The parameters of equation 1.9 are given in Table 1.1.

$$c = \mathrm{D}v = v_{EoS} - v_{exp} = A + B \circ T_r \tag{1.8}$$

$$A, B = f(M_w, W) = k_0 + k_1 \exp\left(\frac{-1}{k_2 M_w W}\right) + k_3 \exp\left(\frac{-1}{k_4 M_w W}\right) + k_5 \exp\left(\frac{-1}{k_6 M_w W}\right) \tag{1.9}$$

6

Table 1.1. Parameters of equation 1.9; k_0 through k_6 for HTHP volume translated PREoS

Constants	A (cm^3/mol)	B (cm^3/mol)
k_0	-4.1034	-0.3489
k_1	31.723	-28.547
k_2	0.0531	0.0687
k_3	188.68	-817.73
k_4	0.0057	0.0007
k_5	20.196	-65.067
k_6	0.0003	0.0076

1.2.2. SAFT-Based Equation of State Models: Perturbed-Chain Statistical Associating Fluid Theory

The SAFT-based EoS models are theoretically derived and are based on the perturbation theory of Wertheim put forth in the mid-80s [40-43]. SAFT-based equations of state are constructed from a summation of the reduced, residual Helmholtz free energies that account for hard sphere repulsion, dispersion interactions, and chain formation resulting from segments bonding to one another, as well as intra- and inter-molecular hydrogen bonding and other specific interactions. For the original SAFT equation proposed by both Chapman *et al*. [44,45] and Huang and Radosz [46,47], the Helmholtz free energy of dispersion is calculated for a reference fluid of hard spheres that is obtained from the power series put forth by Alder [48]. The power series was fit by Chen and Kreglewski [49] to pure component pressure-volume-temperature data and the second virial coefficient of argon. The hard sphere repulsion term itself is based on the theory of Carnahan and Starling [50]. Hard sphere chains are formed from a

7

mixture the hard spheres. Chapman *et al*. [44] derived the term accounting for the chain formation, which is the Helmholtz free energy term needed for the chain formation.

Since their introduction in the early 90s, there have been many modifications to the SAFT equation. The most widely used form of the SAFT equation to represent the thermodynamic properties of hydrocarbons is the perturbed-chain statistical associating fluid theory (PC-SAFT) proposed by Gross and Sadowski in 2001 [51]. The PC-SAFT equation is similar to the original SAFT equation with the only exception being that the dispersion interaction term is directly obtained for the hard sphere mixtures as is done in the SAFT equation, but is obtained for mixtures of whole chains after their formation from hard spheres. The dispersion term is calculated by applying the perturbation theory of Baker and Henderson to a hard-chain reference fluid. The PC-SAFT EoS has been demonstrated to provide superior phase equilibrium predictions for mixtures of both associating and non-associating compounds [51-53]. In this study, the association term of the PC-SAFT is neglected since all the compounds investigated do not have specific interactions like hydrogen bonding and neither do they form complexes such as Lewis acid-Lewis base complexes. Therefore, the reduced residual Helmholtz free energy for non-associating fluids is given in equation 1.10, followed by a synopsis of the PC-SAFT EoS outline since details can be easily found elsewhere [51].

$$\tilde{a}^{res} = \tilde{a}^{hc} + \tilde{a}^{disp} \tag{1.10}$$

The terms $\tilde{a}^{hc}$ and $\tilde{a}^{disp}$ are the reduced hard chain reference and dispersion terms, respectively. Both terms are described by the following equations;

$$\widetilde{a}^{hc} = m\widetilde{a}^{hs} - \sum_i x_i(m-1)\ln g_{ii}^{hs}(\sigma_{ii}) \tag{1.11}$$

$$m = \sum_i x_i m_i \tag{1.12}$$

$$\widetilde{a}^{hs} = \frac{1}{z_0}\left[\frac{3z_1 z_2}{(1-z_3)} + \frac{z_2^3}{z_3(1-z_3)^2} + \left(\frac{z_2^3}{z_3^2} - z_0\right)\ln(1--z_3)\right] \tag{1.13}$$

$$\widetilde{g}^{hs} = \frac{1}{(1-z_3)} + \left(\frac{d_i d_j}{d_i + d_j}\right)\frac{3z_2}{(1-z_3)^2} + \left(\frac{d_i d_j}{d_i + d_j}\right)^2\frac{2z_2^3}{(1-z_3)^3} \tag{1.14}$$

$$z_n = \frac{\rho}{6}\pi\sum_i x_i m_i d_i^n \qquad n = 0,\,1,\,2,\,3 \tag{1.15}$$

$$d_i = \sigma_i\left[1 - 0.12\exp\left(-3\frac{e_i}{k_B T}\right)\right] \tag{1.16}$$

$$\widetilde{a}^{disp} = -2\pi\rho\sum_i\sum_j x_i x_j m_i m_j\left(\frac{e_{ij}}{k_B T}\right)\sigma_{ij}^3 I_1(\eta,m) - \pi\rho C_i m\sum_i\sum_j x_i x_j m_i m_j\left(\frac{e_{ij}}{k_B T}\right)^2\sigma_{ij}^3 I_2(\eta,m) \tag{1.17}$$

$$\sigma_{ij} = 0.5(\sigma_i + \sigma_j) \tag{1.18}$$

$$\varepsilon_{ij} = (1-k_{ij})\sqrt{\varepsilon_i\varepsilon_j} \tag{1.19}$$

Here, $\widetilde{a}^{hs}$ represents the reduced Helmholtz free energy of the hard-sphere fluid, $\widetilde{g}^{hs}$ is the hard-sphere radial distribution function, m is the number of segments in a molecule, k_B is Boltzmann's constant, and η is the reduced fluid density also known as the segment packing fraction. I_1 and I_2 are calculated from power series in density as given in [51]. The parameters ρ, σ, and ε/k_B, are the total number density, temperature-independent segment diameter, and the interaction energy, respectively. The binary interaction parameter, k_{ij}, accounts for the error

9

associated with the geometric mean averaging of the interaction energy parameter of each component. Parameter C_1 is given as;

$$C_1 = \left(1 + m\frac{8\eta - 2\eta^2}{(1-\eta)^4} + (1-m)\frac{20\eta - 27\eta^2 + 12\eta^3 - 2\eta^4}{[(1-\eta)(2-\eta)]^2}\right)^{-1}$$

(1.20)

In the procedure given by Gross and Sadowski [51], the density at a given temperature and pressure is determined by adjusting the value of the reduced density, η, to minimize the difference between the calculated pressure and the system pressure. Therefore, the density is calculated knowing the system temperature, pressure, and the three, pure component parameters, m, σ, and ε/k_B. The three pure component parameters are typically obtained by fitting the PC-SAFT EoS to pure component experimental data. Different parameter sets can be obtained for a compound depending on what experimental data are of interest and/or available. The first set of parameters reported by Gross and Sadowski [51] were obtained by fitting the PC-SAFT EoS to vapor-pressure curves and low-pressure liquid densities of each compound that was described. Another sets of pure component parameters were published by Burgess *et al*. [54] who fitted the equation to high-temperature, high-pressure liquid densities of each compound. In this PhD study, these two sets of parameters are denoted as Low-P and HTHP parameters, respectively. Alternatively, the pure component parameters can be estimated from group contribution schemes when experimental data for a compound of interest is not available. The group contribution methods basically accounts for the contribution of each group in compound to the three fitted pure component parameter for which the experimental data are available. The contributions of each group are then assumed to be the same from one compound to another. The group

10

contribution method of Burgess *et al*. [55] using Low-P and HTHP parameter sets is employed to model one of the binary mixture systems investigated in this study.

1.3. Objectives of This PhD Study

The main focus of this PhD study is to experimentally determine the high-pressure fluid phase behavior and densities for pure compounds and asymmetric binary mixtures of propane, a representative light gas, and heavy hydrocarbons. These compounds represent well-characterized model systems of pure compound and binary mixtures found in the saturate fraction of crude oils. The experimental study on samples of real crude oil are also investigated at similar conditions to the well-characterized model compound systems. The experiments are performed using a variable volume, floating piston, high-pressure view cell that is coupled to a linear variable differential transformer, LVDT, which provides information about the internal volume of the view cell. The floating piston, high-pressure view cell provides a means for simultaneous phase behavior and density determination since the technique allows for visual observation of the cell contents. Finally, the experimental data obtained from this study are used to test the performance of contemporary cubic and SAFT-based equations of state to model the experimental data.

11

Chapter 2 High-Pressure Experimental Techniques

2.1. Methods for Measuring High-Pressure Density

Many methods exist for high-pressure experimental studies depending on what operating conditions are of interest. Among the methods are three main types of instruments for high-pressure density measurement. The methods have varying difficulty, operating condition ranges, and experimental accuracy. Techniques belonging to the first type are collectively called vibrating body technique [21,56-65] that involves measuring the resonance of a vibrating object in the fluid of interest. This class of experimental method can allow for the simultaneous measurement of both density and viscosity data. The vibration of the object is affected by the hydrodynamic drag that is exerted on the body by the fluid of interest, which can be correlated to the density and viscosity of the fluid. The resonant period and the resonance curve of the vibratory body are measured. Since the resonant period and the width of the resonance curve can be directly measured, the density and viscosity of the fluid of interest at different temperatures and pressures can be calculated by simultaneously solving the correlation equations. The two equations however contain both density and viscosity and they can be complicated to solve. In the event that either the density data or the viscosity data can be obtained from other sources, the equations then become easier to solve for the unknown data. Caudwell *et al*. [66] used the vibrating body technique to report density data for five hydrocarbon compounds at temperatures to 473 K and pressures to 200 MPa with a reported uncertainty within 0.2% showing the remarkable accuracy of this technique. However, there are no reported data at temperatures above 473 K using this technique as the elastic properties of the vibration wire starts to significantly vary with temperature beyond, 473 K. Furthermore, the fluid of interest cannot be

visually observed for phase transitions and thus, the technique does not allow for phase behavior measurements.

Another technique commonly used in the study of volumetric properties of hydrocarbons involves the use of bellows. Nobel Laureate, Percy Bridgman, used the apparatus to measure the high-pressure experimental density data for alkanes, cyclic, aromatic hydrocarbons *etc*., at temperatures to 448 K and pressures to 5000 MPa, which is an extremely high pressure [67-70]. The bellows are composed of segments of a hollow elastic material with fixed diameter and the length, hence the volume, can be changed either by compressing of extending the bellows. Therefore, the change in volume of a fluid of certain mass is measured with respect to the applied pressure. This change in volume could be determined by coupling one end of the bellows to a device that can track the change in length of the bellows such as a linear variable differential transformer (LVDT). Although, the bellows can be applied to density measurements at extremely high pressures, however, there can be loss of mechanical properties of the bellows due to repeated stretching and at high temperatures. This can lead to a decrease in accuracy of the apparatus. Recently however, Ito *et al*. [71] used a metal-bellow variable volumometer apparatus to measure the density for propane, butane, and 2-methylpropane at temperatures to 600 K and pressures to 200 MPa. The authors extended the improvement on the temperature limit achieved by Muromachi *et al*. [72] from 500 K to 600 K. In the traditional operation of the bellows apparatus, the fluid of interest is loaded inside the hollow part of the bellow and therefore, does not allow for the visual observation of the bellow contents. Hence, the apparatus cannot be employed for phase behavior experiments. In addition care must also be taken not to exceed the elastic limit of the bellows as this can cause a permanent distortion of the bellows. The bellows

are also fragile and care must be taken when operating the apparatus so as not to allow for the differential pressure across the view cell to exceed 0.2 MPa, which can damage bellows.

The third technique is the floating-piston view cell densimeter and it is the technique that is primarily used in this PhD study. The operation of this technique is similar to the operation of the bellow apparatus where the LVDT tracks the location of a floating piston and the information from the LVDT can be correlated to the change in volume of the view cell. Knowing the volume and the mass of the fluid injected, the density can be obtained. The major advantage of this apparatus is that the contents of the cell can be visually observed throughout the course of the experiment from ambient conditions to HTHP conditions with temperatures to 535 K and pressures to 275 MPa. Figure 2.1 shows the layout of one of the high-pressure view cells used in this PhD study while Figure 2.2 shows the overview of the entire experimental apparatus. Liu *et al*. [4] described in some detail how this methodology is used for their density measurements of five relatively low molecular weight alkanes.
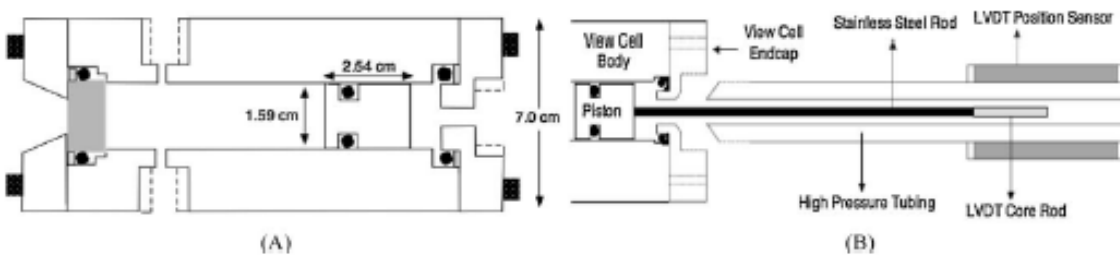
Figure 2.1. (A) Schematic diagram of the high-pressure view cell that was first used in this study. (B) Schematic diagram showing the rod connecting from the piston to the LVDT.
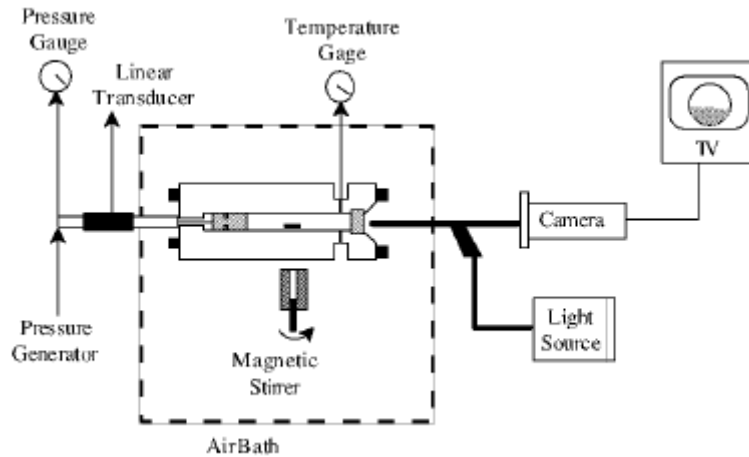
Figure 2.2. Schematic diagram of the experimental setup used in this PhD study.

Briefly, the view cell is constructed of a high nickel content metal alloy, such as Nitronic 50, Inconel 625, and Inconel 718. The internal diameter of the cell is about 1.59 cm and has a working fluid of approximately 35 ml. A sapphire window is fitted to one end of the cell with an o-ring and a backup o-ring. Once, the window is secured on the cell, the end cap is bolted to the cell body in a symmetrical fashion. The cell is then flipped over followed by insertion of a magnetic stir bar, shown in Figure 2.2, to ensure proper mixing of the cell contents. The piston with a fitted o-ring is then inserted that separates the contents of the cell from the overburden fluid which is used to pressurize the cell. After the piston is installed, the second end cap is fastened to the cell body in a similar fashion to the first end cap. Selection of o-rings is based on their compatibility with the fluid that they are in contact with. For the hydrocarbons studied here, Viton o-rings are used both on the window and on the piston for the experimental measurements. Prior to an experiment, the o-rings are pretreated in pure propane at about 320 K and 55 MPa for more than 8 hours. This step ensures that the elastomeric o-rings are saturated with propane and minimizes sorption of the fluid of interest into the o-ring that can potentially lead to substantial

15

experimental error in the density measurement. Furthermore, use of o-rings is reduced as the study progressed whereby the o-ring and backup o-ring previously required to seal the window have been eliminated for the mixture experiments in this PhD study. The sapphire window is now encased in a window-holder constructed from similar material as the high-pressure view cell. Sealing is achieved by a metal-to-metal conical mating of the window-holder to the cell body. Therefore, only the o-ring on the piston is needed which is pretreated as described earlier for the experiments.

As shown in Figure 2.1B, a rod is connected to the piston through the end cap and the other end of the rod is connected to a magnetic core that travels through the LVDT (Schaevitz Corporation, Model 2000 HR) region. The LVDT provides information on the position of the piston as the cell is pressurized or depressurized. From the information on the location of the piston, the volume occupied by the fluid of interest is obtained and hence the density is calculated from the knowledge of the amount of material loaded. A rupture disk is connected to one of the ports on the high-pressure vessel for safety, while a valve and a type-K thermocouple are also connected on the other ports of the cell. The valve allows for the transfer of the fluid of interest, while the thermocouple allows for temperature measurement of the contents of the view cell. The pressure is measured on the water-side of the piston with a Heise pressure gauge (Heise Corporation, Model CC, accurate to ± 10 psig (or 0.07 MPa)) for pressures below 10,000 psi (68.9 MPa) and a Viatran pressure transducer (Viatran Corporation, Model 245, accurate to ± 50 psig (or 0.35 MPa)) for pressures between 10,000 and 40,000 psi (68.9 to 275 MPa).

The calibration data for the Viatran pressure transducer is obtained from Viatran Corporation and the information is presented in Table 2.1 and Figure 2.3. This calibration equation thus obtained is used to convert the measured pressure values to the actual absolute

16

pressure values. The uncertainty in the pressure calibration, and hence the uncertainty in pressure measurements in this study, is 50 psi (0.35 MPa) at pressures to 40,000 psi (275 MPa). Similarly, the type-K thermocouple is calibrated against an Isotech F150 precision thermometer, accurate to ± 0.03 K and the result is presented in Table 2.2 and Figure 2.4. However, the calibration equation obtained for the thermocouple is only good to ± 0.2 K, hence, the uncertainty of the temperature measurements for this study is ± 0.2 K. Note that the σ_{slope} and $\sigma_{intercept}$ refer to the percent error in the slope and intercept values obtained from the respective calibrations. The small error in the slope of both calibrations indicates the linearity of both the pressure transducer and the thermocouple. The value for the $\sigma_{intercept}$ in the thermocouple plot is somewhat high given the calibration did not start from zero and it involves extrapolating the equation over 50 °C (50 K). This is not much of concern since the temperature range in this study is primary from 50 to 250 °C (323 to 523 K).

Table 2.1. Calibration data for the Viatran pressure transducer ($P_{viatran}$) obtained from Viatran Corporation.

Calibration Standard Pressure (psi)	Measured Viatran Pressure (psi)	Calibration Equation Pressure (psi)	Equation – Standard Δ Pressure (psi)	Equation – Standard Δ Pressure (MPa)
0	6	12.3	12.3	0.09
7992.5	7995	7984.6	-7.9	-0.05
15986.2	16007	15979.7	-6.5	-0.04
23982.7	24025	23980.9	-1.8	-0.01
31982.2	32042	31981.1	-1.1	-0.01
39985.9	40073	39995.2	9.3	0.06

17
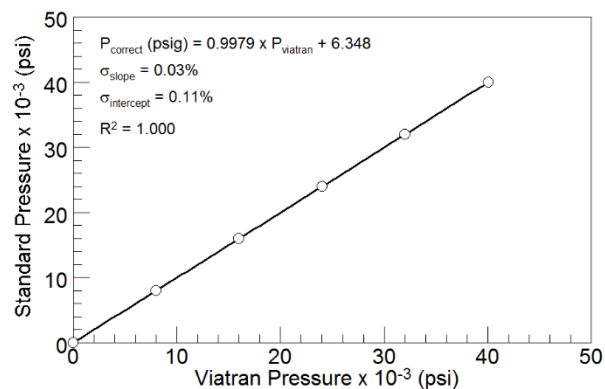
Figure 2.3. Calibration curve for the Viatran pressure transducer used in this study.

Table 2.2. Calibration data for the type-K thermocouple against the Isotech F150 precision thermometer.

Calibration Standard Temperature (°C)	Measured Type-K Temperature (°C)	Calibration Equation Temperature (°C)	Equation – Standard Δ Temperature (°C)
53.70	53.70	53.71	0.01
102.61	103.08	102.52	-0.09
153.62	154.98	153.81	0.19
200.52	202.09	200.37	-0.15
250.82	253.17	250.86	0.04

18
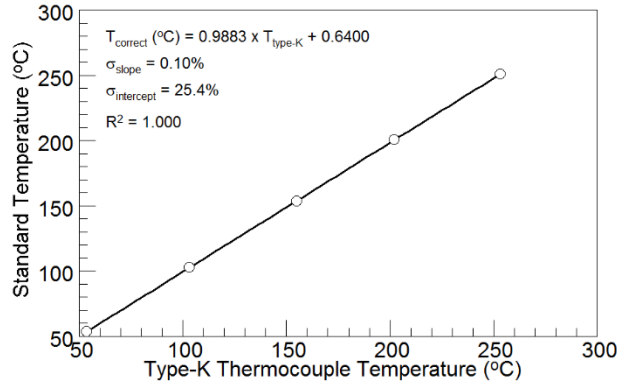
Figure 2.4. Calibration curve for the type-K thermocouple used in this study.

2.2. Experimental Techniques

2.2.1. Internal View Cell Volume Calibration and Density Measurements

The floating-piston technique is not an absolute technique for density measurements. As such, the internal volume of the cell needs to be calibrated with a fluid of known density at various temperature and pressure ranges before the density measurements for the fluid of interest can be completed. First, the linear range of the LVDT is established by measuring the reading of the LVDT against a vernier caliper. This process is done three times for reproducibility. The LVDT model used in this work has a linear range of 4 inches and this corresponds to LVDT readings between 0 and 120 as shown in Figure 4. The percent error of the slope gives an indication of the linearity of the LVDT, which was found to be within 0.12 % and is less than half of the 0.25 % specified by the manufacturer. However, the intercept depends on the starting length of the vernier caliper which explains the variation in the values of the intercepts between the three lines shown in Figure 5.
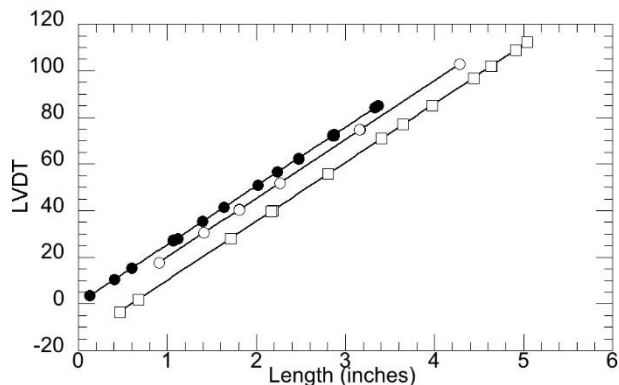
Figure 2.5. Plot showing the linearity range of the Linear Variable Differential Transformer (LVDT) used in this study for density measurement experiments. The procedure was conducted three times as indicated by the three curves.

The procedure for calibrating the internal volume of the view cell and the density measurement experiment are essentially the same and thus described. After assemblage, the cell is flushed with a suitable gas, for instance propane, and then vacuumed. This process is done three times to remove any residual air that will not dissolve in the hydrocarbon fluid of interest. The fluid of interest is then charged into the cell. For the calibration procedure, a calibrating fluid with known density data over wide temperature and pressure conditions, typically decane, can then be loaded into the cell using a hypodermic syringe. The mass of the fluid loaded is obtained with a weighing balance that is accurate to within ±0.0001 g. When working with a fluid that is a gas at ambient conditions, e.g. propane, the gas is charged into the cell using a high-pressure transfer vessel. The transfer vessel comprises of a Swagelok sample cylinder (Swagelok 304L-HDF4-50) plugged at one end and the other end is attached to 1/16 inch valve (HiP 15-11AF1) from which a 1/16 inch OD tubing that is about five inches long is attached. First the transfer vessel is filled with gas by chilling the vessel in ice and weighed. The transfer vessel is then

20

connected to the cell with the 1/16 inch tubing to the aforementioned valve on the cell. Once a satisfactory amount of gas has been transferred in to the view cell, the valve on the view cell is closed while leaving the valve on the transfer vessel opened. The transfer vessel is chilled in liquid nitrogen for a few minutes and then the second valve is closed before disconnecting the transfer line from the view cell. Chilling the transfer vessel in liquid nitrogen minimizes the loss of gas from the transfer line when the transfer vessel is disconnected from the view cell. The transfer vessel is then weighed and the amount of gas transferred is obtained. Since the transfer vessel weighs about 400 g, another scale with a larger maximum load capacity (OHAUS Ex 1103) accurate to within ±0.001 g is used to determine the amount of gas that is transferred. In a gas-liquid mixture experiment both loading routines are employed whereby the liquid is loaded first followed by addition of the gas.

The cell is heated to a desired temperature, say 50, 150, or 250 °C, by using heating bands encasing the view cell and the cell is allowed to stabilize for at least an hour. The cell is pressurized to selected pressures from about 3 to 275 MPa in a non-monotonous fashion to reduce experimental artifacts in the measurements. Often times, data points are repeated in duplicates or triplicates. At each pressure, the cell is allowed to stand for at least a minute after the rate of pressure change is less than 10 psi (0.07 MPa) per minute. Once this is achieved, the temperature, pressure, and LVDT position are recorded. All of this is done with magnetic stirring to ensure proper mixing of the view cell contents.

In a calibration process, the density data for the calibrating fluid are obtained from a reliable literature source at the temperature and pressure conditions obtained from the experiment. For instance, density data for decane are reported in the NIST webbook [73] at temperatures to 800 MPa and pressures to 673 K and are routinely used for calibrating the

internal volume of the view cell at 323, 423, and 523 K. The volume at each temperature and pressure condition recorded is calculated by dividing the known mass of fluid by the density value obtained from the literature. A volume calibration plot is generated by plotting the calculated volume data against the corresponding LVDT position data that were recorded. Figure 2.6 shows a typical calibration curve thus obtained.
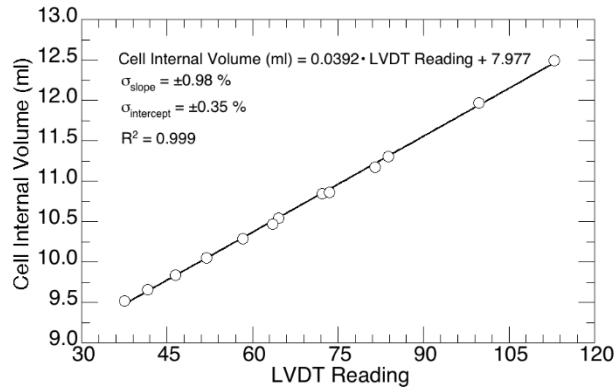
Figure 2.6. Calibration curve generated in this study for the internal volume of the view cell as a function of Linear Variable Differential Transformer (LVDT) position using decane as a calibrating fluid.

However, for density measurement experiments, the recorded LVDT positions at each temperature and pressure condition is used to calculate the volume from the previously obtained calibration equation. The density is then obtained by dividing the known mass of material by the calculated volume. The robustness of this technique has been demonstrated in reporting the density data for a variety of pure compounds[4,14,74-76], binary mixtures [77,78], and a polymer [79] at temperatures to 533 K and pressures to 275 MPa.

2.2.2. Procedure for Phase Behavior Determination

Phase behavior experiments are conducted with the same apparatus and loading techniques as described in the previous section. The phase transitions are however obtained visually at which point the temperature and pressure information are recorded. The phase transition is always approached isothermally by changing the pressure, starting from a single phase region until two phases are observed. Bubble point and dew point data are obtained by decreasing the pressure, while solidification data points are thus obtained with increase in pressure. For each experiment, the cell is stabilized at a desired temperature and the pressure is adjusted accordingly until a single, usually clear, phase is obtained. The search for the transition pressure is carried out by a stepwise adjustment of pressure. The cell is left to stand for about 5 to 10 minutes after each pressure adjustment. If phase of the cell contents remains single, the pressure is again adjusted. This process is repeated until the first bubble is observed for bubble point experiment, or mists are observed for dew point experiments, or the first crystal is observed in a solidification experiment. For each experiment, the phase transition is repeated until the pressure difference between the single phase region and the two-phase region is within 0.1 MPa. The transition pressure is chosen as the midpoint between the pressures of the two phases.

Visual observation of view cell contents at various temperature and pressure conditions is achieved by using a borescope (Olympus Corporation, Model F100-024-000-55) that is connected to a camera (Olympus Corporation, Model STC-N63CJ). The borescope is placed against the sapphire window of the cell while the camera transmits the image on to a monitor screen. The experimental technique has been used to obtain various phase behavior data including solidification, vapor-liquid equilibria, and cloud point data [80,81].

2.3. Error Analysis

2.3.1. Uncertainty Associated with Reported Density Data

As stated in section 2.1, the standard uncertainty associated with the temperature measurement, σ_T, is 0.2 K and uncertainty associated with pressure measurements σ_P, is 0.07 MPa for pressures below 68.9 MPa and 0.35 MPa for pressures between 68.9 and 275 MPa. The accumulated uncertainty associated with density data measured in this study, σ_ρ, is obtained from the measurements of both mass, m, and volume, V, through the propagation of error as given in equation 2.1. In equation 2.1 σ_m, is the standard uncertainty in mass of fluid and is obtained from the weighing scale, which is typically 0.0001 for liquid samples. The uncertainty in the volume, σ_V, is obtained from the calibration equation of the internal volume of the view cell against the LVDT position, $T.R.$, as given in equation 2.2 and equation 2.3 gives the expression for σ_V.

$$\sigma_\rho = \sqrt{\left(\frac{\delta\rho}{\delta m}\right)^2 \bullet \sigma_m^2 + \left(\frac{\delta\rho}{\delta V}\right)^2 \bullet \sigma_V^2} = \sqrt{\left(\frac{1}{V}\right)^2 \bullet \sigma_m^2 + \left(\frac{m}{V^2}\right)^2 \bullet \sigma_V^2} \qquad (2.1)$$

$$V = I + S \circ T.R \qquad (2.2)$$

$$\sigma_V = \sqrt{\left(\frac{\delta V}{\delta I}\right)^2 \bullet \sigma_I^2 + \left(\frac{\delta V}{\delta S}\right)^2 \bullet \sigma_s^2 + \left(\frac{\delta V}{\delta T.R}\right)^2 \bullet \sigma_{T.R}^2} = \sqrt{\sigma_I^2 + (T.R)^2 \bullet \sigma_s^2 + (S)^2 \bullet \sigma_{T.R}^2} \quad (2.3)$$

Therefore, equation 2.1 can be expanded with the information of the calibration equation and the expanded equation is given in equation 2.4. Note that σ_I and σ_S correspond to the error obtained from the linear fit of the internal volume calibration equation for the intercept and slope, while $\sigma_{T.R}$, is the uncertainty of the LVDT position, which is 0.0025, as specified by

24

Schaevitz Corporation. Thus the estimated accumulated uncertainty in the reported density data obtained in this study is calculated from equation 2.4 and is within 0.9% of the density value, i.e., $\sigma_\rho = 0.9 \cdot \rho$.

$$\sigma_\rho = \sqrt{\left(\frac{1}{V}\right)^2 \bullet \sigma_m^2 + \left(\frac{m}{V^2}\right)^2 \bullet \sigma_l^2 + \left(\frac{m}{V^2}\right)^2 \bullet (T.R)^2 \bullet \sigma_s^2 + \left(\frac{m}{V^2}\right)^2 \bullet (S)^2 \bullet \sigma_{T.R}^2} \qquad (2.4)$$

2.3.2. Uncertainty Associated with Reported Mixture Compositions

Similarly, the uncertainty in the mixture molar composition is estimated through the propagation of error. The mole fraction of component 1 is related to the mass of each component in a binary mixture according to equation 2.5. Therefore, the uncertainty in mole fraction of composition 1, σ_{x1}, is calculated according to equation 2.6. Note that σ_{m1} and σ_{m2} in equation 2.6 are the uncertainty in measuring the mass of components 1 and 2 respectively. Through mathematical manipulation, the final expression for σ_{x1} is given in equation 2.7. The average accumulated uncertainty for the propane mole fraction in the binary mixtures reported in this work is within 0.0003.

$$x_1 = \frac{n_1}{n_1 + n_2} = \frac{\dfrac{m_1}{M_1}}{\dfrac{m_1}{M_1} + \dfrac{m_2}{M_2}} \qquad (2.5)$$

$$\sigma_{x_1} = \sqrt{\left[\frac{\delta x_1}{\delta m_1}\sigma_{m_1}\right]^2 + \left[\frac{\delta x_1}{\delta m_2}\sigma_{m_2}\right]^2} \qquad (2.6)$$

$$\sigma_{x_1} = \sqrt{\frac{1}{\left(\dfrac{m_1}{M_1} + \dfrac{m_2}{M_2}\right)^4}\left[\left[\left(\dfrac{m_1}{M_1} + \dfrac{m_2}{M_2}\right)\dfrac{1}{M_1} - \dfrac{m_1}{M_1^2}\right]^2 \bullet \sigma_{m_1}^2 + \left(\dfrac{m_1}{M_1} \bullet \dfrac{1}{M_2}\right)^2 \bullet \sigma_{m_2}^2\right]} \qquad (2.7)$$

3.1. Experimental Results

3.1.1. Propane

The thermodynamic properties of propane have been studied over wide temperature and pressure conditions leading to development of several reference equations of state (EoS). Lemmon *et al*. [82] developed the latest in the series of reference EoS that represent the thermodynamic properties of propane and covers temperatures to 650 K and pressures to 1000 MPa. In the development and validation of the reference EoS, Lemmon *et al*. [82] utilized a very large pool of experimental data from almost two hundred references. The uncertainty in the density data calculated from the reference EoS is less than 0.1% and the calculated data also agree with the data reported in the NIST webbook [73] within 0.1 %. However, at temperatures in excess of 480 K, experimental density data are lacking beyond 60 MPa, and especially lacking at the HTHP conditions related to oil recovery processes in ultra-deep reservoirs. This study reports the experimental density data for propane at 324.1, 424.6, and 514.4 K at pressures to 210 MPa. Under these conditions the density ranges from 336 to 536 kg m^{-3} and are presented in Table 3.1. Recently, Ito *et al*. [71], using a metal-bellows variable volumometer technique, reported the density data for propane to 673 K and 200 MPa with average uncertainty within 0.3% of the density data. Thus, Figure 3.1 shows the deviation plots of the data calculated from the Lemmon *et al*. reference EoS [82] from the experimental data of Ito *et al*.[71] and the data obtained in this study. The mean absolute percent deviation (δ, equation 3.1) between the density reported in this study and the density predicted with the Lemmon *et al*. reference EoS is 0.4 at 324.1 K, 0.4 at 424.6 K, and 0.3 at 514.4 K, which are well within the experimental uncertainty

for the reported density in this study and are well within the experimental uncertainty, which 0.9%.

Table 3.1. Experimental propane density data, ρ, as a function of temperature, T, and pressure, P, obtained in this study. Listed are values for the mean absolute percent deviation, δ, obtained by comparing experimental data to values calculated from a reference equation of state for propane developed by Lemmon *et al.* [82].

	P /MPa	ρ /kg·m^{-3}	P /MPa	ρ /kg·m^{-3}	P /MPa	ρ /kg·m^{-3}
$T =$	324.1 ± 0.1 K		424.6 ± 0.2 K		514.4 ± 0.1 K	
$\delta =$	0.4		0.4		0.3	
	3.9	455	21.7	386	30.4	336
	7.3	471	22.1	387	36.8	361
	7.7	471	30.6	420	37.0	361
	13.9	493	30.9	420	49.9	401
	14.5	493	31.1	420	49.9	402
	24.9	517	42.0	451	50.7	402
	25.3	518	43.1	452	65.2	433
	26.0	516	43.5	453	65.7	434
	35.8	533	54.5	474	66.3	435
	37.9	533	54.5	474	82.4	460
	46.7	547	69.3	497	82.6	460
	46.9	547	72.2	499	97.7	480
	49.5	546	72.7	499	98.2	481
	60.4	560	88.9	517	116.7	501
	80.8	577	89.0	517	118.7	503
	105.5	593	111.7	536	138.7	520

27

105.5	593	111.8	537	140.7	521
138.5	610	137.9	557	161.0	536
168.7	623	167.1	575	188.9	553
180.5	627	172.4	578	190.7	554
203.2	635	202.3	593		
209.9	636	207.4	596		

$$\delta = \frac{1}{n} \sum_{1}^{n} \left| \frac{\rho_{i,\text{experimental}} - \rho_{i,\text{predicted}}}{\rho_{i,\text{experimental}}} \right| \bullet 100$$

(3.1)
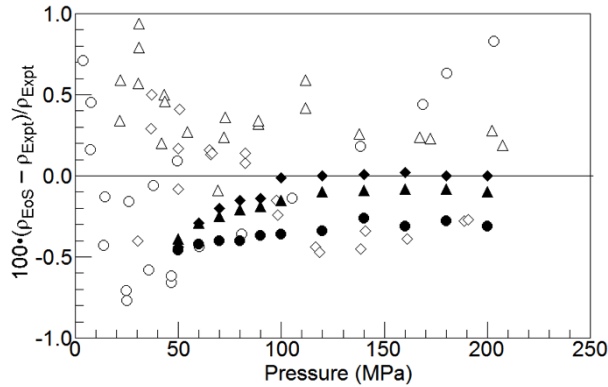
Figure 3.1. Percent density deviations for experimental propane densities (ρ_{Expt}) obtained in this study (open symbols) and data reported by Ito *et al.*[71] (filled symbols) from predicted densities using Lemmon *et al.*'s reference EoS [82] (ρ_{EoS}) at (○), 324.1 K; (●), 360.0 K; (Δ), 424.6 K; (▲), 440.0 K; (◊), 514.4 K; and (♦), 550.0 K.

3.1.2. Squalane

In this study, experimental density data for pure squalane are measured and presented at 323.4, 423.7, and 511.5 K and at pressure to 240 MPa and are presented in Table 2. The high-pressure density of squalane has been reported in the literature at temperatures to 473 K and pressures to 200 MPa. The present study extends the literature data to 511.5 K and to 240 MPa. Figure 3.2 compares the range of experimental conditions for density data obtained in this study with the experimental conditions reported in the literature for squalane. The figure does not include references that only reported density data at atmospheric pressures [83-93]. Similar comparison is presented in Table 3.3 showing how the range of experimental conditions for squalane studied here extends the conditions of each literature source. Mylona *et al.* [91] correlated the modified Tait equation [20] to the available literature density data at both atmospheric and high pressures, but only to a maximum temperature of 473 K. The Tait equation, with the parameters reported by Mylona *et al.* is used to compare the experimental data obtained in this study to data available in the literature. The δ between the Tait equation and the reported data in the present study is 0.7 at temperatures to 423.7 K. When the parameters of the Tait equation are extrapolated to 511.5 K, which is beyond the limits of the experimental data used to obtain the parameters, the δ becomes 0.9, a value almost equal to the estimated uncertainty for the reported density data in the present study.

Table 3.2. Experimental squalane density data, ρ, as a function of temperature, T, and pressure, P, obtained in this study. Listed are values for the mean absolute percent deviation, δ, obtained by comparing experimental data to values calculated from a Tait equation correlation of the available literature data for Squalane [91].

P /MPa	ρ /kg•m^{-3}	P /MPa	ρ /kg•m^{-3}	P /MPa	ρ /kg•m^{-3}
$T =$	323.4 ± 0.1 K		423.7 ± 0.1 K		511.5 ± 0.2 K
$\delta =$	0.5		0.9		1.3
7.5	786	3.1	716	12.1	667
13.8	792	5.0	718	22.5	682
22.5	798	11.9	726	22.6	683
23.5	798	12.3	726	34.6	703
28.8	806	14.8	735	35.2	698
37.3	808	27.3	741	50.9	722
44.3	815	27.5	741	56.1	720
44.7	815	29.0	749	56.6	720
55.6	819	29.2	750	71.4	740
55.9	818	44.1	763	90.5	754
60.8	824	47.0	760	91.0	755
67.6	826	48.2	759	91.5	754
82.3	836	63.3	777	111.1	768
84.3	836	81.7	789	139.4	785
97.0	843	83.7	791	139.7	785
109.3	848	103.0	802	172.1	802
110.4	848	152.7	828	206.4	819
111.2	848	194.7	846	206.4	819
135.8	859			239.5	833

30
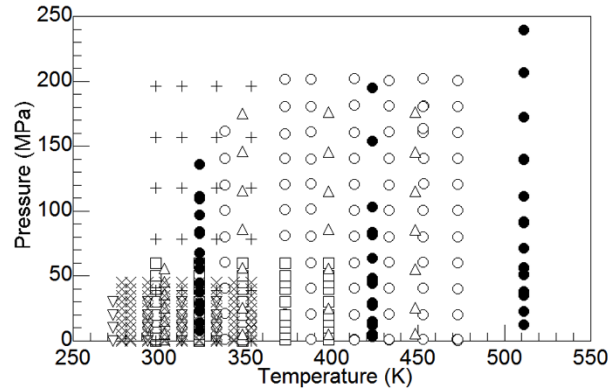
Figure 3.2. Temperature and pressure distribution of literature density data for squalane as compared to the squalane density data obtained in the present study. The figure excludes literature data only collected at 0.1 MPa [83-93]. The data of Schmidt *et al*. [94] (○), Fandino *et al*. [95] (□), Ciotta *et al*. [96] (Δ), Tomida *et al*. [97] (◊), Kumagai *et al*. [98] (▽), Fandino *et al*. [99] (x), Kuss *et al*.[100] (+), and the data obtained in this study (●).

Table 3.3. Comparison of data obtained in this study to that available in the literature for squalane.

Literature reference	Literature temperature range (K)	Literature maximum pressure (MPa)	Literature data points	Temperatures (K) and pressures (MPa) for density data obtained in the present study that differ from reference data
Schmidt *et al*. [97]	338-473	202	86	323 K: P < 136 523 K: P < 240
Fandino *et al*. [95]	298-398	60	53	323 K: 60 < P < 136 423 K: P < 195

				523 K: P < 240
Ciotta *et al*. [96]	303-448	176	32	423 K: 176 < P < 195
				523 K: P < 240
Tomida *et al*. [97]	293-353	20	12	323 K: 20 < P < 136
				423 K: P < 195
				523 K: P < 240
Kumagai *et al*. [98]	273-333	30	16	323 K: 30 < P < 136
				423 K: P < 195
				523 K: P < 240
Fandino *et al*. [99]	278-353	45	99	323 K: 45 < P < 136
				423 K: P < 195
				523 K: P < 240
Kuss *et al*. [100]	298-353	196	24	423 K: P < 195
				523 K: P < 240

3.1.3 *Bis* (2-ethylhexyl) Phthalate (DEHP)

Table 3.4 lists the experimental DEHP densities as functions of temperature and pressure obtained in this study. Figure 3.3 shows the effect of pressure, to 270 MPa, on the density of DEHP at different temperatures. DEHP density data range from 811 to 1046 kg•m^{-3} for the temperature and pressure conditions investigated.

Table 3.4. Experimental density data, ρ, at different temperatures, T, and pressures, P, for DEHP obtained in this study.

	P/MPa	ρ/kg•m^{-3}	P/MPa	ρ/kg•m^{-3}	P/MPa	ρ/kg•m^{-3}
T/K =	373.3		423.4		476.2	
	3.8	921	4.2	878	5.5	847
	7.6	924	7.9	885	9.5	853
	12.2	928	11.1	890	9.4	853
	15.9	931	14.5	895	15.7	861
	18.1	933	18.0	898	15.2	861
	22.3	936	21.2	901	15.2	861
	28.3	940	27.8	908	27.5	874
	34.8	945	35.2	914	27.3	874
	42.2	950	42.1	918	26.8	874
	48.9	954	49.2	924	46.9	894
	56.1	959	55.7	930	46.7	894
	69.5	967	70.7	939	59.8	905
	83.7	974	83.7	948	71.5	913
	104.2	984	104.2	960	70.7	914
	125.4	994	125.4	970	96.4	931
	138.9	1001	139.9	977	95.7	931
	152.9	1007	153.7	983	114.8	942
	174.4	1015	173.4	992	114.2	942
	208.3	1029	207.1	1006	140.4	958
	240.0	1041	239.4	1018	139.8	959
	262.1	1046	263.8	1028	176.2	975
					206.9	990
					240.2	1002

33

			269.0	1013	

Table 3.4 continued. Experimental density data, ρ, at different temperatures, T, and pressures, P, for DEHP obtained in this study.

P/MPa	ρ/kg•m^{-3}	P/MPa	ρ/kg•m^{-3}
T/K =	491.9		523.7
3.9	830	5.7	811
4.1	830	9.2	817
3.9	831	9.2	817
10.5	839	16.1	827
9.9	840	16.1	827
23.3	856	21.6	835
23.3	856	21.6	835
22.8	856	27.5	842
37.5	870	27.3	842
37.2	870	35.7	851
51.1	885	35.5	851
50.7	886	44.4	860
71.5	902	44.6	860
71.9	902	44.3	860
95.0	918	44.2	860
94.8	918	56.3	871
121.7	934	55.8	871
121.8	934	68.9	882
145.4	948	68.5	882
145.6	948	82.5	892
177.2	964	82.2	893

177.4	964	97.3	903
204.3	977	97.0	903
206.0	978	117.0	916
230.8	988	117.7	916
229.4	989	117.4	916
253.7	998	155.7	939
258.1	1000	156.1	939
		181.5	952
		181.2	952
		209.5	964
		209.9	964
		233.9	974
		234.0	974
		253.6	983
		253.4	983
		263.5	987

3.2. Correlations with the Modified Tait Equation

The modified Tait equation [20], equation 3.2, is fitted to the experimental density data for the pure compounds studied here to provide a facile method for density calculations at different temperatures and pressures. Although, the modified Tait equation has been widely used to correlate experimental liquid density data, the equation does not provide very good representation for the volumetric properties of gases like propane. Therefore, the Tait equation is only correlated to the density data for pure squalane and DEHP, as well as the propane binary mixtures with heavier alkanes (in chapter 4). The reference equation proposed by Lemmon *et al*. [82] is in good agreement with the experimental data obtained in this study and it is thus used to represent the pure propane data for the purpose of interpolating the experimental data.

35

$$\frac{\rho - \rho_0}{\rho} = C \log_{10} \frac{P + B}{P_0 + B} \qquad (3.2)$$

$$\delta = \frac{1}{n} \sum_1^n \left| \frac{\rho_{i,\text{experimental}} - \rho_{i,Tait}}{\rho_{i,\text{experimental}}} \right| \bullet 100 \qquad (3.3)$$

In the above equation, P_0 equals 0.1 MPa, ρ_0 is the density at P_0, while B and C are adjustable parameters determined from fitting the equation to experimental density data. Parameter C is independent of temperature, while ρ_0 and B are temperature-dependent and, for hydrocarbons, both parameters decrease as the temperature increases. For each compound, the Tait equation is fitted to each isotherm independently to obtain initial values for the three parameters ρ_0, B, and C by minimizing the mean absolute percent deviation (δ) as defined in equation 3.3. Next, the values of parameter C are averaged, followed by refitting the Tait equation to the experimental density data. This time however, only a single value C is used for all the isotherms and it is adjusted along with the other two parameters, ρ_0 and B, while minimizing the δ. The optimized values for the three parameters are listed in the Table 3.5 for squalane and Table 3.6 for DEHP, along with the corresponding final δ and λ for the fit of the Tait equation to the experimental data. As an example the comparison of the DEHP density data obtained in this study to the modified Tait equation with fitted parameters is shown in Figure 3.3 at 373.3, 423.4, 476.2, 491.9, and 523.7 K.

36

Table 3.5. Tait equation parameters, mean absolute percent deviation, δ, and standard deviation values, λ, for each δ, obtained for each squalane density isotherm. $C = 0.2232$.

Data Points	T /K	ρ_0 /kg•m^{-3}	B /MPa	δ	λ
19	323.4	780	85.364	0.12	0.11
18	423.7	711	46.565	0.26	0.22
21	511.5	638	23.676	0.19	0.20

Table 3.6. Tait equation parameters, mean absolute percent deviation, δ, and the standard deviation, λ, values obtained for each DEHP density isotherm. C has a constant value of 0.2275.

Data Points	T /K	ρ_0 /kg•m^{-3}	B /MPa	δ	λ
21	373.3	918	103.621	0.09	0.06
21	423.5	878	76.074	0.18	0.13
24	476.2	839	55.210	0.11	0.09
28	491.9	823	50.590	0.16	0.07
37	523.7	799	43.438	0.23	0.11
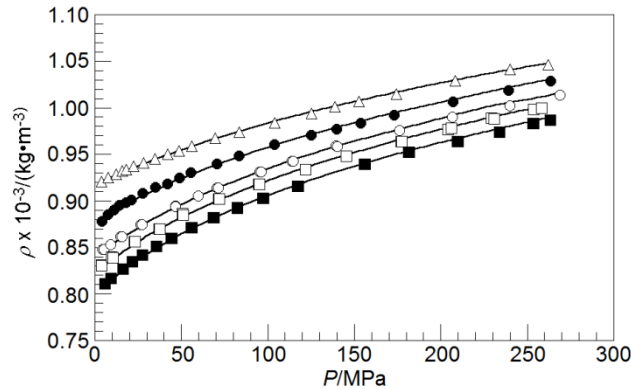
Figure 3.3. Comparison of DEHP density data, ρ, (symbols) obtained at different pressures, P, in this study to a fit of the modified Tait equation (lines). Temperatures are 373.3 K (Δ), 423.4 K ($\bullet$), 476.2 K ($\circ$), 491.9 K ($\square$), 523.7 K ($\blacksquare$). Lines serve to guide the eyes.

37

The Tait equation has already been used to compare the experimental data obtained in this study for squalane to the literature data by using the set of Tait equation parameters reported by Mylona *et al*. [91]. In addition to this, the Tait equation, with the parameters listed in Table 3.6, are used to compare density data obtained in this study with the data of Agaev *et al*. [101], reported with an uncertainty of 0.03%, from 373.29 to 523.15 K to a maximum pressure of 80 MPa. The δ from this comparison is less than 0.60, which is less than the estimated accumulated experimental uncertainty in the data reported in the present study. In fact, a δ value of 0.57 is obtained when comparing data of Agaev *et al*. to those predicted with the Tait equation from $T = 303.15$ K to $T = 548.15$ K, which are temperatures well outside the range used to determine the Tait parameters in the present study. Hence, it is reasonable to conclude that the Tait equation parameters reported here provides a reliable method to estimate DEHP densities from 303.15 to 548.15 K and pressures to 270 MPa. To the best of our knowledge, the data reported by the Agaev *et al*. are the only density data for DEHP that have been reported at similar conditions to the conditions investigated in this study.

3.3. Equation of State Modeling

The high-temperature, high-pressure (HTHP) experimental density data obtained in this study are modeled with the Peng-Robinson (PR) [24], the volume-translated Peng-Robinson (VT-PR) [27], and the Perturbed Chain Statistical Associating Fluid Theory (PC-SAFT) [51] equations of state (EoS). As mentioned in chapter 1, both the PR and the VT-PR Eos require the critical temperature, T_c, critical pressure, P_c, and the acentric factor, ω, of each compound for calculations. For low molecular weight compounds like propane, the properties are easily obtained from open literature. However, for thermally-labile, high-molecular weight compounds

that undergo thermal decomposition before reaching the critical point, such as squalane and

DEHP, these properties must be estimated by other methods. As such, there can be discrepancies

in the performance of the cubic EoS depending on the estimation methods for the physical

properties. In the case of the PC-SAFT EoS, the three pure-component parameters are required

for calculations for the non-associating propane, squalane, and DEHP fluids studied here. Again,

the pure component parameters are the number of segments, m, the temperature-independent

segment diameter, σ, and the interaction energy, ε/k_B. The performance of each model is

characterized by the mean absolute percent deviation, δ, as defined in equation 3.4.

$$\delta = \frac{1}{n} \sum_{1}^{n} \left| \frac{\rho_{i,\text{experimental}} - \rho_{i,\text{calculated}}}{\rho_{i,\text{experimental}}} \right| \bullet 100$$

(3.4)

3.3.1. Peng-Robinson (PR) and Volume-Translated (VT) PR Equations of State (EoS)

Table 3.7 shows the critical properties and acentric factor for propane and squalane that

are used for calculations with the PREoS and the VT-PREoS along with δ and the standard

deviation, λ obtained for each δ. Table 3.8 contains similar information for DEHP as well as

comparison with different methods of estimating the critical properties for DEHP. Unlike

squalane and DEHP, the critical properties and acentric factor for propane are readily obtained

from Reid *et al.* [102]. The critical properties for squalane are estimated using a flow method

[103], which is an indirect method for inferring the critical points of thermally-labile compounds.

The acentric factor is then calculated using equation 3.5, where P_r^{sat} is the reduced saturated

vapor pressure at a reduced temperature, T_r, of 0.7. Unfortunately, the vapor pressure data also

reported by VonNiederhausern *et al.* [103] are only between reduced temperatures of 0.79 and

1.0. Therefore the vapor pressure data are fitted to the Riedel [102] equation and was extrapolated to reduced temperature of 0.7, from which the acentric factor is then calculated.

In the case of DEHP, Nikitin *et al*. reported T_c ($\pm$ 10 K) and P_c ($\pm$ 0.04 MPa) that are obtained using a pulse-heating method [104], which is another indirect method for estimating the critical properties, since phthalates also undergo thermal decomposition at temperatures below their critical temperatures [104,105]. The acentric factor for DEHP is calculated using equation 3.6 [102] since the vapor pressure data are not readily available as in the case of squalane. Instead the acentric factor is calculated using the information from the boiling temperature, T_b (in K) and P_c, which is the critical pressure in atmospheres. These physical properties are used with the PREoS and VT-PREoS models to calculate density data for propane, squalane, and DEHP. The results of the DEHP density calculations are compared to calculations using these models with three different group contribution methods to estimate the critical properties [102,106,107].

$$\omega = -\log_{10}\left(P_r^{sat}\right) - 1, \quad \text{at } T_r = 0.7 \tag{3.5}$$

$$\omega = \frac{3}{7}\left[\frac{\left(\dfrac{T_b}{T_c}\right)}{\left(1 - \dfrac{T_b}{T_c}\right)}\right]\log_{10}\left(P_c / atm\right) - 1 \tag{3.6}$$

Table 3.7. Critical temperature, T_c, critical pressure, P_c, and acentric factor, ω, for propane and squalane along with the mean absolute percent deviation (δ) and the standard deviation (λ) obtained from density calculations using the Peng-Robinson (PR), the volume-translated Peng-Robinson (VT-PR) equations of state (EoS).

	M_w	T_c /K	P_c /MPa	ω	δ PREoS	λ PREoS	δ VT-PREoS	λ VT-PREoS
Propane [102]	44.1	369.8	0.4246	0.152	8.34	2.16	1.16	0.73
Squalane [103]	422.8	795.9	0.590	1.340	41.18	2.32	29.14	1.78

Table 3.8. Critical temperature, T_c, critical pressure, P_c, and acentric factor, ω, for DEHP from four different sources, along with the mean absolute percent deviation (δ) and the standard deviation (λ) obtained using the Peng-Robinson (PREoS) and the volume-translated Peng-Robinson (VT-PREoS). The normal boiling point of DEHP, T_b, is 657.2 K and the molecular weight is 390.6 g/mol [108].

	T_c /K	T_b/T_c	P_c /MPa	ω	δ PREoS	λ PREoS	δ VT-PREoS	λ VT-PREoS
Nikitin *et al.* [104]	835.0	0.787	1.070	0.622	21.29	2.54	7.65	2.11
Marrero and Gani [107]	868.7	0.757	1.220	0.439	14.03	2.72	2.22	1.71

Constantinou and Gani [106]	853.5	0.770	0.982	0.415	29.32	2.25	21.72	1.99
Reid *et al*. [102]	806.8	0.815	0.989	0.863	24.50	2.50	9.74	2.02

From the results in Tables 3.7 and 3.8, it can be clearly observed that both the PREoS and the VT-PREoS provide better HTHP density predictions for propane, a low-molecular weight compound whose critical properties are readily measurable, than either squalane or DEHP. In addition to the easy availability of the critical properties for propane, the value of the acentric factor, 0.152, is also small as compared to that for squalane, estimated as 1.34, and that for DEHP estimated to be between 0.415 and 0.863. The cubic EoS are notorious for providing poor density predictions for high-molecular weight compounds possessing acentric factor that is greater than 0.4. In all the cases, the VT-PREoS does provide an improvement on the PREoS following the addition of the fourth parameter in the equation of state. Figure 3.4 shows the comparison of the modeling performance of both the PREoS and the VT-PREoS with the HTHP experimental density data for propane (a), squalane, (b), and DEHP (c) using the set of physical parameters obtained from Nikitin *et al*. [104].
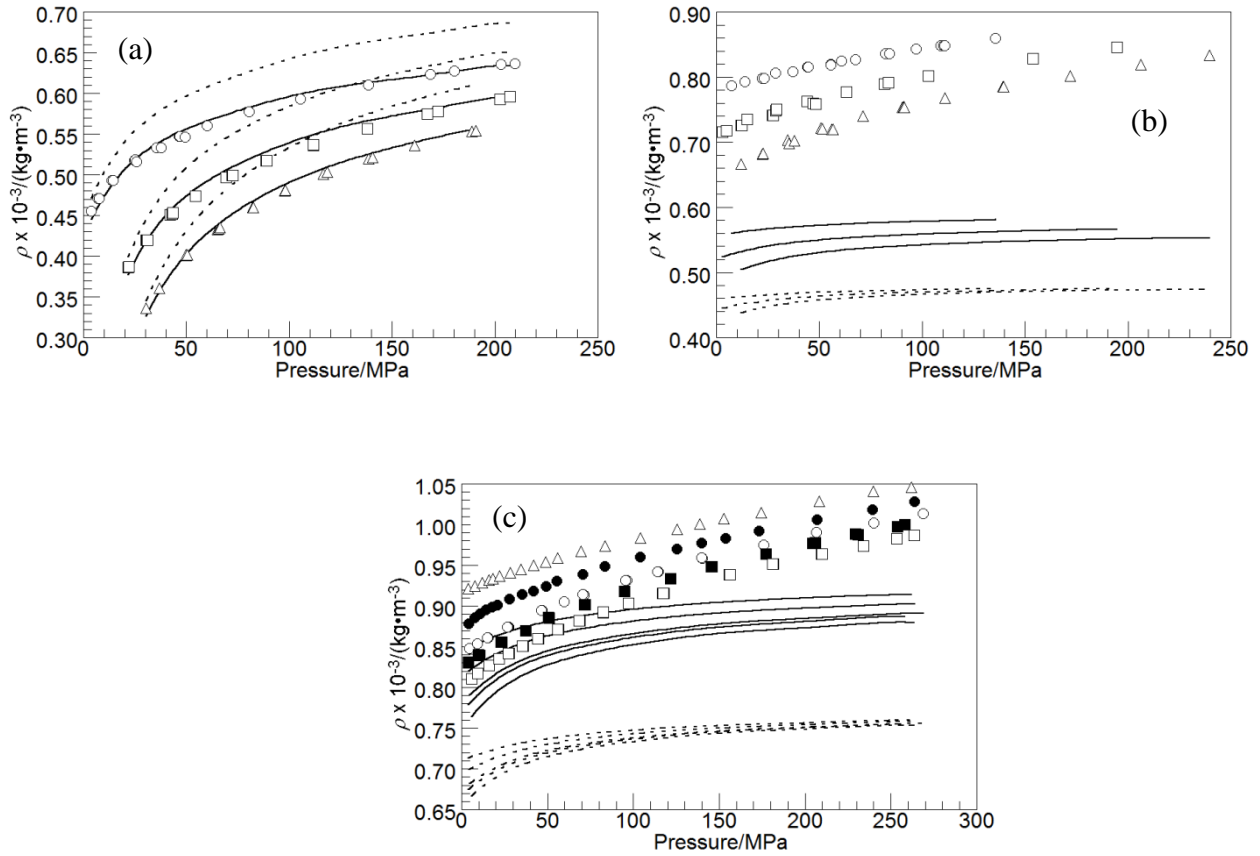
Figure 3.4. Comparison of the performance of the PREoS (·········) and the VT-PREoS (——) with the HTHP experimental density data obtained in this study. Propane results are presented in (a) at 324.1 K (○), 424.6 K (□), and (Δ), 514.4 K. Squalane results are presented in (b) at 323.4 (○), 423.7 (□), and 511.5 K (Δ). DEHP results are presented in (c) at 373.3 K (Δ), 423.4 K (●), 476.2 K (○), 491.9 K (□), 523.7 K (■) using the set of physical properties obtained from Nikitin *et al*. [104].

The sensitivity of the PREoS and especially the VT-PREoS to changes in the estimated physical properties can be evaluated by comparing the performance of each model to the DEHP experimental density data when using sets of physical properties obtained either by indirect

experimental methods or by group contribution schemes. As shown in Table 3.8, the δ values for the VT-PREoS are a factor of at least 2.5 less than those found for the original PREoS except when using the parameters reported by Constantinou and Gani [106], which shows only a little improvement in a very large δ value. It is not apparent why the δ does not improve substantially when the VT-PREoS is used with the group contribution approach of Constantinou and Gani [106]. However, consider the performance of the PREoS and VT-PREoS models when the DEHP critical properties are adjusted slightly. The δ with the VT-PREoS for the 373 K isotherm can be reduced to 7.65 rather than 23.41 if the Constantinou and Gani calculated value of T_c is used along with a P_c of 1.220 MPa, rather than the Constantinou and Gani calculated value of 0.982 MPa, and with a newly calculated ω of 0.551, rather than 0.415. Likewise, the δ with the PREoS is also reduced from 31.71% to 15.23% when the adjusted critical properties and acentric factor are used. Given that the adjusted critical properties and acentric factor are within the range of the values reported in Table 3.8, it is reasonable to conclude that a cubic-based equation of state is not capable of reliably modeling such a high molecular weight, polar compound.

3.3.2. Perturbed-Chain Statistical Associating Fluid Theory (PC-SAFT) EoS

As mentioned earlier, the PC-SAFT EoS requires three pure-component parameters for each non associating compound density calculations. In this work, the pure component parameters are obtained primarily from two sources in the literature. The first set of parameters is obtained from the works of Gross and Sadowski (Low-P parameters) [51] who fitted the equation to vapor-pressure curves and low-pressure liquid densities of each compound, while the second source is obtained from Burgess *et al*. (HTHP parameters) [54] who fitted the equation to high-temperature, high-pressure liquid densities of each compound. Generally, the Low-P parameters

44

provide good predictions for vapor pressure and saturated density values while the HTHP parameters provide good predictions for HTHP density data. However, the Low-P parameters yields poorer HTHP density predictions and conversely, the HTHP parameters perform poorer than the Low-Parameters in the prediction of vapor pressure and saturated liquid densities. Due to the need for pure component parameters that are not always available, group contribution methods can be used to estimate the parameters and are available in the literature [55]. The group contribution methods are set up to yield pure component parameters that are either similar to the Low-P parameters or similar to the HTHP parameters.

For propane, both the Low-P [51] and HTHP [54] parameters have been reported in the literature, while only the Low-P parameters have been reported for squalane [109]. Therefore, new HTHP parameters are obtained for squalane by fitting the PC-SAFT EoS to the HTHP density data for pure squalane obtained in this study. These fitted pure-component parameters are listed in Table 3.9. Table 3.11 lists pure component parameters obtained from group contribution (GC) methods [55] using Low-P and HTHP parameter sets and using the functional groups provided in Table 3.10. These GC parameters are then used for the PC-SAFT EoS density predictions for propane and squalane investigated in this study.

Table 3.9. Fitted PC-SAFT pure component parameters, m, σ, and ε/k_B for propane, $M_w = 44.1$ g/mol, and for squalane, $M_w = 422.8$ g/mol.

Type	Compound	m	$\sigma/\text{Å}$	$\varepsilon/k_B/\text{K}$
Low-P	Propane [51]	2.0020	3.6184	208.11
	Squalane[109]	10.5257	4.1189	254.95
HTHP	Propane [54]	2.1994	3.5381	204.81
	Squalane [a]	16.6709	3.5360	227.53

[a] HTHP parameters for squalane obtained from fit of pure squalane experimental density data obtained in this study.

45

Table 3.10. Values for the PC-SAFT group contribution of each functional group for both Low-P and HTHP parameters from Burgess *et al*. [55].

Type	Group	# of Groups in Propane	# of Groups in Squalane	m	$m\sigma^3$ (Å^3)	$m\varepsilon/k_B$ (K)
Low-P	–CH$_3$	2	8	0.6960	35.425	144.63
	–CH$_2$–	1	16	0.4193	24.410	107.50
	–CH<	0	6	0.0665	10.784	47.48
HTHP	–CH$_3$	2	8	1.0667	35.468	179.27
	–CH$_2$–	1	16	0.5775	24.175	150.85
	–CH<	0	6	-0.0799	12.361	57.54

Table 3.11. PC-SAFT pure component parameters, m, σ, and ε/k_B for propane, M_w = 44.1 g/mol, and for squalane, M_w = 422.8 g/mol, from the group contribution parameters of Burgess *et al*. [55].

Type	Compound	m	σ /Å	ε/k_B /K
Low-P	Propane	1.8113	3.7466	219.05
	Squalane	11.8772	3.9620	266.22
HTHP	Propane	2.7109	3.2737	187.90
	Squalane	17.2942	3.5051	242.45

Table 3.12 lists the mean absolute percent deviation, δ, and the standard deviation, λ, for calculations with the PC-SAFT EoS using Low-P and HTHP parameters for propane and squalane at ~324, ~424, and ~518 K. Table 3.13 contains similar information using the GC estimated Low-P and HTHP pure-component parameters. Not surprisingly, the PC-SAFT EoS provides a better representation of the experimental density data when the HTHP or the GC HTHP pure-component parameters are used as compared to the representation obtained when the Low-P or the GC Low-P parameters are used. On average, the difference between the δ values is

greater than 1% when comparing the PC-SAFT EoS performance using the HTHP parameters to the performance with the Low-P parameters. The HTHP parameters typically underpredict the density especially at high pressures, while the Low-P parameters virtually overpredict the density for all the experimental conditions. Furthermore, the δ values show that the predictions for the ~ 324 K isotherms are consistently better than predictions at higher temperatures when using the Low-P or the GC Low-P parameters. Figure 3.5 shows the comparison of the PC-SAFT EoS using both the Low-P parameters and the HTHP parameters with the experimental density data obtained in this study for propane. Similar comparison of the PC-SAFT EoS is presented in Figure 3.6 for squalane

Table 3.12. Mean absolute percent deviation (δ) and its standard deviation (λ) for calculations with the PC-SAFT EoS, using pure component parameters obtained from fitting pure component vapor pressure and saturated liquid density data (Low-P) [51,109] and high-temperature, high-pressure (HTHP) density data [54] for modeling propane and squalane HTHP density data.

Data Points	T /K	δ Low-P	λ Low-P	δ HTHP	λ HTHP
Propane					
22	324.1	1.29	1.09	0.81	0.44
22	424.6	2.18	1.04	0.31	0.23
20	514.4	1.94	0.98	0.44	0.43
Squalane					
19	323.4	3.36	0.71	0.18	0.12
18	423.7	3.39	0.65	0.36	0.28
21	511.5	5.05	0.38	0.29	0.27

Table 3.13. Mean absolute percent deviation (δ) and its standard deviation (λ) for calculations with the PC-SAFT EoS, using parameters obtained from group contribution, GC, estimation of both Low-P and HTHP pure component parameters [55] for modeling propane and squalane HTHP density data.

Data Points	T /K	δ GC Low-P	λ GC Low-P	δ GC HTHP	λ GC HTHP
		Propane			
22	324.1	1.77	1.09	0.74	0.84
22	424.6	2.95	1.11	0.29	0.19
20	514.4	2.89	1.09	1.09	0.68
		Squalane			
19	323.4	3.48	0.29	0.23	0.23
18	423.7	3.76	0.42	0.67	0.41
21	511.5	4.89	0.69	0.83	0.73
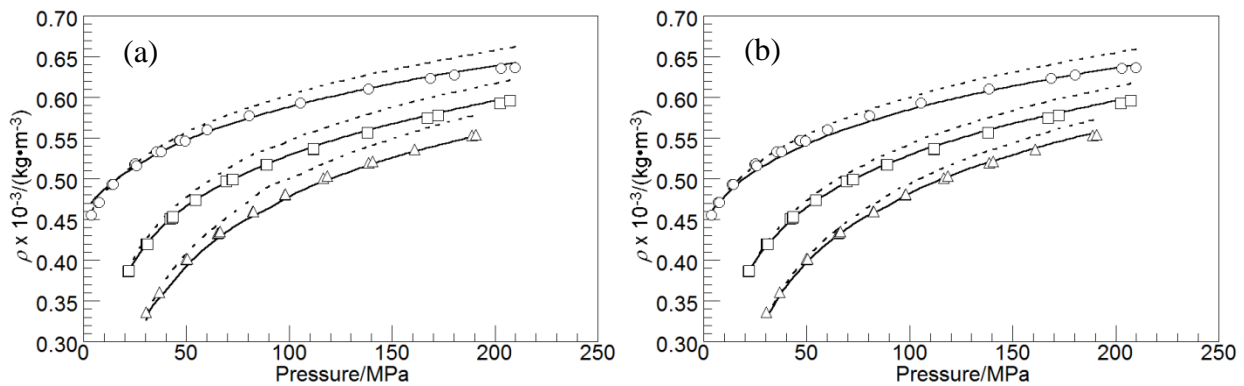
Figure 3.5. Comparison of the performance of the PC-SAFT EoS using Low-P (⋯⋯⋯) and the HTHP (——) pure component parameters with the HTHP experimental density data, ρ, (symbols), for propane at 324.1 K (○), 424.6 K (□), and 514.4 K (Δ). Fitted parameters are presented in (a) and GC parameters are presented in (b).
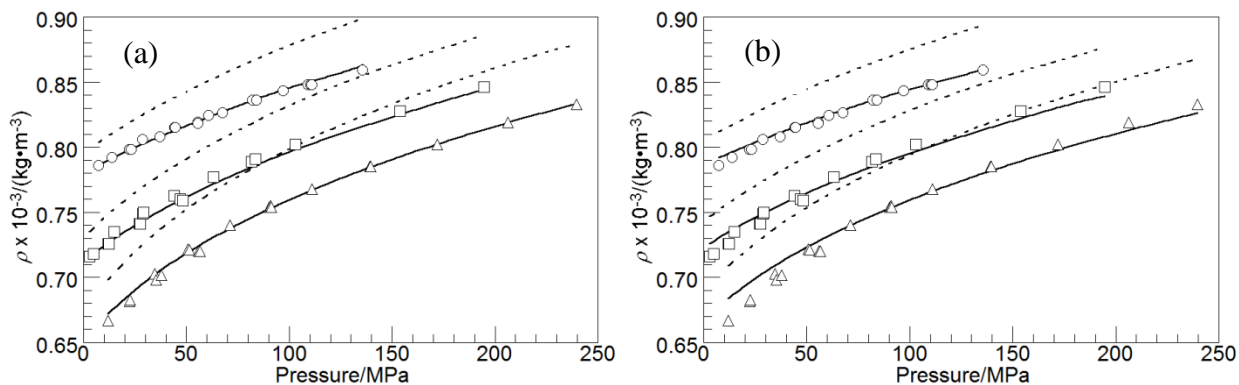
Figure 3.6. Comparison of the performance of the PC-SAFT EoS using Low-P (·········) and the HTHP (——) pure component parameters with the HTHP experimental density data, ρ, (symbols), for squalane at 323.4 K ($\circ$), 423.7 K ($\square$), and 511.5 K (Δ). Fitted parameters are presented in (a) and GC parameters are presented in (b).

The HTHP density data of DEHP are also modeled with the PC-SAFT EoS using similar approaches to obtain the pure component parameters. In the first approach, the first order group contribution method (GC PC-SAFT) proposed by Tihic *et al*. [110] is used to calculate DEHP pure component parameters since the groups present in DEHP are not completely defined in Burgess *et al*.'s method [55]. As shown in Figure 3.7, DEHP has an aromatic core and two, long-chain, ester arms. The DEHP core contains four aromatic carbons, each with a single hydrogen atom, whose group contribution value is listed as an ACH group by Tihic and coworkers. Each of the other two carbons in the aromatic ring (denoted as AC) contains one ester group (denoted as COO) connected to a long chain saturated, branched alkyl group containing one methine (denoted as $-CH<$), five methylene (denoted as $-CH_2$), and two methyl groups (denoted as $-CH_3$). Each GC PC-SAFT parameter is calculated as a sum of the contributions from the groups. Second order group contribution parameters are not considered because the parameters

49

accounting for the exact arrangements of groups present in DEHP, such as the *ortho* positioning of the two ester groups on the aromatic ring, have not been published. It is worth noting that Tihic *et al*. [110] reported first order group contribution parameters for an aromatic carbon connected to a methine group (ACCH<), a methylene group (ACCH$_2$−), and to a methyl group (ACCH$_3$). However, Tihic and coworkers do not report first order group contribution parameters for an aromatic carbon connected to an ester group (ACCOO). The values for the pure component parameters obtained through the group contribution approach are listed in Table 3.14.

The GC PC-SAFT EoS overpredicts the HTHP density data for DEHP at all of the temperatures and pressures considered in this study. The averaged δ for the calculations listed in Table 3.15 is 2.12 and the overprediction is as much as 3% at the high end of the pressure range. Nevertheless, these results demonstrate the utility of using a first order group contribution method with the PC-SAFT equation of state as compared to a cubic equation of state when calculating the density of a high molecular weight compound. It is worth noting that the trends in the calculated densities using the PC-SAFT equation with GC parameters are similar to the modeling trends for HTHP densities of saturated alkanes from pentane to eicosane [4,14] when using parameters fitted to low pressure density and vapor pressure data.
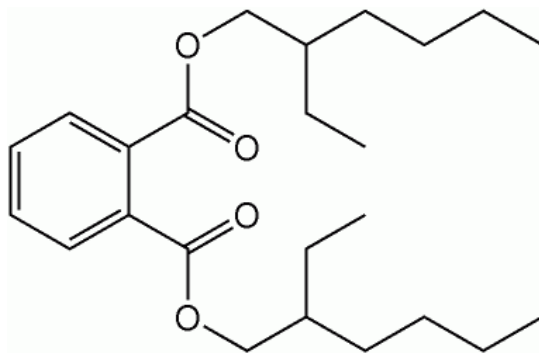
Figure 3.7. Chemical structure of DEHP.

50

Table 3.14. PC-SAFT pure component parameters, m, σ, and ε/k_B obtained from the two approaches considered in this study for DEHP. GC PC-SAFT pure component parameters are determined from the first order group contribution method of Tihic *et al*. [110]. HTHP PC-SAFT pure component parameters are determined from a simultaneous fit of all of the density isotherms reported in this study.

EoS Model	m	σ	ε/k_B
GC PC-SAFT	10.873	3.750	274.351
HTHP PC-SAFT	15.497	3.321	249.031

Table 3.15. Performance of the two PC-SAFT EoS approaches considered in this study characterized by the listed mean absolute percent deviation, δ, and standard deviation, λ, for both approaches.

Data Points	T /K	δ GC	λ GC	δ HTHP	λ HTHP
21	373.3	1.63	0.74	0.23	0.22
21	423.5	1.73	0.54	0.19	0.17
25	476.2	1.56	0.29	0.36	0.20
28	491.9	2.20	0.31	0.17	0.19
37	523.7	2.39	0.43	0.14	0.12

In the second approach, the PC-SAFT EoS is fit simultaneously to all of the HTHP density isotherms reported in this study to obtain pure component parameters for DEHP. Table 3.14 shows the values of the pure component parameters obtained from this method. Furthermore, Table 3.15 shows that the performance of the PC-SAFT EoS is greatly improved in this instance with better δ values. Figure 3.8 also shows the good fit of calculations with the HTHP PC-SAFT EoS to the experimental data. For these calculations the pure component

51

parameters estimated from the first order group contribution approach are used as initial guesses and new set of parameters, m, σ, and ε/k_B, are calculated by minimizing the δ of the calculated and experimental densities. It is important to note that the set of parameters obtained with the second approach differ from the set obtained with the GC method. In this instance, there are more than one set of parameters that give satisfactory density predictions since only the fit of liquid density data is used as the criteria for determining the parameters [111]. When fitting liquid density data, changing the value of ε/k_B has less of an effect on the fit than changing the values for m and σ. For example, the overall averaged δ decreases from 2.12 to 1.32 when ε/k_B is changed from 275 to 250 while using m and σ from the GC method. However, the overall averaged δ increases by more than an order of magnitude if either m and/or σ are changed from the GC values to those from the fit of the PC-SAFT EoS to the data, while using the ε/k_B value from the GC method.
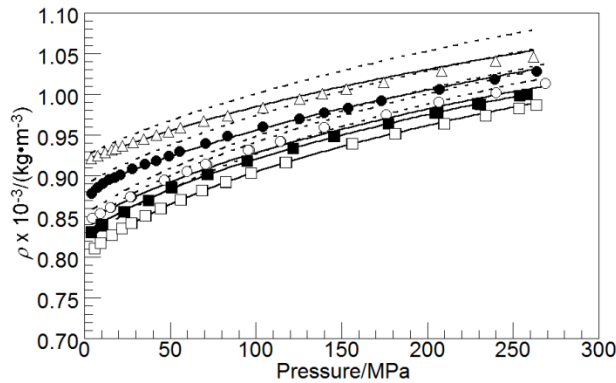
Figure 3.8. Comparison of the performance of the PC-SAFT EoS using Low-P (·········) and the HTHP (——) pure component parameters to the density data, ρ, (symbols) of DEHP obtained in this study at temperatures: 373.29 K (Δ), 423.35 K ($\bullet$), 476.20 K ($\circ$), 491.86 K ($\square$), 523.69 K ($\blacksquare$).

52

3.4. Final Comments

In this chapter, the density for a low-molecular weight compound, propane, along with two high-molecular weight compounds, squalane and *bis* (2-ethylhexyl) phthalate (DEHP), are experimentally measured at temperatures to 525 K and pressures to 265 MPa. The reported data have thus extend the current database for these three compounds to HTHP conditions. When correlated with suitable equations, the experimental data for all the three compounds compare well to available literature data. The performance of predictive models are compared against the experimental data where the PC-SAFT EoS, especially when using HTHP pure component parameters provide the best predictions among the models investigated. Within the cubic EoS family, the utility of using a volume translated PREoS model over the traditional, non-translated PREoS has been demonstrated. For the modeling evaluation, the pure component parameters required for each model are obtained from the literature except the PC-SAFT HTHP parameters that are not already available. As such, HTHP parameters are reported in this study by fitting the equation to the experimental data obtained in this study.

53

Chapter 4 Experimental and Modeling Results: Propane Binary Mixtures

4.1. Experimental Results

4.1.1. Propane-Decane (C_3-C_{10}) Binary Mixture Density

Tables 4.1a-d present the density data for the C_3-C_{10} system as a function of composition, temperature, and pressure. Although the densities are listed in order of increasing pressure in the tables, the pressure for a given measurement is chosen in a non-monotonic manner to minimize any experimental artifacts that might occur in the measurements. For the C_3-C_{10} system approximately two-thirds of all the data are reproduced at the same or very close to the same, pressure. As expected, the mixture density decreases with an increase in propane concentration and/or temperature, while the mixture density increases with increasing pressure. The mole fractions of the C_3-C_{10} binary mixtures studied here differ slightly from those previously reported by Reamer and Sage [17]. Nevertheless, the mixture density data obtained in this study are in close agreement with these literature data, which were only reported to 70 MPa, at comparable mole fractions as shown in Figures 4.1a-c. The average absolute percent deviation between the interpolated mixture density data obtained in this study from the data reported by Reamer and Sage is 0.7 % for ~ 344 K, 0.9 % for ~ 444 K, and 1.2 % for ~ 510 K isotherm. Although not shown here, the C_3-C_{10} mixture density data are also in good agreement with the limited data reported to 40 MPa for three compositions by Saryazdi *et al.* [16]. As an example, the average absolute percent deviation between data obtained in this study at $x_1 = 0.1597$ for 444 K and the data reported by Saryazdi and coworker at $x_1 = 0.17$ for 448 K is within 1.1 %. The data obtained in this study are always higher in value, which is expected because of the slight differences in temperature and propane composition.

54

Table 4.1a. Experimental density data, ρ, at different temperatures, T, and pressures, P, for C_3 (1) - C_{10} (2) binary system at a propane mole fraction, x_1, = 0.3041 and 0.1597 obtained in this study.

P /MPa	ρ /kg·m^{-3}	P /MPa	ρ /kg·m^{-3}	P /MPa	P /kg·m^{-3}
T/K =	344.2		444.3		510.5
x_1=	0.3041		0.1597		0.1597
8.4	665	14.8	617	24.6	597
8.6	666	14.8	617	38.5	619
32.1	689	28.4	636	38.6	619
32.4	689	28.6	636	45.0	627
52.2	705	48.0	656	45.2	627
52.2	705	48.0	656	63.4	647
74.1	720	66.3	671	63.7	647
74.1	720	66.4	671	81.9	664
98.2	734	86.6	686	82.1	664
98.2	734	86.8	686	102.7	679
124.3	747	109.1	700	103.0	680
124.5	747	108.8	700	126.2	695
146.7	758	128.7	711	126.5	695
147.0	758	128.8	711	152.1	710
169.6	769	155.4	724	152.2	710
170.3	769	155.5	724	175.6	722
192.7	780	184.1	739	175.6	722
219.9	793	184.3	739	202.5	731
258.5	807	209.2	747	229.9	744
		242.6	759	260.9	754
		243.4	759		

55

Table 4.1b. Experimental density data, ρ, at different temperatures, T, and pressures, P, for C_3 (1) - C_{10} (2) binary system at a propane mole fraction, x_1, = 0.4210 obtained in this study.

P /MPa	ρ /kg·m^{-3}	P /MPa	ρ /kg·m^{-3}	P /MPa	ρ /kg·m^{-3}
T/K =	344.2		444.4		511.0
3.5	641	11.6	569	17.9	523
3.6	641	17.6	583	18.3	523
8.1	645	27.0	600	33.9	565
11.5	651	34.9	613	34.4	565
22.7	663	49.3	631	51.2	595
32.0	672	53.1	636	51.8	595
37.8	677	70.7	653	67.5	615
51.3	688	71.0	653	67.9	615
51.5	688	90.6	669	86.3	635
73.2	703	90.6	669	86.8	635
73.2	703	112.2	684	107.1	653
97.4	718	112.6	684	107.8	653
97.7	718	136.7	699	130.0	671
123.6	732	137.4	699	130.3	670
123.8	732	161.7	713	151.9	685
146.2	743	189.7	728	152.6	685
146.8	743	221.0	740	177.0	699
167.1	755	251.5	755	202.0	710
167.5	755			202.3	710
193.4	769			232.1	724
194.0	769			232.8	724
217.3	778			260.2	736

56

P /MPa	ρ /kg•m⁻³			P /MPa	ρ /kg•m⁻³
248.6	789			260.2	735
248.9	788				

Table 4.1c. Experimental density data, ρ, at different temperatures, T, and pressures, P, for C$_3$ (1) - C$_{10}$ (2) binary system at a propane mole fraction, x_1, = 0.6052 obtained in this study.

P /MPa	ρ /kg•m^{-3}	P /MPa	ρ /kg•m^{-3}	P /MPa	ρ /kg•m^{-3}
T/K =	344.3		444.3		513.2
19.7	631	14.6	537	29.9	520
20.0	632	25.9	566	30.3	521
30.8	644	26.1	566	44.9	555
31.2	644	40.4	591	44.9	554
48.7	661	40.5	591	61.3	581
48.9	661	58.0	613	61.8	581
63.8	673	58.0	613	84.1	608
65.3	673	74.9	631	84.6	608
86.9	689	75.0	631	104.2	627
87.8	689	97.8	650	104.7	627
113.7	704	98.2	650	131.2	649
141.4	719	119.1	666	131.5	649
160.2	729	119.8	666	152.4	664
161.5	729	143.2	681	153.1	664
185.1	743	143.8	682	176.2	679
185.3	743	169.1	696	176.4	679
220.1	759	170.2	697	196.9	689
220.1	759	198.7	711	198.7	689
248.2	770	198.7	712	224.0	701
249.6	770	231.6	727	224.3	700

57

P /MPa	ρ /kg•m^{-3}	P /MPa	ρ /kg•m^{-3}
259.1	737	254.0	713
259.8	738		

Table 4.1d. Experimental density data, ρ, at different temperatures, T, and pressures, P, for C$_3$ (1) - C$_{10}$ (2) binary system at a propane mole fraction, x_1, = 0.8156 obtained in this study.

P /MPa	ρ /kg•m^{-3}	P /MPa	ρ /kg•m^{-3}
T/K =	344.2		444.3
18.4	556	9.9	411
23.7	564	10.7	416
23.7	564	17.2	462
31.5	575	17.7	462
31.8	575	24.4	488
44.7	590	24.9	488
44.9	590	34.9	511
59.4	604	52.4	540
59.5	604	52.9	540
59.7	604	68.9	561
79.2	620	69.9	561
79.6	620	82.8	574
89.7	628	101.0	592
107.5	639	101.8	592
127.0	651	117.6	605
153.5	665	118.3	605
176.2	675	144.3	623
206.7	688	168.6	638
233.0	700	168.8	639
261.4	713	190.0	650

58

190.0	650
212.1	662
212.8	662
236.8	672
262.5	685
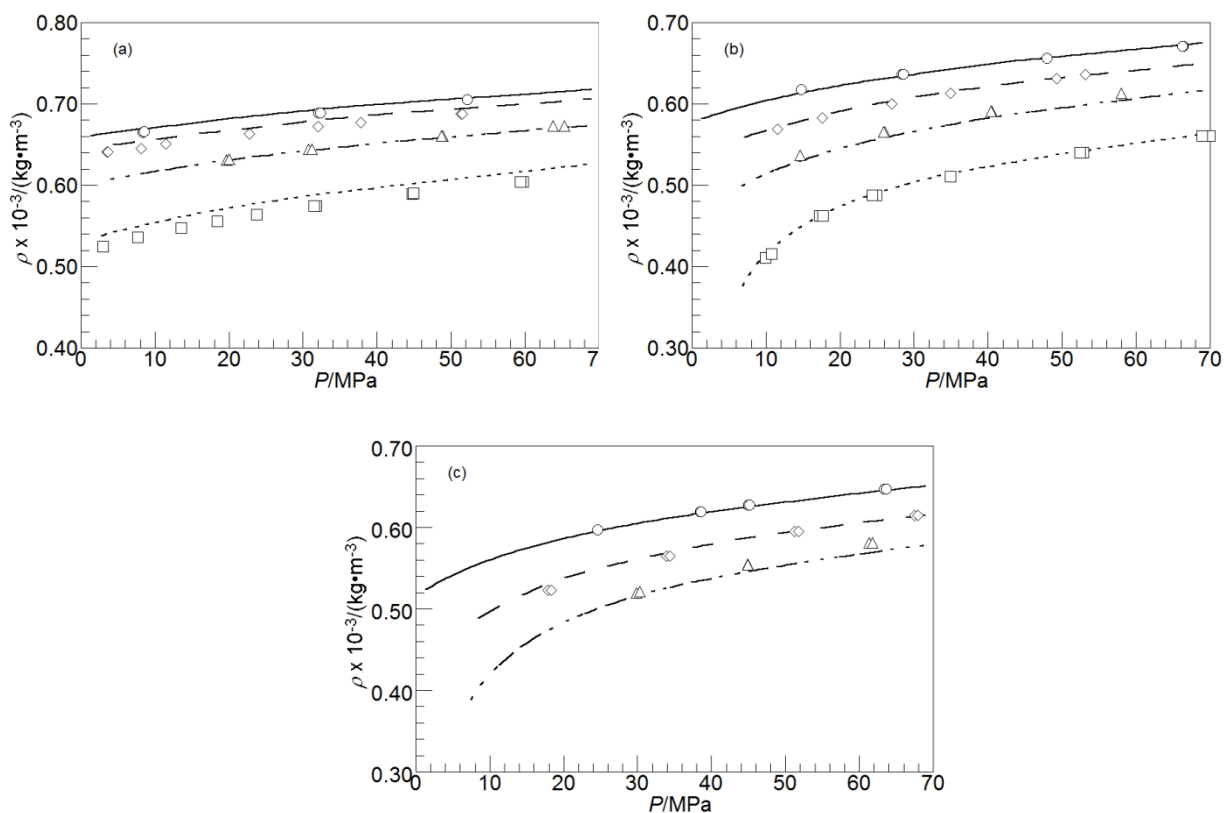
Figure 4.1. Comparison of C_3-C_{10} binary density data for x_1 = 0.3041 in (a) and 0.1597 in (b) and (c) (○), 0.4210 (◇), 0.6052 (Δ), and 0.8156 (□) obtained in this study with curves representing the data of Reamer and Sage [17] at x_1 = 0.30 in (a) and 0.20 in (b) and (c) (———), 0.40 (— — —), 0.60 (·· — — ··), and 0.80 (········), (a) = ~344 K, (b) = ~444 K, and (c) = ~510 K.

59

4.1.2. Propane-Eicosane (C_3-C_{20}) Binary Mixture Density

Experimental density data are obtained for the C_3-C_{20} system at five different mixture compositions and are presented in Tables 4.2 a-e for three isotherms at ~325, ~425, and ~520 K and pressures to 260 MPa. The density data for the C_3-C_{20} system follow similar trend with those of the C_3-C_{10} data, and the density values for the C_3-C_{20} mixtures are larger than those for C_3-C_{10} mixtures at similar temperatures, pressures, and propane-concentrations. Approximately one-third of all the C_3-C_{20} mixture density data are reproduced at the same, or very close to the same, pressure. However, at ~325 K, a liquid-solid phase boundary is encountered for all the C_3-C_{20} mixture compositions except at x_1 = 0.9310 as shown in the tables. Unfortunately there are no available literature density data for C_3-C_{20} mixtures to compare with the data presented here.

Table 4.2a. Experimental density data, ρ, at different temperatures, T, and pressures, P, for C_3 (1) − C_{20} (2) binary system at a propane mole fraction, x_1, = 0.3025 obtained in this study.

P /MPa	ρ /kg•m^{-3}	P /MPa	ρ /kg•m^{-3}	P /MPa	ρ /kg•m^{-3}
T/K =	324.7		422.9		516.2
6.6	724	6.8	663	17.8	626
18.6	737	18.3	680	34.7	648
31.1	748	32.8	694	59.6	671
51.3	761	51.1	709	82.0	687
84.2	778	73.4	724	108.9	702
Solidification Boundary		73.6	724	135.8	718
		96.2	737		
		125.1	752		
		125.8	752		

60

P /MPa	ρ /kg•m⁻³
156.6	767
188.9	780
188.9	780
221.0	793
236.8	798
236.9	798
264.4	808

Table 4.2b. Experimental density data, ρ, at different temperatures, T, and pressures, P, for C_3 (1) − C_{20} (2) binary system at a propane mole fraction, x_1, = 0.6483 obtained in this study.

P /MPa	ρ /kg•m⁻³	P /MPa	ρ /kg•m⁻³	P /MPa	ρ /kg•m⁻³
T/K =	325.1		420.4		520.7
6.6	687	10.6	620	23.7	566
19.0	698	10.7	620	48.0	609
33.6	709	13.8	623	70.7	635
52.9	721	23.7	640	98.6	660
53.3	721	23.8	640	125.6	679
77.8	735	31.5	647	152.2	695
91.2	742	41.2	660	180.2	710
105.3	749	48.2	664	203.4	721
119.8	755	59.6	677	214.9	726
132.1	761	60.0	678		
Solidification Boundary		72.3	684		
		87.1	698		
		98.6	701		
		98.7	701		

115.1	715
129.2	719
159.5	734
159.7	734
191.7	748
214.3	757
214.6	757

Table 4.2c. Experimental density data, ρ, at different temperatures, T, and pressures, P, for C_3 (1) − C_{20} (2) binary system at a propane mole fraction, x_1, = 0.7375 obtained in this study.

P /MPa	ρ /kg•m^{-3}	P /MPa	ρ /kg•m^{-3}	P /MPa	ρ /kg•m^{-3}
T/K =	319.1		424.5		521.5
14.6	676	17.5	593	29.3	533
22.5	681	25.5	608	38.0	553
37.3	695	30.2	616	48.5	572
38.4	695	37.6	627	57.8	588
50.6	706	48.0	640	59.3	588
59.3	710	59.2	651	69.9	600
65.3	715	69.9	661	85.2	616
76.9	721	80.8	670	104.1	632
91.6	731	91.5	678	105.4	633
94.0	731	103.1	685	121.1	643
102.5	737	115.6	693	136.4	652
110.9	739	136.7	704	163.7	666
117.6	745			196.4	680
126.8	747			162.8	666
Solidification Boundary				196.4	680
				222.8	690

Table 4.2d. Experimental density data, ρ, at different temperatures, T, and pressures, P, for C_3 (1) $- C_{20}$ (2) binary system at a propane mole fraction, x_1, $= 0.8367$ obtained in this study.

P /MPa	ρ /kg$\cdot$m^{-3}	P /MPa	ρ /kg$\cdot$m^{-3}
$T/K =$	324.6		421.0
6.1	632	10.8	539
15.7	645	10.8	539
15.9	645	22.6	568
33.3	663	23.0	568
53.5	680	43.3	600
54.2	680	59.2	622
54.7	681	68.3	629
79.0	698	90.7	649
83.4	699	90.9	649
103.9	713	92.7	652
104.6	713	93.0	652
112.7	718	116.0	669
113.1	718	119.4	670
146.3	733	145.9	689
172.4	747	146.7	687
Solidification Boundary		177.5	704
		177.8	704
		214.1	721
		258.0	740

Table 4.2e. Experimental density data, ρ, at different temperatures, T, and pressures, P, for C_3 $(1) - C_{20}$ (2) binary system at a propane mole fraction, x_1, = 0.9310 obtained in this study.

P /MPa	ρ /kg•m^{-3}	P /MPa	ρ /kg•m^{-3}	P /MPa	ρ /kg•m^{-3}
T/K =	322.9		422.2		524.5
5.0	547	11.8	412	35.3	420
13.0	562	18.3	457	49.4	464
23.0	577	24.6	482	68.9	500
36.8	592	36.0	513	86.1	521
51.5	605	50.9	540	111.6	544
70.1	618	64.9	557	132.0	558
95.7	634	84.3	576	165.4	575
120.9	647	104.2	592	188.9	586
142.8	657	131.1	607	218.7	598
168.6	668	151.8	621	241.4	607
203.4	680	172.1	630	247.3	610
		208.8	646		

4.1.3. Propane-Squalane (C_3-C_{30}) Binary Mixture Density

Experimental density data are reported in Tables 4.3 a-e for five mixture compositions for the C_3-C_{30} mixtures. The mixtures contain 0.6555, 0.7960, 0.9208, 0.9439, and 0.9752 mole fraction of propane corresponding to 0.1653, 0.2892, 0.5480, 0.6368, and 0.8040 weight fraction of propane, respectively. The temperature (~324, ~424, and ~518 K) and pressure ranges (4 to 265 MPa) are similar to the experimental ranges investigated for the C_3-C_{20} binary mixture. It can be observed from Table 4.3a-e that mixture densities increase with increase in pressure and decreases with increase in temperature and/or propane concentration. To our knowledge, there

64

are no high-pressure density data in the literature to compare to the propane-squalane mixture density data obtained in this study. Furthermore, no liquid-solid solidification boundary was encountered for the propane-squalane system which was observed for the propane-eicosane system, despite that squalane, compared to eicosane, contains four more carbon atoms in its straight chain, and ten more carbons overall in its molecular structure. This is easily attributed to the structure of squalane that contains six methyl branches that gives rise to higher degree of free volume and the squalane molecules cannot align to form rigid crystal structures unlike the linear eicosane molecules. As representation of how the mixture data reported in this study fall within the pure component boundaries, Figure 4.2 shows the mixture density obtained the C_3-C_{30} binary mixture along with the pure component densities for propane and squalane.

Table 4.3a. Experimental density data, ρ, at different temperatures, T, and pressures, P, for C_3 $(1) - C_{30}$ (2) binary mixture at propane mole fraction, x_1, $= 0.6550$ obtained in this study.

P /MPa	ρ /kg•m^{-3}	P /MPa	ρ /kg•m^{-3}	P /MPa	ρ /kg•m^{-3}
T/K=	323.6		423.6		516.0
3.2	729	18.9	677	21.9	627
4.4	729	20.1	677	23.5	630
11.9	744	27.1	690	28.3	639
14.3	745	29.7	689	33.7	648
17.5	749	35.1	700	34.6	649
17.7	749	39.1	699	48.7	667
25.0	749	47.0	713	48.7	667
29.3	759	59.7	724	57.5	677
29.5	759	60.9	724	70.9	691

65

P	ρ	P	ρ	P	ρ
42.7	768	76.8	738	78.8	698
56.7	778	77.0	737	90.6	709
57.2	777	98.0	752	107.8	722
57.7	778	99.3	753	110.0	724
75.0	789	120.7	765	140.5	744
89.8	797	124.7	768	142.6	746
91.8	798	145.0	778	160.1	756
109.9	807	150.3	782	166.7	759
112.4	808	168.8	788	188.7	771
137.9	820	178.7	796	195.1	774
140.3	821	199.8	804	218.5	785
161.5	830	205.6	808	223.2	788
170.7	834	229.5	815	247.3	798
201.9	846	237.3	820	255.8	802
206.6	847				

Table 4.3b. Experimental density data, ρ, at different temperatures, T, and pressures, P, for C_3 (1) − C_{30} (2) binary mixture at propane mole fraction, x_1, = 0.7960 obtained in this study.

P /MPa	ρ /kg•m^{-3}	P /MPa	ρ /kg•m^{-3}	P /MPa	ρ /kg•m^{-3}
$T/K =$	324.2		420.5		523.5
6.9	684	7.1	590	29.5	550
7.3	684	16.2	612	38.2	572
26.5	706	17.2	613	38.2	572
29.3	707	32.4	642	58.0	609
43.6	720	33.4	641	73.2	629
56.0	731	45.6	660	89.3	645
58.3	731	46.8	660	95.3	652

P /MPa	ρ /kg·m⁻³	P /MPa	ρ /kg·m⁻³	P /MPa	ρ /kg·m⁻³
67.9	739	62.1	677	120.2	672
86.5	749	63.3	677	141.8	690
111.9	763	91.0	703	170.4	708
137.3	776	115.7	720	210.7	730
165.1	787	134.6	733	239.8	743
207.5	804	135.7	733	259.8	753
		170.6	751	260.9	753
		209.0	768		
		214	772		

Table 4.3c. Experimental density data, ρ, at different temperatures, T, and pressures, P, for C_3 $(1) - C_{30}$ (2) binary mixture at propane mole fraction, x_1, = 0.9208 obtained in this study.

P /MPa	ρ /kg·m^{-3}	P /MPa	ρ /kg·m^{-3}	P /MPa	ρ /kg·m^{-3}
$T/K =$	324.5		424.0		515.3
7.4	580	36.4	547	50.7	520
14.5	591	38.3	549	72.8	546
15.5	590	47.1	562	77.6	551
21.0	604	47.4	562	77.9	551
29.1	617	47.8	562	92.6	565
29.7	616	55.2	572	92.6	565
41.9	636	55.9	573	101.1	573
42.9	636	69.1	587	111.5	582
53.4	651	69.9	586	119.3	588
56.7	652	71.2	587	129.8	600
75.8	672	94.9	618	145.0	616
76.3	671	95.2	619	145.4	616
98.6	691	115.0	639	169.2	637

67

P	ρ	P	ρ	P	ρ
99.6	692	119.4	639	195.4	658
103.4	693	139.6	661	197.9	659
125.9	709	139.6	661	221.2	675
129.7	710	165.8	680	224.3	677
145.4	721	169.0	682	258.3	698
150.7	723	195.8	699	262.3	700
165.3	731	199.6	701		
174.9	736	219.9	711		
202.6	749	253.6	728		
209.6	752	260.7	732		
250.0	769				
256.6	771				

Table 4.3d. Experimental density data, ρ, at different temperatures, T, and pressures, P, for C_3 (1) − C_{30} (2) binary mixture at propane mole fraction, x_1, = 0.9439 obtained in this study.

P /MPa	ρ /kg·m^{-3}	P /MPa	ρ /kg·m^{-3}	P /MPa	ρ /kg·m^{-3}
$T/K =$	324.4		426.5		522.5
4.8	562	24.6	479	46.6	448
8.4	572	31.4	503	48.7	451
14.2	585	38.4	522	53.6	472
16.1	585	48.5	545	56.2	472
22.5	600	56.1	559	59.6	487
31.7	613	69.6	580	62.5	488
34.9	614	86.4	601	69.5	503
41.7	626	103.2	618	74.3	518
52.4	637	122.9	634	77.2	518
57.5	637	124.7	645	86.8	540

P /MPa	ρ /kg·m⁻³	P /MPa	ρ /kg·m⁻³	P /MPa	ρ /kg·m⁻³
62.0	646	143.1	648	90.1	541
62.7	646	163.9	661	104.2	560
75.9	656	170.4	665	118.2	577
82.6	656	200.9	681	138.9	598
95.8	670			161.9	619
98.2	671			165.3	622
116.1	681			189.8	639
119.0	683			194.4	642
134.2	691			214.9	655
137.2	693			220.1	658
162.4	703			250.0	674
171.6	709				
199.0	719				
207.0	724				
219.9	726				

Table 4.3e. Experimental density data, ρ, at different temperatures, T, and pressures, P, for C_3 (1) − C_{30} (2) binary mixture at propane mole fraction, x_1, = 0.9752 obtained in this study.

P /MPa	ρ /kg·m⁻³	P /MPa	ρ /kg·m⁻³	P /MPa	ρ /kg·m⁻³
T/K =	324.4		426.5		522.5
11.0	528	21.3	433	47.3	434
17.7	546	22.3	433	50.0	436
24.2	563	26.0	445	57.2	447
26.6	563	26.6	445	65.1	464
35.1	576	34.3	467	69.1	467
43.0	590	34.9	467	79.0	487
46.4	590	43.1	490	99.5	520

56.3	601	52.0	511	116.9	544
66.7	613	52.0	511	123.1	549
67.6	613	62.7	531	145.4	570
69.5	613	76.0	551	178.4	595
86.1	626	76.8	551	203.5	612
101.3	638	90.0	568	208.7	615
104.4	638	110.7	589	245.5	637
125.3	651	112.8	589	248.9	638
145.3	662	138.0	610		
149.9	664	172.9	631		
172.1	675	193.3	648		
179.7	678	197.9	645		
206.0	689	211.9	649		
212.1	692	224.0	658		
239.7	704	251.3	669		
250.7	706	256.5	672		
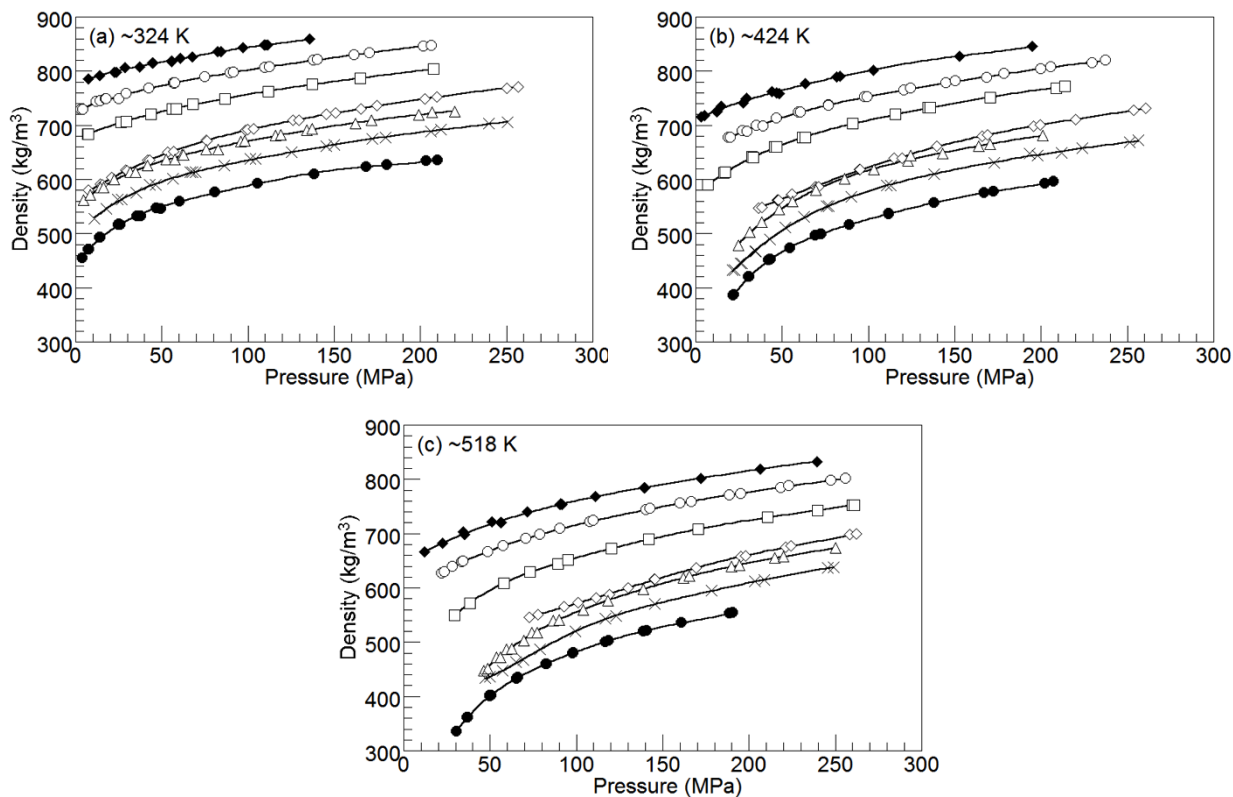
Figure 4.2. Experimental density data for the propane (1) − squalane (2) binary mixtures measured in this study at about 324 K (a), 424 K (b), and 518 K (c). The propane mole fractions, x_1, are: 0, (♦); 0.6550, (○); 0.7960, (□); 0.9208, (◊); 0.9439, (Δ); 0.9708, (x); and 1.0000, (●). Lines are drawn to guide eyes through data points.

4.1.4. Propane-Eicosane (C_3-C_{20}) Binary Mixture Phase Behavior

Table 4.4 lists the *P-T* isopleths data obtained in this study for the propane-eicosane mixtures at 10 different compositions and at temperatures to 485 K. The types of phase transitions are also listed in the table where the dew points are only encountered in the mixture with 0.9754 mole fraction of propane. More than 90% of the data points are obtained in duplicate with a selected few data points obtained in triplicate.

71

Table 4.4. Experimental vapor-liquid equilibrium data for the propane (1) – eicosane (2) system at fixed molar composition. The bubble point transitions are designated as BP, while dew point transitions are designated as DP.

x_1	Transition	T/K	P/MPa	T/K	P/MPa
0.3025	BP	324.7	0.7	324.6	0.8
		349.3	0.8	349.3	0.8
		381.3	1.1	381.4	1.0
		422.8	1.6	422.8	1.6
0.3965	BP	322.1	0.7	322.2	0.7
		349.1	0.8	349.0	0.8
		379.7	1.2	379.8	1.3
		421.0	2.0	421.1	2.0
		468.2	2.9	468.5	2.9
0.6483	BP	324.9	1.0	325.0	1.0
		350.0	1.8	350.1	1.0
		382.1	2.9	382.1	2.9
		420.4	4.3	420.5	4.3
		460.1	6.7	460.4	6.8
		496.1	8.2	496.2	8.2
0.7375	BP	319.7	1.2	320.1	1.1
		349.9	2.0	349.9	2.1
		381.6	3.3	381.7	3.4
		424.6	5.7	424.6	5.7
		470.2	8.5	470.4	8.6
0.8367	BP	324.7	1.3	324.7	1.3
		348.7	2.4	348.8	2.4
		377.9	3.9	377.9	3.9
		421.2	6.8	421.3	6.8
		479.3	10.0	479.3	10.0
0.8723	BP	325.0	1.7	325.4	1.8
		349.6	2.7	349.7	2.7
		392.3	5.2	392.3	5.2
		427.6	8.0	427.8	8.0
		436.1	8.6	477.1	11.2
		484.8	11.7	484.8	11.7
0.9217	BP	323.1	1.7	323.3	1.7
		347.7	2.7	347.7	2.7

		380.4	4.8	380.4	4.8
		406.8	7.0	424.0	8.4
		424.2	8.4	434.5	9.0
		440.2	9.7	441.4	9.8
		451.4	10.4	473.9	11.4
0.9310	BP	322.7	1.6	322.8	1.6
		350.2	2.8	350.4	2.8
		384.2	5.3	384.3	5.4
		398.7	6.7	398.9	6.8
		404.3	7.4	404.6	7.4
0.9754	BP	322.0	1.5	322.1	1.6
		347.9	2.6	348.1	2.6
		363.9	3.9	363.9	4.0
		384.0	5.4	385.4	5.8
		393.8	6.5	398.7	6.8
	DP	405.0	7.3	418.5	8.1
		418.8	8.1	419.0	8.1
		429.4	8.4	429.4	8.5
		442.4	8.7	442.4	8.8
		478.6	10.6	479.5	10.5
0.9798	BP	327.3	2.0	334.7	2.3
		356.7	3.4	365.9	3.9
		366.3	3.9	370.5	4.2
		370.8	4.3	375.0	4.6
		382.6	5.3	383.4	5.4

The C_3-C_{20} P-T traces can be represented with polynomial curves as shown in Figure 4.3 for select isopleths. A single phase exists at pressures above each curve, while liquid and vapor phases exist at pressures below each curve. The transitions along the curves are bubble points except at a propane mole fraction of 0.9754, where dew points occurred at temperatures above 400 K. No liquid-liquid immiscibility is observed for this system under the experimental conditions studied here, which is not surprising since liquid-liquid immiscibility is only expected to occur for propane binary mixtures with *n*-alkanes that are in excess of 30 carbon atoms [112,113]. From the polynomial fit of the isopleths, *P*-*x* isotherms are generated by interpolating

73

the phase transition pressures for each isotherm and are shown in Figure 4.4 at 323, 348, 373, 423, and 473 K. Note that the abscissa in Figure 4.4 is eicosane mole fraction and not propane mole fraction. The shape of the *P-x* isotherms also suggests that C_3-C_{20} mixture exhibits type-1 phase behavior with a continuous mixture-critical curve, having a maximum in the *P-T* plane [6,114]. Figure 4.4 also shows a good agreement between the experimental phase behavior data obtained in this study and the literature data reported by Gregorowicz *et al*. [115] who obtained data only to 353 K. Hence, the present PhD study extends the phase behavior data for the C_3-C_{20} mixture to temperatures beyond the critical point of propane (T_c = 369.8 K) and to temperatures in excess of 473 K.
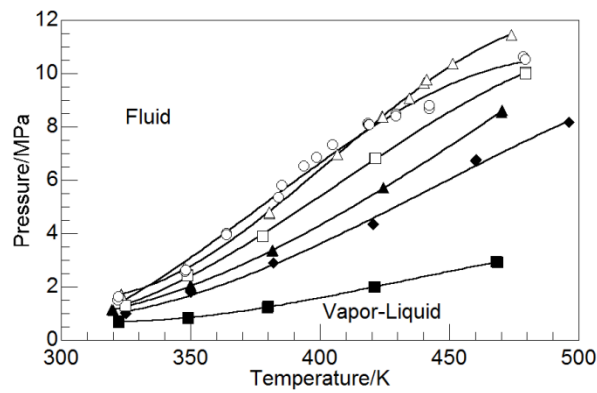
Figure 4.3. Pressure–temperature isopleths for propane-eicosane mixtures obtained in this study at propane mole fractions of 0.3965 (■), 0.6483 (♦), 0.7375 (▲), 0.8367 (□), 0.9217 (Δ), and 0.9754 (○). The *P-T* traces for isopleths at propane mole fraction of 0.3025, 0.8723, 0.9310, and 0.9798 are not shown to reduce clutter in the graph.

74
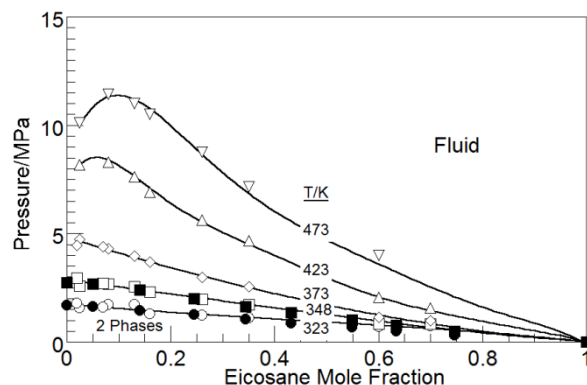
Figure 4.4. Pressure-composition isotherms for propane-eicosane mixtures. Data points are obtained from a cross plot of isopleth data from this study (open symbols) and from the data of Gregorowicz *et al*. (filled symbols) [115]. Lines are drawn through the data to guide the eye.

4.2. Correlations and Excess Volume Properties

4.2.1. Modified Tait Equation

In the previous section, the experimental *P-T* phase behavior data are correlated with polynomial equations to facilitate ease of interpolation of experimental data, from which the isothermal *P-x* cross plots are constructed. However, the Tait equation is a more useful tool for representing the experimental density data for the binary mixtures studied here. The modified Tait equation [20] is fitted to the experimental density data obtained in this study to facilitate interpolating between data at different mixture compositions, temperatures, and pressures. The modified Tait equation is again given in equation 4.1.

$$\frac{\rho - \rho_0}{\rho} = C \log_{10} \frac{P + B}{P_0 + B}$$

(4.1)

In the above equation P_0 equals 0.1 MPa, ρ_0 is the density at P_0, and B and C are adjustable parameters determined from fitting the equation to experimental density data. Parameters ρ_0 and B are temperature dependent and, for hydrocarbons, both parameters are expected to decrease as the temperature increases. C is approximately equal to 0.2 for many hydrocarbons [21-23]. In this study, the Tait equation is first fitted to each set of isopleth densities at different temperatures to obtain values for ρ_0, B, and C. The value of C for each isotherm for a given isopleth only varied slightly, therefore updated values for ρ_0 and B are obtained by refitting the Tait equation using a value of C averaged over all the isotherms for the given isopleth. In fact, the averaged value of C did not vary significantly between isopleths nor did this averaged value vary significantly between the C_3-C_{10} and the C_3-C_{20} systems, although C does differ slightly for the C_3-C_{30} system. Hence, a new averaged value of C is determined using data for all of the isopleths for both C_3-C_{10} and the C_3-C_{20} binary mixtures and the Tait equation is again fitted to density data to obtain values for ρ_0 and B as function of mixture composition and temperature. Similarly the Tait equation is fitted to the density data for all the isopleths of the C_3-C_{30} system using a value of C averaged over all the isopleths. The values for ρ_0 and B as function of mixture composition and temperature are thus obtained from the fit of the Tait equation to the experimental data.

The fitting results are presented in Table 4.5 for the C_3-C_{10} mixture, in Table 4.6 for the C_3-C_{20} mixture, and in Table 4.7 for the C_3-C_{30} mixture along with the mean absolute percent deviation (δ, equation 4.2) for each isotherm at a fixed composition. Note that the δ values shown in Tables 4.5 and 4.6, as well as the deviation plots shown in Figures 4.5and 4.6 exclude data at low pressures and high temperatures, especially at high concentrations of propane. Specifically, deviation values are not presented for pressures below 11 MPa for the C_3-C_{10}

mixture at x_1 = 0.8156 and 444.3 K, for pressures below 25 MPa for the C_3-C_{20} mixture at x_1 = 0.9310 and 422.2 K, and for pressures below 50 MPa for the same C_3-C_{20} mixture at x_1 = 0.9310 and 524.5 K. Similarly, Table 4.7 shows that the Tait equation provides a poor representation of the C_3-C_{30} experimental mixture density data for mixtures at the higher propane concentrations and at the highest temperatures. Likewise the density deviation plots for the propane mole fraction of 0.9439 (□) and 0.9752 (♦) isopleths in Figure 4.7 for the C_3-C_{30} system also show the largest deviations especially at ~424 and ~518 K. At these conditions, the mixture exhibits gas-like behavior and the Tait equation is not expected to reliably represent the volumetric properties of expanded, low density mixtures.

$$\delta = \frac{1}{n}\sum_{1}^{n}\left|\frac{\rho_{i,\text{Tait}} - \rho_{i,\text{experimental}}}{\rho_{i,\text{experimental}}}\right| \bullet 100$$

(4.2)

Table 4.5. Tait equation parameters, mean absolute percent deviations, δ, and standard deviation values, λ, for δ, obtained for each density isotherm and isopleth for the C_3 (1) - C_{10} (2) binary mixtures. Parameter C = 0.2157.

x_1	Data Points	T /K	ρ_0 /kg•m^{-3}	B /MPa	δ	λ
0.1597	21	444.3	590	24.932	0.07	0.09
0.1597	20	510.5	535	11.801	0.07	0.13
0.3041	19	344.2	654	44.078	0.21	0.33
0.4210	24	344.2	634	38.635	0.31	0.35
0.4210	18	444.4	532	11.463	0.08	0.08
0.4210	23	511.0	441	3.437	0.40	0.46
0.6052	20	344.3	595	25.735	0.33	0.24
0.6052	22	444.3	477	5.901	0.12	0.08
0.6052	21	511.1	389	1.771	0.46	0.52
0.8156	20	344.2	514	15.124	0.22	0.24
0.8156	25	444.3	366	1.743	0.59[*]	0.35[*]

[*] The δ and λ values reported exclude the data at the two lowest pressure values for the isotherm, where the Tait equation does not provide a good fit having δ values of 7.12 and 7.52.

77
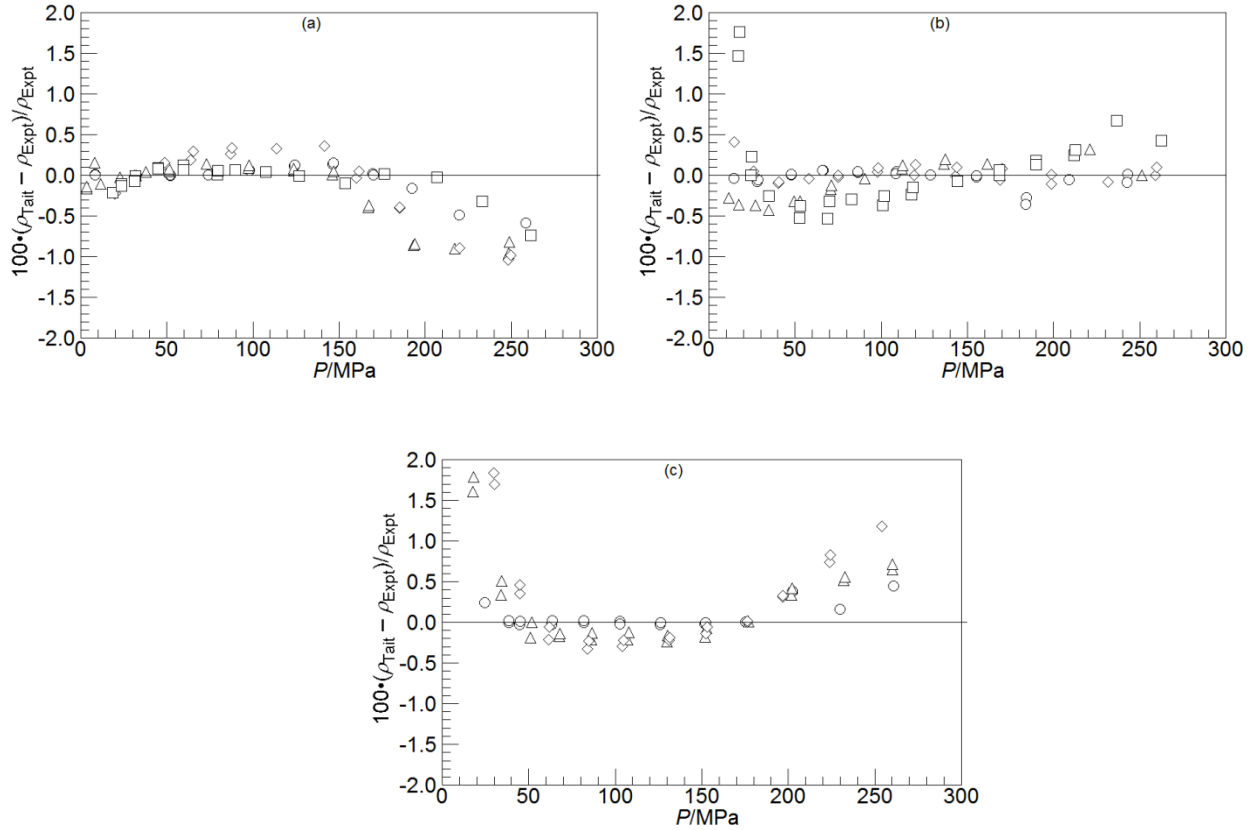
Figure 4.5. Deviation plots of the C$_3$-C$_{10}$ mixture density data (symbols) obtained in this study from the fit of the modified Tait equation at (a) = ~344 K, (b) = ~444 K, and (c) = ~510 K, where x_1 = 0.3041 or 0.1597 (○), 0.4210 (◊), 0.6052 (Δ), and 0.8156 (□).

Table 4.6. Tait equation parameters, mean absolute percent deviations, δ, and standard deviation values, λ, for δ, obtained for each density isotherm and isopleth for the C$_3$ (1) - C$_{20}$ (2) binary mixtures. Parameter C = 0.2157.

x_1	Data Points	T /K	ρ_0 /kg•m^{-3}	B /MPa	δ	λ
0.3025	5	324.7	720	66.383	0.14	0.13
0.3025	16	422.9	655	41.312	0.11	0.09
0.3025	6	516.2	596	25.947	0.11	0.10
0.6483	10	325.1	680	63.674	0.02	0.03
0.6483	21	420.4	601	26.484	0.19	0.14

78

0.6483	9	520.3	492	6.915	0.12	0.21
0.7375	14	319.1	660	50.664	0.13	0.10
0.7375	12	424.5	550	13.946	0.15	0.10
0.7375	16	521.5	444	4.589	0.55	0.59
0.8367	16	324.6	623	36.509	0.08	0.09
0.8367	19	421.0	496	7.869	0.08	0.09
0.9310	11	322.9	543	26.231	0.16	0.24
0.9310	12	422.2	395	3.109	0.45[*]	0.26[*]
0.9310	11	524.5	348	2.431	0.39[*]	0.40[*]

[*] The δ and λ values reported excludes the data at the three and two lowest pressure values for the two isotherms, respectively, where the Tait equation does not provide a good fit having δ values ranging from 3 – 12.
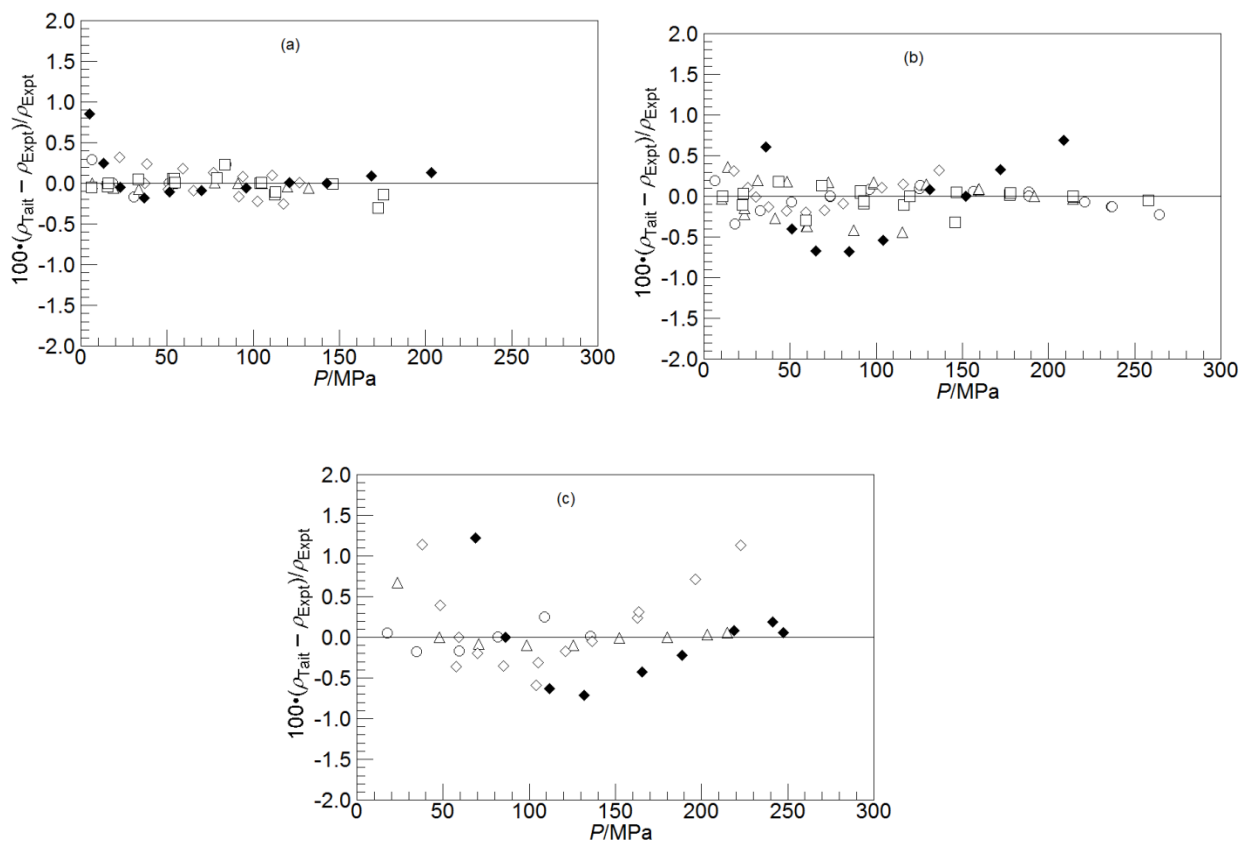
Figure 4.6. Deviation plots of the C_3-C_{20} mixture density data (symbols) obtained in this study from the fit of the modified Tait equation at (a) = ~323 K, (b) = ~423 K, and (c) = ~523 K, where x_1 = 0.3025 (○), 0.6483 (◊), 0.7375 (Δ), 0.8367 (□), and 0.9310 (♦).

Table 4.7. Tait equation parameters, mean absolute percent deviation, δ, and standard deviation Values, λ, for each δ, obtained for each density isotherm and isopleth for the C_3 (1) - C_{30} (2) binary mixtures. Parameter $C = 0.2232$.

x_1	Data Points	T /K	ρ_0 /kg·m^{-3}	B /MPa	δ	λ
0.0000	19	323.4	780	85.364	0.12	0.11
0.0000	18	423.7	711	46.565	0.26	0.22
0.0000	21	511.5	638	23.676	0.19	0.20
0.6550	24	323.6	731	67.144	0.16	0.27
0.6550	23	423.6	648	30.713	0.15	0.18
0.6550	23	516.0	569	13.393	0.04	0.03
0.7960	14	324.2	675	48.697	0.09	0.11
0.7960	16	420.5	569	15.051	0.15	0.11
0.7960	14	523.5	422	2.603	0.54	0.30
0.9208	25	324.5	550	13.929	0.15	0.22
0.9208	23	424.0	388	1.934	0.37	0.33
0.9208	19	515.3	295	0.576	0.39	0.49
0.9439	25	322.6	555	20.000	0.32	0.20
0.9439	14	424.2	339	0.951	0.90	0.65
0.9439	21	521.5	223	0.124	1.42	1.07
0.9752	23	324.4	507	14.120	0.26	0.35
0.9752	23	426.5	286	0.537	1.47	1.04
0.9752	15	522.5	211	0.137	1.08	0.84
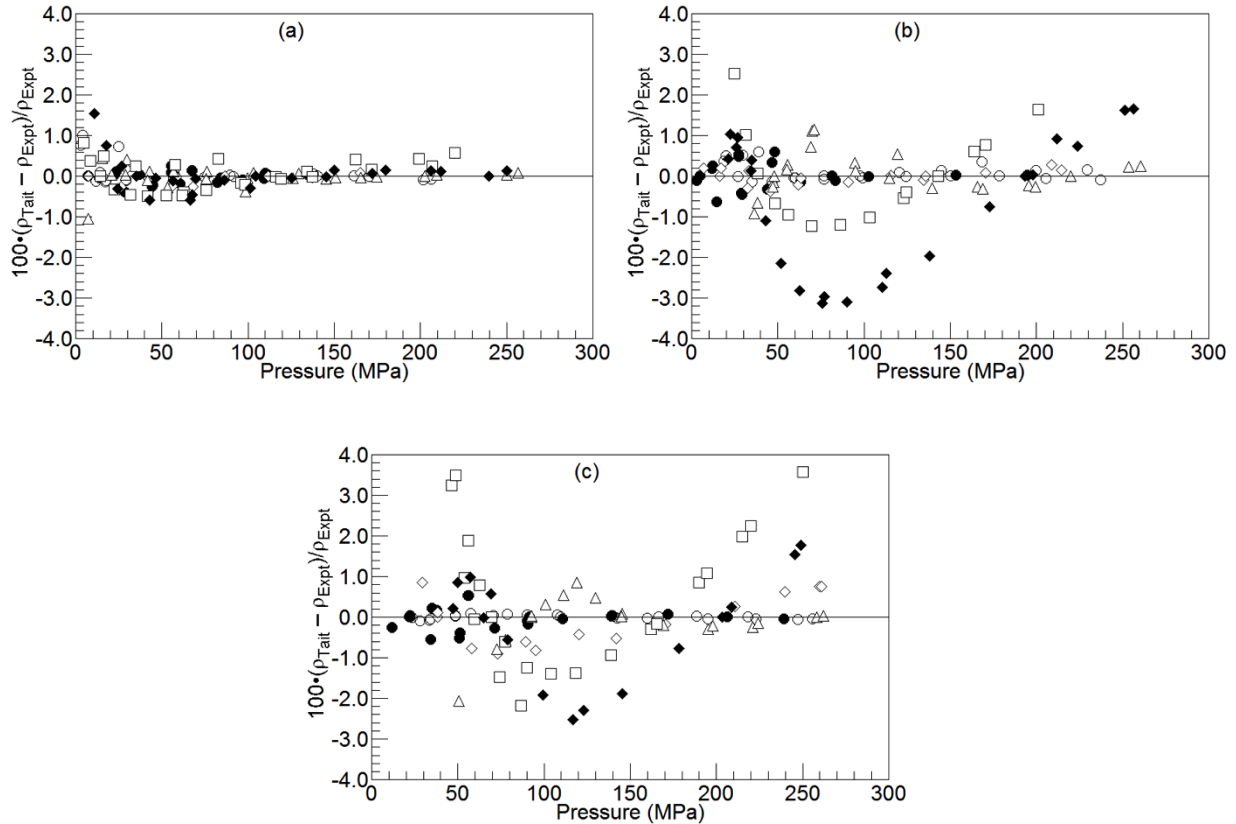
Figure 4.7. Deviation plots of the C_3-C_{30} mixture density data (symbols) obtained in this study from the fit of the modified Tait equation at (a) = 324 K, (b) = 424 K, and (c) = 518 K, where x_1 = 0.0000 ($\bullet$), 0.6550 ($\circ$), 0.7960 ($\Diamond$), 0.9208 (Δ), 0.9439 ($\square$), and 0.9752 ($\blacklozenge$).

4.2.2. Mixture Molar Volumes and Excess Mixture Molar Volumes

Molar volumes are calculated at constant temperatures and pressures using the modified Tait equation parameters as means of interpolating experimental data. Figure 4.8 shows the plots of the molar volume for the C_3-C_{10} system against propane mole fractions at 444 K and at 30, 70, 160, and 250 MPa, while Figure 4.9 shows a similar graph for the 160 MPa isobar at 344, 444, and 511 K. The figures show that the mixture molar volumes exhibit a smooth linear trend with propane mole fraction. Similar trends, not shown here, are observed at other conditions for the

C_3-C_{10} system, as well as for the C_3-C_{20} and the C_3-C_{30} system. The pure component end points are obtained from the literature using a reference EoS by Lemmon *et al.* [82] for propane, taken from the NIST webbook [73] for decane, and obtained from [14] for eicosane. The pure component end point for the squalane mixture system is obtained from the experimental data reported in this study.
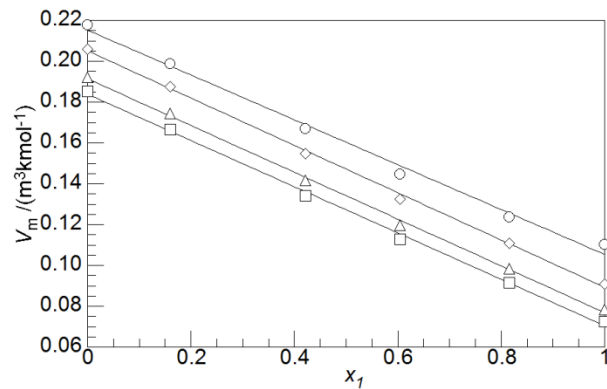
Figure 4.8. Representation of the C_3-C_{10} mixture molar volume as a function of propane mole fraction for 444 K at 30 MPa (○), 70 MPa (◊), 160 MPa (Δ), and 250 MPa (□). Lines serve to guide the eyes.
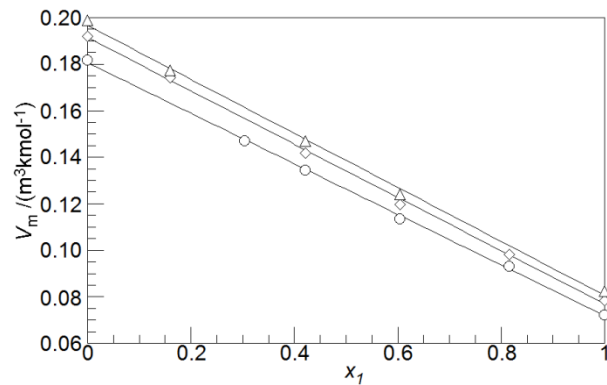
Figure 4.9. Representation of the C_3-C_{10} mixture molar volume as a function of propane mole fraction for 160 MPa 344 K (○), 444 K (◊), and 511 K (Δ). Lines serve to guide the eyes.

The excess volumes are computed using equation (4.3) where V^{Ex} is the excess volume, ρ_m is the density of the mixture and x_i, M_i, and ρ_i are the mole fraction, molar mass, and density of component i, respectively. The excess volumes are calculated using the modified Tait equation for interpolating experimental mixture density data at constant temperatures and pressures. Figure 4.10 shows representative results for the excess volume of the C_3-C_{10} mixture as a function of propane mole fraction for the 444 K isotherm at 30, 70, and 160 MPa, while Figure 4.11 shows a similar plot for the 160 MPa isobar at 344, 444, and 511 K. Similarly, Figures 4.12a-c show representative results for the excess volume of the C_3-C_{30} mixture as a function of propane mole fraction for the 324 K, 424, and 518 K isotherms at 30, 100, and 160 MPa. Figure 4.12d shows a similar plot for the 30 MPa isobar at 324, 424, and 518 K.

$$V^{Ex}/(m^3 \bullet kmol^{-1}) = \frac{1}{\rho_m/(kg \bullet m^{-3})} \sum_{i=1}^{2} x_i M_i (kg \bullet kmol^{-1}) - \sum_{i=1}^{2} \frac{x_i M_i/(kg \bullet kmol^{-1})}{\rho_i/(kg \bullet m^{-3})} \qquad (4.3)$$
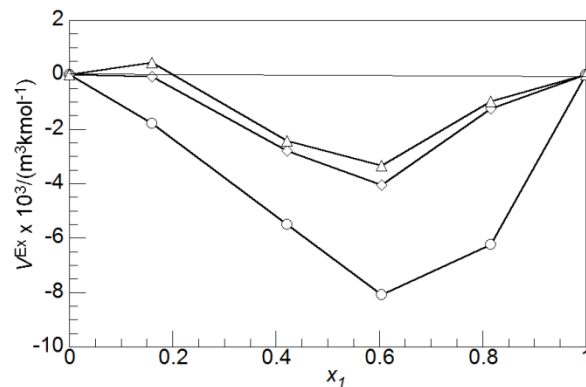
Figure 4.10. Excess volumes for the C_3-C_{10} mixture as a function of propane mole fraction at 444 K for 30 MPa (○), 70 MPa (◊), and 160 MPa (Δ). Lines serve to guide the eyes.

83
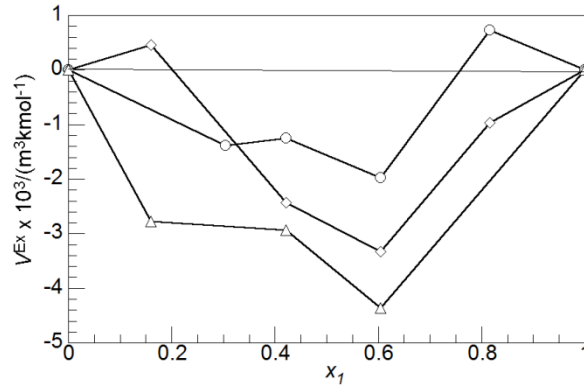
Figure 4.11. Excess volumes for the C_3-C_{10} mixture as a function of propane mole fraction at 160 MPa for 344 K (○), 444 K (◊), and 511 K (Δ). Lines serve to guide the eyes.
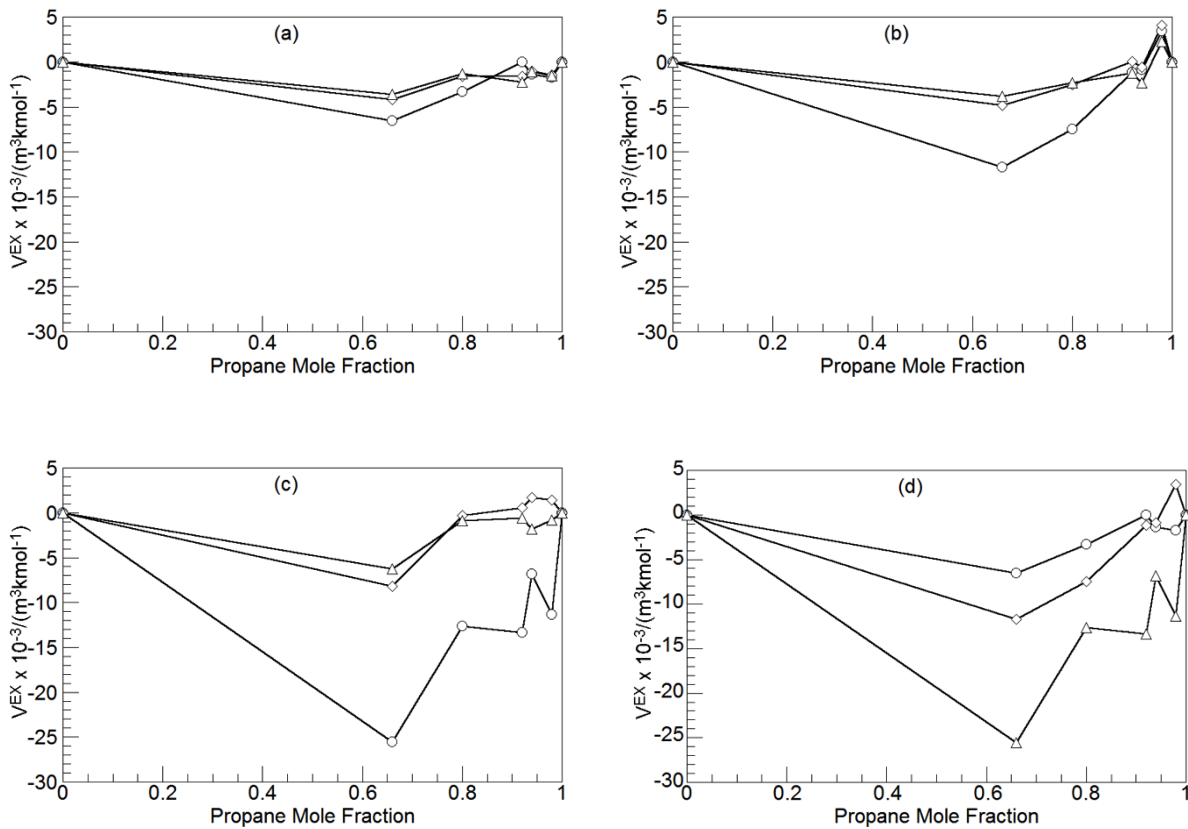
Figure 4.12. Excess volumes for propane-squalane mixtures as a function of propane mole fraction for isotherms (a) 324 K, (b) 424 K, (c) 518 K for 30 MPa (○), 100 MPa (◊), and 160 MPa (Δ), while (d) is for 30 MPa isobar at 324 K (○), 424 K (◊), and 518 K (Δ). Lines serve to guide the eyes.

The excess volumes are mostly negative for the C_3-C_{10}, C_3-C_{20}, and the C_3-C_{30} systems, which is similar to the behavior exhibited for systems of compounds in the same chemical family. It has been theorized that the negative excess volumes observed in asymmetric systems such as this one result from the small molecules filling the void spaces between the much larger molecules [15]. The magnitude of the excess volume decreases as the pressure increases and the excess volume increases as the temperature increases. The trends of the excess volume with pressure and temperature are similar for all the propane-alkane mixtures studied here and are also similar to those observed for propane-*n*-octane mixtures reported by Milanesio *et al*. [15]. The absolute magnitude of the C_3-C_{20} excess volumes are also similar to those calculated for the C_3-C_{10} system. In the present study, the most negative value of the excess volume for the C_3-C_{10} mixture is obtained at $x_1 = 0.6052$ while it occurs at $x_1 = 0.6550$ for the C_3-C_{30} mixture. At these points, it appears that the highest degree of packing for the mixtures exists. However, it is important to note that the absolute values of the excess volumes are only 1 to 2% of the value of the mixture molar volume itself, which means that the absolute value of the excess volume is only slightly greater than the accumulated error in the values of the mixture volumes. In addition, the trends depicted in Figure 4.12for the C_3-C_{30} mixture exhibit some hysteresis especially at high propane concentrations due to the relatively small magnitude of the excess volumes. As an explanation for these observations, Pecar and Dolecek [116] noted how a small difference in density can lead to large difference in the calculated excess volumes. Note also that the Tait equation used to interpolate data at constant temperatures and pressures performed poorly at high propane concentrations where most of the hysteresis exists. Therefore, more precise experimental data and a more accurate correlation are needed to obtain more accurate values for the excess volume of these mixtures.

4.3. Equation of State Modeling

Although the Tait equation is useful for interpolating mixture density data at specific mixture compositions, it is not an appropriate tool for representing the thermodynamic properties of mixtures over wide ranges of temperature, pressure, and composition. During petroleum production and transportation, the oil can undergo changes in composition due to a release of gas phase, or mixing of the petroleum oil with injected fluids. Therefore, the high-temperature, high-pressure (HTHP) experimental density data for the C_3-C_{10}, C_3-C_{20}, and the C_3-C_{30} binary mixture systems obtained in this study are modeled with the Peng-Robinson (PR) [24], the volume-translated Peng-Robinson (VT-PR) [27], and the Perturbed Chain Statistical Associating Fluid Theory (PC-SAFT) [51] equations of state (EoS). The performance of each model is again characterized by the mean absolute percent deviation, δ, as defined in equation 4.4.

$$\delta = \frac{1}{n} \sum_{1}^{n} \left| \frac{\rho_{i,\text{experimental}} - \rho_{i,\text{calculated}}}{\rho_{i,\text{experimental}}} \right| \bullet 100$$

(4.4)

4.3.1. Peng-Robinson (PR) and Volume-Translated (VT) PREoS

The PREoS [24] and the VT-PREoS [27] approach by Baled *et al.* are used to model the high-temperature, high-pressure (HTHP) C_3-C_{10}, C_3-C_{20}, and the C_3-C_{30} binary mixture density data obtained in this study. The typical van der Waals one-fluid mixing rules are used with the PREoS and VT-PREoS to calculate mixture values for *a* and *b*, while *c* is calculated as a mole fraction weighted average [27]. Table 4.8 lists the physical properties of the pure component hydrocarbons required for the PREoS and the VT-PREoS calculations. For these calculations the

86

binary interaction parameter used in the PREoS and the VT-PREoS, k_{ij}, is set to zero given that propane, *n*-decane, *n*-eicosane, and squalane are all from the same chemical family. δ values, presented in Tables 4.9, 4.10, and 4.11 are calculated using equation (4.4), where $\rho_{i,predicted}$ is the value of density predicted with the equation of state at the same conditions with the experimental density, $\rho_{i,experimental}$.

Table 4.8. Molecular weight, M_w, critical temperature, T_c, critical pressure, P_c, and acentric factor, ω, for propane, *n*-decane, and *n*-eicosane from Reid *et al.* [102]. Properties for squalane are the same as described for pure squalane in chapter 3.

Compound	M_w	T_c /K	P_c /MPa	ω
Propane	44.1	369.8	4.256	0.152
n-Decane	142.3	617.6	2.108	0.490
n-Eicosane	282.6	767.0	1.115	0.907
Squalane	422.8	795.9	0.590	1.340

Table 4.9. Mean absolute percent deviation (δ) and the standard deviation (λ) showing the performance of the Peng-Robinson equation of state (PREoS) and the volume-translated (VT) PREoS for C_3 (1) - C_{10} (2) binary mixture. All calculations are done with $k_{ij} = 0$.

x_1	Data Points	T /K	δ PREoS	λ PREoS	δ VT-PREoS	λ VT-PREoS
0.1597	21	444.3	3.74	1.64	1.52	0.74
0.1597	20	510.5	3.66	1.49	1.15	1.22
0.3041	19	344.2	6.41	2.07	1.60	1.20
0.4210	24	344.2	5.23	2.14	1.68	1.06
0.4210	18	444.4	3.15	1.62	1.16	1.25
0.4210	23	511.0	2.41	1.86	1.72	1.62
0.6052	20	344.3	3.92	3.19	1.77	1.76
0.6052	22	444.3	2.60	1.59	2.20	1.58
0.6052	21	511.1	1.80	1.25	2.74	1.29
0.8156	20	344.2	3.37	1.39	2.24	0.89
0.8156	25	444.3	2.72	1.50	2.03	1.77

Table 4.10. Mean absolute percent deviation (δ) and the standard deviation (λ) showing the performance of the Peng-Robinson equation of state (PREoS) and the volume -translated (VT) PREoS for C_3 (1) - C_{20} (2) binary mixture. All calculations are done with $k_{ij} = 0$.

x_1	Data Points	T /K	δ PREoS	λ PREoS	δ VT-PREoS	λ VT-PREoS
0.3025	5	324.7	19.65	1.02	2.32	0.93
0.3025	16	422.9	19.08	2.45	3.76	2.40
0.3025	6	516.2	14.44	0.98	1.03	0.71
0.6483	10	325.1	16.48	0.58	3.43	0.45
0.6483	21	420.4	14.77	1.29	3.80	1.14
0.6483	9	520.3	12.98	1.74	3.76	1.43
0.7375	14	319.1	14.80	0.75	3.70	0.60
0.7375	12	424.5	11.94	0.63	3.14	0.41
0.7375	16	521.5	8.66	1.04	1.38	0.69
0.8367	16	324.6	12.30	0.88	5.05	0.83
0.8367	19	421.0	10.31	1.51	4.87	1.66
0.9310	11	322.9	1.86	1.09	0.88	0.90
0.9310	12	422.2	0.62	0.50	0.70	0.57
0.9310	11	524.5	2.53	0.93	1.00	0.58

Table 4.11. Mean absolute percent deviation (δ) and the standard deviation (λ) showing the performance of the Peng-Robinson equation of state (PREoS) and the volume -translated (VT) PREoS for C_3 (1) - C_{30} (2) binary mixture. All calculations are done with $k_{ij} = 0$.

x_1	Data Points	T /K	δ PREoS	λ PREoS	δ VT-PREoS	λ VT-PREoS
0.6550	24	324.7	38.42	1.18	28.01	1.10
0.6550	23	422.9	36.21	1.68	27.20	1.59
0.6550	23	516.2	34.73	1.99	27.15	1.86
0.7960	14	323.6	32.84	0.97	24.03	0.88
0.7960	16	423.6	30.61	1.49	23.29	1.40
0.7960	14	516.0	29.19	3.03	22.70	2.41
0.9208	25	324.2	21.32	2.15	16.60	2.02
0.9208	23	420.5	17.95	2.73	14.67	2.65
0.9208	19	523.5	16.28	2.76	14.27	3.39
0.9439	25	324.5	17.25	0.91	14.34	0.94
0.9439	14	424.0	13.45	1.97	12.03	1.86
0.9439	21	515.3	10.54	3.73	10.41	3.73
0.9752	23	322.6	7.62	1.19	8.80	1.20
0.9752	23	424.2	5.22	1.81	7.61	1.97

88

0.9752	15	521.5	3.25	2.33	6.56	2.89

Both the PREoS and the VT-PREoS models provide better HTHP density predictions for C_3-C_{10} mixtures than for C_3-C_{20} mixtures, which is also better than the predictions obtained for the C_3-C_{30} mixtures. This result is not surprising given the large difference in δ values found when modeling the HTHP density for pure n-decane, $\delta = 6.13$, for pure n-eicosane, $\delta = 22.05$ [27], and for pure squalane $\delta = 41.18$ (as obtained in chapter 3), with the PREoS given the large value of the acentric factor of n-eicosane and for squalane [26]. It is important to note that for light hydrocarbons such as propane, the PREoS overpredicts the HTHP density while for higher hydrocarbons the PREoS underpredicts the HTHP density [4,14]. In all of these cases the VT-PREoS underpredicts the density at high pressures. Since the volume translated term, c, accounts for the volume difference between the values calculated by the EoS and the experimental value, the sign of c switches from positive to negative as propane-hydrocarbon mixtures become expanded due to an increase in either temperature or propane concentration. Therefore, at certain temperatures and propane concentrations, the PREoS and VT-PREoS yield similar predictions. As an example of these effects, consider the representative comparison of calculated and experimental densities shown in Figures 4.13a and 4.13b for the C_3-C_{10} mixture at $x_1 = 0.4210$. The improved performance of the VT-PREoS relative to the PREoS is readily apparent at 344.2 and 444.4 K, however, at the highest temperature, 511.0 K, the difference between the performances of the two models is minimal. Similar observations are obtained for the C_3-C_{20} mixtures with $x_1 = 0.9310$ at 524 K and for the C_3-C_{30} mixtures with $x_1 = 0.9439$ at 515.3 K.
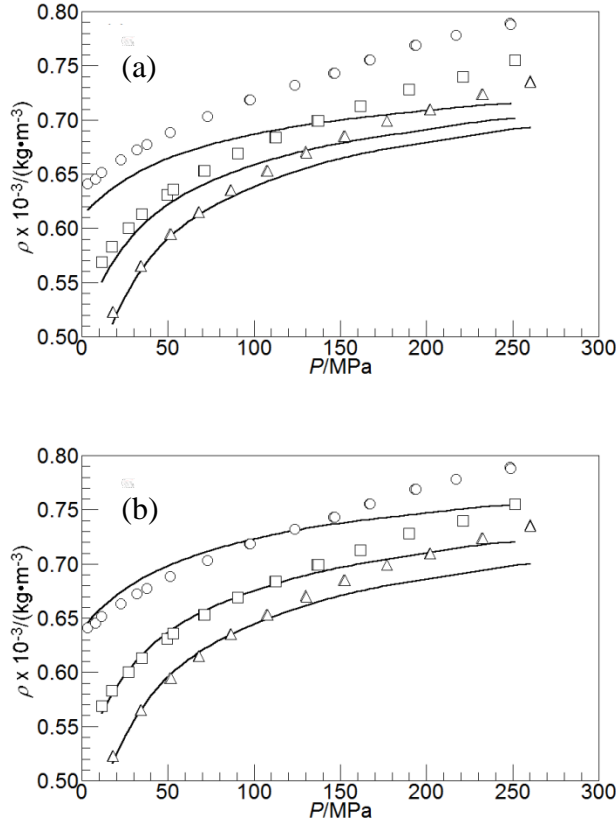
Figure 4.13. Representative comparison of C_3-C_{10} binary density data for $x_1 = 0.4210$ obtained in this study (symbols) with the EoS model predictions (lines) using (a) PREoS and (b) VT-PREoS at 344.2 K ($\circ$), 444.4 K ($\square$), and 511.0 K (Δ).

4.3.2. Perturbed-Chain Statistical Associating Fluid Theory (PC-SAFT) EoS

The PC-SAFT equation for non-associating fluids is obtained from the residual Helmholtz free energy, $\tilde{a}^{res}$, written as a sum of Helmholtz free energy contributions from a hard-sphere term, $\tilde{a}^{hs}$, chain term, $\tilde{a}^{hc}$, and a dispersion term, $\tilde{a}^{disp}$ detailed equations for these terms are found in [51].

90

$$\tilde{a}^{res} = m\tilde{a}^{hs} + \tilde{a}^{chain} + \tilde{a}^{disp} \tag{6}$$

The parameters m_i, σ_i, and ε_i which are the segment number, temperature-independent segment diameter, and the interaction energy, respectively, are required for each pure-component i for PC-SAFT calculations. For a binary mixture, the combining rules for each parameter is given in equations 4.6 to 4.8.

$$m = \sum_i x_i m_i , \tag{4.6}$$

$$\sigma_{ij} = 0.5(\sigma_i + \sigma_j) , \tag{4.7}$$

$$\varepsilon_{ij} = (1 - k_{ij})\sqrt{\varepsilon_i \varepsilon_j} , \tag{4.8}$$

In the above equations, x_i is the mole fraction of component i, and k_{ij} is binary interaction parameter that corrects for the geometric mean averaging of the interactions between two dissimilar molecules. The performance of both the Low-P and HTHP pure-component parameters (as previously described) are evaluated against the binary mixture density data reported here. Both Low-P [51] and HTHP [54] parameters are obtained from the literature for propane, decane, and eicosane while only the Low-P parameters have been reported for squalane [109]. HTHP parameters used here are those obtained for squalane in chapter 3 by fitting the PC-SAFT EoS to the HTHP density data for pure squalane. Just as was the case for the cubic EoS,

the binary interaction parameter, k_{ij}, is set to zero for the mixture calculations given that propane, decane, eicosane, and squalane both belong to the same chemical family. Table 4.12 lists the Low-P parameters fit to low pressure data and Table 4.13 lists the Burgess parameters fit to HTHP data. Alternatively for the C_3-C_{30} system, PC-SAFT parameters are estimated from group contribution (GC) methods [55] using Low-P and HTHP parameter sets and using the functional groups as described in chapter 3.

Table 4.12. Values for the PC-SAFT Low-P parameters from the literature that are used for predicting binary mixture density data investigated in this study. Parameters for propane, decane, and *n*-eicosane are obtained from Gross and Sadowski [51], while parameters for squalane are obtained from Garcia *et al*. [109].

Compound	M_w	m	σ /Å	ε/k_B /K
Propane	44.1	2.0020	3.6184	208.11
n-Decane	142.3	4.6627	3.8384	243.87
n-Eicosane	282.6	7.9849	3.9869	257.75
Squalane	422.8	10.5257	4.1189	254.95

Table 4.13. Values for the HTHP PC-SAFT parameters from Burgess *et al*. [54] for used for predicting binary mixture density data investigated in this study. Parameters for squalane are obtained from a fit of the PC-SAFT EoS to HTHP pure squalane density data in chapter 3.

Compound	M_w g/mol	m	σ /Å	ε/k_B /K
Propane	44.1	2.1994	3.5381	204.81
n-Decane	142.3	6.9000	3.3665	226.86
n-Eicosane	282.6	10.8881	3.6193	263.86
Squalane	422.8	16.6709	3.5360	227.53

92

The δ values and the λ obtained for the PC-SAFT EoS modeling results with the Low-P parameters and the HTHP parameters are listed in Table 4.14 for C_3-C_{10} mixtures, in Table 4.15 for C_3-C_{20} mixtures, and in Table 4.19 for the C_3-C_{30} mixtures. In addition to the results listed in Table 4.16 with fitted parameters for the C_3-C_{30} mixtures, Table 4.17 also lists the δ values and the λ obtained when the GC estimated Low-P and HTHP pure-component parameters are used with the PC-SAFT EoS.

Table 4.14. Mean absolute percent deviation (δ) and standard deviation (λ) showing the performance of the PC-SAFT EoS for propane (1) - decane (2) binary mixtures using pure-component Low-P parameters from Gross and Sadowski (GS) [51] and HTHP parameters from Burgess and coworkers [54]. All calculations are done with $k_{ij} = 0$.

| x_1	Data Points	T /K	δ Low-P	λ Low-P	δ HTHP	λ HTHP
0.1597	21	444.3	2.47	1.20	0.20	0.16
0.1597	20	510.5	1.36	0.87	1.66	0.36
0.3041	19	344.2	1.13	0.54	0.68	0.41
0.4210	24	344.2	1.17	0.58	0.62	0.46
0.4210	18	444.4	0.97	0.58	1.11	0.39
0.4210	23	511.0	1.22	0.48	1.48	0.44
0.6052	20	344.3	0.55	0.33	1.30	0.67
0.6052	22	444.3	0.54	0.28	1.90	0.57
0.6052	21	511.1	0.46	0.33	2.48	0.53
0.8156	20	344.2	3.04	0.31	1.31	0.59
0.8156	25	444.3	1.69	0.81	0.84	1.53

93

Table 4.15. Mean absolute percent deviation (δ) and standard deviation (λ) showing the performance of the PC-SAFT EoS for propane (1) – eicosane (2) binary mixture using pure-component Low-P parameters from Gross and Sadowski [51] and HTHP parameters from Burgess and coworkers [54]. All calculations are done with $k_{ij} = 0$.

x_1	Data Points	T /K	δ Low-P	λ Low-P	δ HTHP	λ HTHP
0.3025	5	324.7	3.60	0.37	2.37	0.57
0.3025	16	422.9	4.95	0.97	2.18	0.54
0.3025	6	516.2	4.95	1.31	2.91	0.31
0.6483	10	325.1	2.67	0.87	1.10	0.10
0.6483	21	420.4	2.90	0.96	1.29	0.73
0.6483	9	520.3	3.77	0.56	1.34	1.12
0.7375	14	319.1	2.01	0.43	0.41	0.36
0.7375	12	424.5	2.51	0.29	1.21	1.10
0.7375	16	521.5	5.32	0.87	3.23	1.05
0.8367	16	324.6	0.50	0.31	1.44	0.45
0.8367	19	421.0	1.31	0.34	1.26	0.86
0.9310	11	322.9	3.52	1.17	1.92	0.41
0.9310	12	422.2	4.29	1.64	3.39	3.63
0.9310	11	524.5	6.07	2.15	3.81	1.33

Table 4.16. Mean absolute percent deviation (δ) and its standard deviation (λ) for calculations with the PC-SAFT EoS, setting k_{ij} to zero, using pure component parameters obtained from fitting pure component vapor pressure and saturated liquid density data (Low-P) [51,109] and high-temperature, high-pressure (HTHP) density data [54] for modeling propane (1) - squalane (2) mixture density data.

x_1	Data Points	T /K	δ Low-P	λ Low-P	δ HTHP	λ HTHP
0.6550	24	323.6	1.11	0.83	1.77	0.32
0.6550	23	423.6	1.98	0.67	1.68	0.25
0.6550	23	516.0	1.86	0.81	2.48	0.27
0.7960	14	324.2	1.58	0.72	0.88	0.21
0.7960	16	420.5	2.62	0.28	0.92	0.44
0.7960	14	523.5	4.23	0.59	0.79	0.78

94

0.9208	25	324.5	1.79	1.29	1.86	0.91
0.9208	23	424.0	3.62	1.51	1.88	0.82
0.9208	19	515.3	4.23	1.43	1.54	0.71
0.9439	25	322.6	1.16	0.40	1.31	0.49
0.9439	14	424.2	3.38	2.50	2.51	2.45
0.9439	21	521.5	5.91	2.43	3.26	2.42
0.9752	23	324.4	0.62	0.35	1.81	0.49
0.9752	23	426.5	2.08	1.28	1.99	0.89
0.9752	15	522.5	2.33	1.33	1.62	0.72

Table 4.17. Mean absolute percent deviation (δ) and its standard deviation (λ) for calculations with the PC-SAFT EoS, setting k_{ij} to zero, using parameters obtained from group contribution, GC, estimation for both Low-P and HTHP pure component parameters [55] for modeling propane (1) - squalane (2) mixture density data.

x_1	Data Points	T /K	δ GC Low-P	λ GC Low-P	δ GC HTHP	λ GC HTHP
0.6550	24	323.6	1.31	0.41	1.25	0.43
0.6550	23	423.6	2.04	0.28	1.31	0.61
0.6550	23	516.0	1.94	0.13	2.02	0.57
0.7960	14	324.2	2.05	0.25	0.55	0.27
0.7960	16	420.5	3.25	1.03	1.36	1.17
0.7960	14	523.5	4.64	1.46	1.42	1.35
0.9208	25	324.5	2.25	1.76	2.15	1.40
0.9208	23	424.0	4.18	1.95	2.36	1.20
0.9208	19	515.3	4.70	1.67	1.73	0.71
0.9439	25	322.6	1.71	0.50	1.17	0.62
0.9439	14	424.2	4.31	3.24	2.38	2.18
0.9439	21	521.5	7.05	2.86	3.51	2.59
0.9752	23	324.4	1.09	0.43	1.29	0.60
0.9752	23	426.5	3.03	1.79	2.35	1.36
0.9752	15	522.5	3.29	1.65	1.78	0.83

As was the case with the cubic EoS modeling, the PC-SAFT EoS provides the best HTHP density predictions for C_3-C_{10} mixtures than the C_3-C_{20} and C_3-C_{30} mixtures. The poor fits of the C_3-C_{20} and the C_3-C_{30} densities with the PC-SAFT EoS are attributed to the difference in the molecular size of the mixture compounds where the C_3-C_{20} and the C_3-C_{30} system exhibits more

size asymmetry than the C_3-C_{10} system. There is not much difference in the overall performance of the PC-SAFT EoS to represent C_3-C_{10} density data when using parameters from either of the two sources. Nevertheless, the HTHP parameters provide marginally superior PC-SAFT EoS predictions. Figure 4.14 shows a representative example of the performance the PC-SAFT EoS with the two different pure component parameters for the C_3-C_{10} mixture at $x_1 = 0.4210$. The PC-SAFT EoS with the Low-P parameters provides good agreement between model calculations and experimental data at low pressures to about 70 MPa, beyond which the model overpredicts the mixture density. In contrast the PC-SAFT EoS with HTHP parameters provides good agreement between model calculations and experimental data to approximately 150 MPa, above which the model slightly underpredicts the mixture density. However for the C_3-C_{20} mixture, the PC-SAFT EoS always overpredicts the experimental density data with any sets of parameters. However, predictions obtained with the Low-P parameters overpredict the density relatively more often than the predictions using the HTHP parameters.

For the C_3-C_{30} mixture, the PC-SAFT EoS unsurprisingly provides a better representation of the experimental density data when the HTHP or the GC HTHP pure-component parameters are used as compared to the prediction obtained with either the Low-P or the GC Low-P parameters are used. On average, the difference between the δ values is greater than 1% when comparing the PC-SAFT EoS performance using the HTHP parameters to the performance with the Low-P parameters. The HTHP parameters typically underpredict the density especially at high pressures, while the Low-P parameters overpredict the density for virtually all of the experimental conditions. Furthermore, the δ values show that the predictions for the $\sim$ 324 K isotherms are consistently better than predictions at higher temperatures when using the Low-P or the GC Low-P parameters. This trend is also observed when the GC HTHP parameters are

96

used except for the mixture at propane mole fraction of 0.9201 and for pure propane. However, the PC-SAFT EoS with the HTHP parameters does not show any particular temperature sensitivity for all the mixture compositions studied. For the three mixtures studied, the PC-SAFT EoS density predictions are generally poor for propane-rich mixtures at pressures below 25 MPa and at temperatures greater than the critical temperature of propane. This observation is in agreement with results reported by Burgess *et al*. [54]. In the present study the poorest predictions are obtained for C_3-C_{20} mixtures at $x_1 = 0.9310$, 422.2 K, and pressures below 25 MPa where the percent deviations in two instances are in excess of 10%.
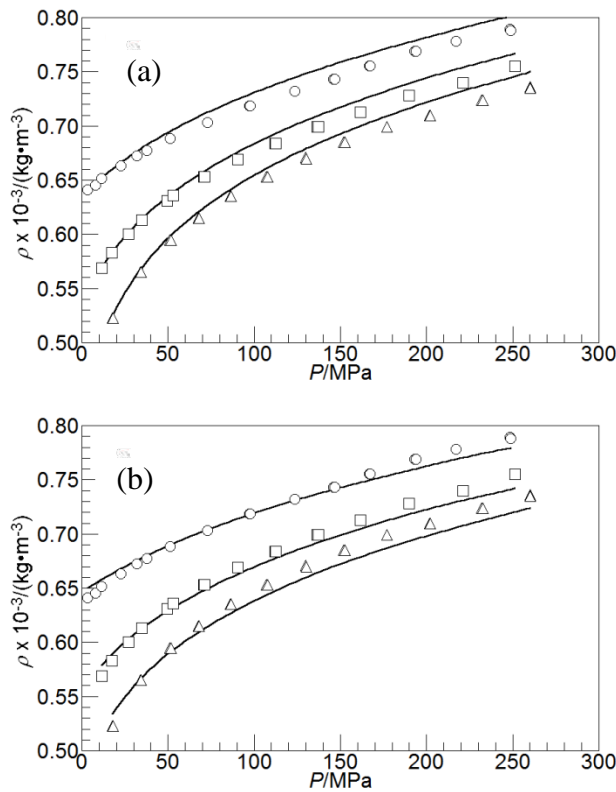
Figure 4.14. Representative comparison of C_3-C_{10} binary density data for $x_1 = 0.4210$ obtained in this study (symbols) with the EoS model predictions (lines) using PC-SAFT EoS with Low-P (a), and HTHP (b) parameters at 344.2 K ($\circ$), 444.4 K ($\square$), and 511.0 K (Δ).

4.3.3. Comparison of Equation of State Model Predictions for Binary Mixture Density

Figures 4.15-4.23 show the comparison of the predictive performance of the PREoS (a), the VT-PREoS (b), and the PC-SAFT EoS with either the Low-P (c) or the HTHP (d) pure component parameters the three binary mixture systems studied here. The comparisons with the C_3-C_{10} experimental data are shown in Figure 4.15 at ~344 K, in Figure 4.16 at ~444 K, and in Figure 4.17 at 510 K. Similarly, the comparisons with the C_3-C_{20} experimental data are shown in Figure 4.18 at ~323 K, in Figure 4.19 at ~423 K, and in Figure 4.20 at 520 K., while the comparison with the C_3-C_{30} experimental data are shown in Figure 4.21 at ~323 K, in Figure 4.22 at ~423 K, and in Figure 4.23 at 520 K. From the plots, it can be seen clearly how the PREoS provides the worst density predictions for the binary mixtures investigated in this study. The VT-PREoS provides improved density predictions over the PREoS especially for the C_3-C_{10} and the C_3-C_{20} mixtures, but provides only marginally better predictions for the C_3-C_{30}. In addition, the PREoS predictions for all the mixture compositions cross one another for the C_3-C_{20} and the C_3-C_{30} mixtures. The VT-PREoS provides an improvement on the predictions in this aspect as well whereby the VT-PREoS predictions do not cross one another, except for the C_3-C_{30} mixtures albeit at a higher pressure than is obtained for the PREoS predictions at all the three isotherms.

98
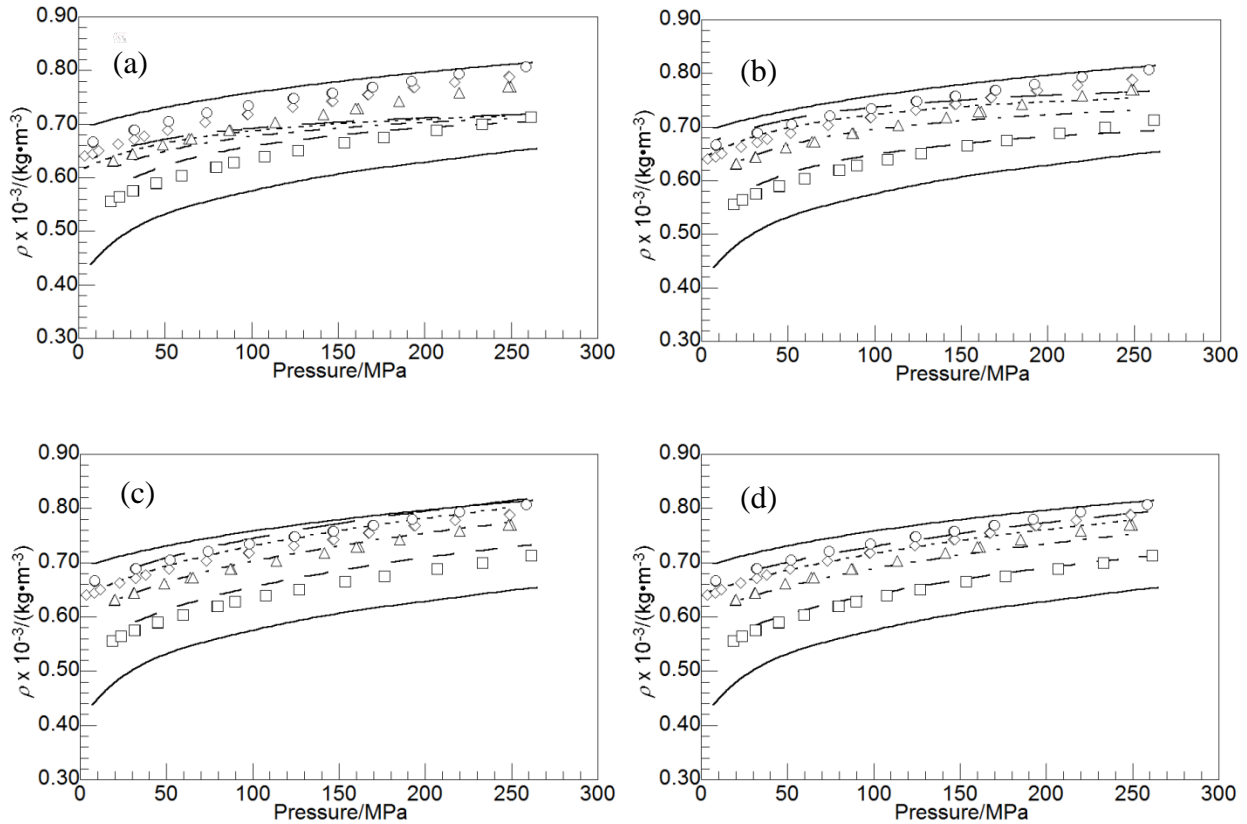
Figure 4.15. Comparison of the performance of (a) PREoS, (b) VT-PREoS, (c) Low-P PC-SAFT EoS, and (d) HTHP PC-SAFT EoS predictions (dashed lines) with the experimental density data (symbols) at ~344 K for the C_3-C_{10} mixture at 0.3041 (○) and (—— ——); 0.4210 (◊) and (- —- —); 0.6052 (Δ) and (········);and 0.8156 (□) and (— — —) propane mole fraction. The solid lines represent pure eicosane density (top) and propane density data (bottom).
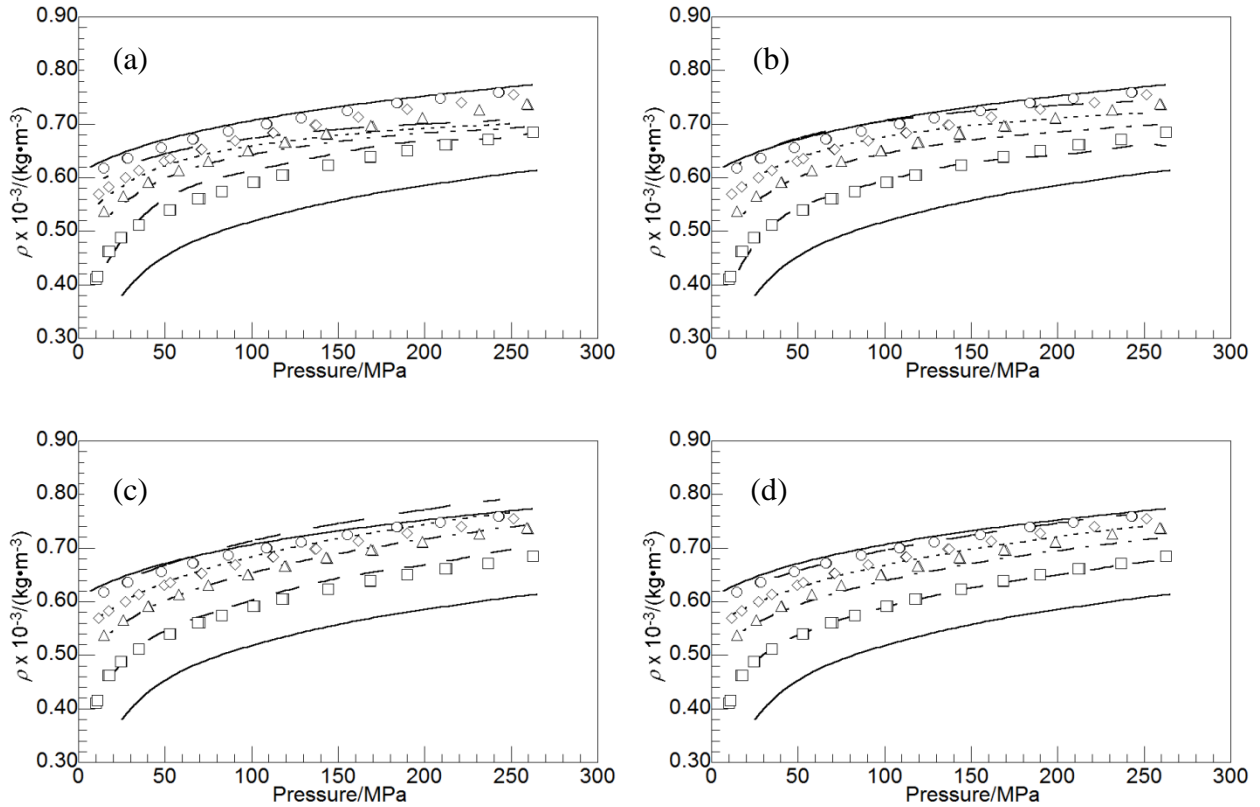
Figure 4.16. Comparison of the performance of (a) PREoS, (b) VT-PREoS, (c) Low-P PC-SAFT EoS, and (d) HTHP PC-SAFT EoS predictions (dashed lines) with the experimental density data (symbols) at ~444 K for the C_3-C_{10} mixture at 0.1597 (○) and (—— ——); 0.4210 (◊) and (- — - —); 0.6052 (Δ) and (·········);and 0.8156 (□) and (— — —) propane mole fraction. The solid lines represent pure eicosane density (top) and propane density data (bottom).

100
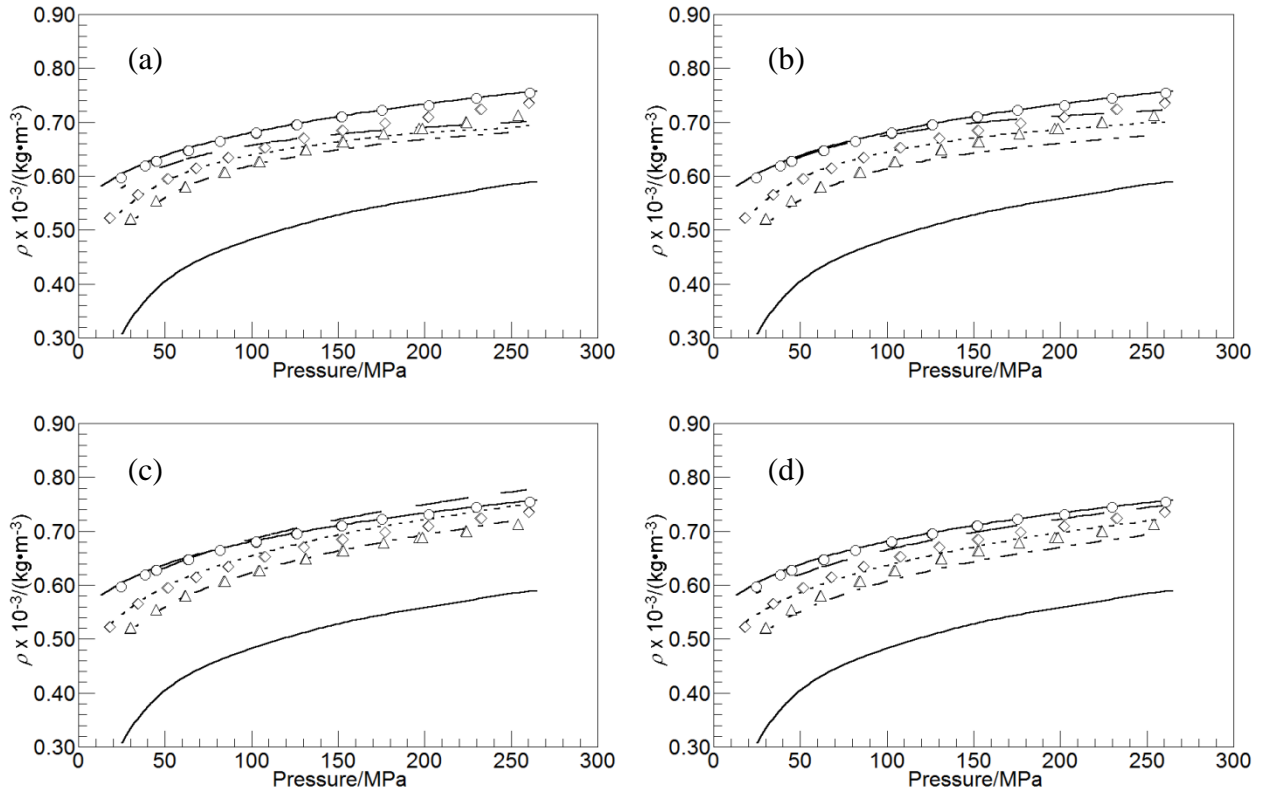
Figure 4.17. Comparison of the performance of (a) PREoS, (b) VT-PREoS, (c) Low-P PC-SAFT EoS, and (d) HTHP PC-SAFT EoS predictions (dashed lines) with the experimental density data (symbols) at ~510 K for the C_3-C_{10} mixture at 0.1597 (○) and (—— ——); 0.4210 (◊) and (- — - —); 0.6052 (Δ) and (········);and 0.8156 (□) and (— — —) propane mole fraction. The solid lines represent pure eicosane density (top) and propane density data (bottom).
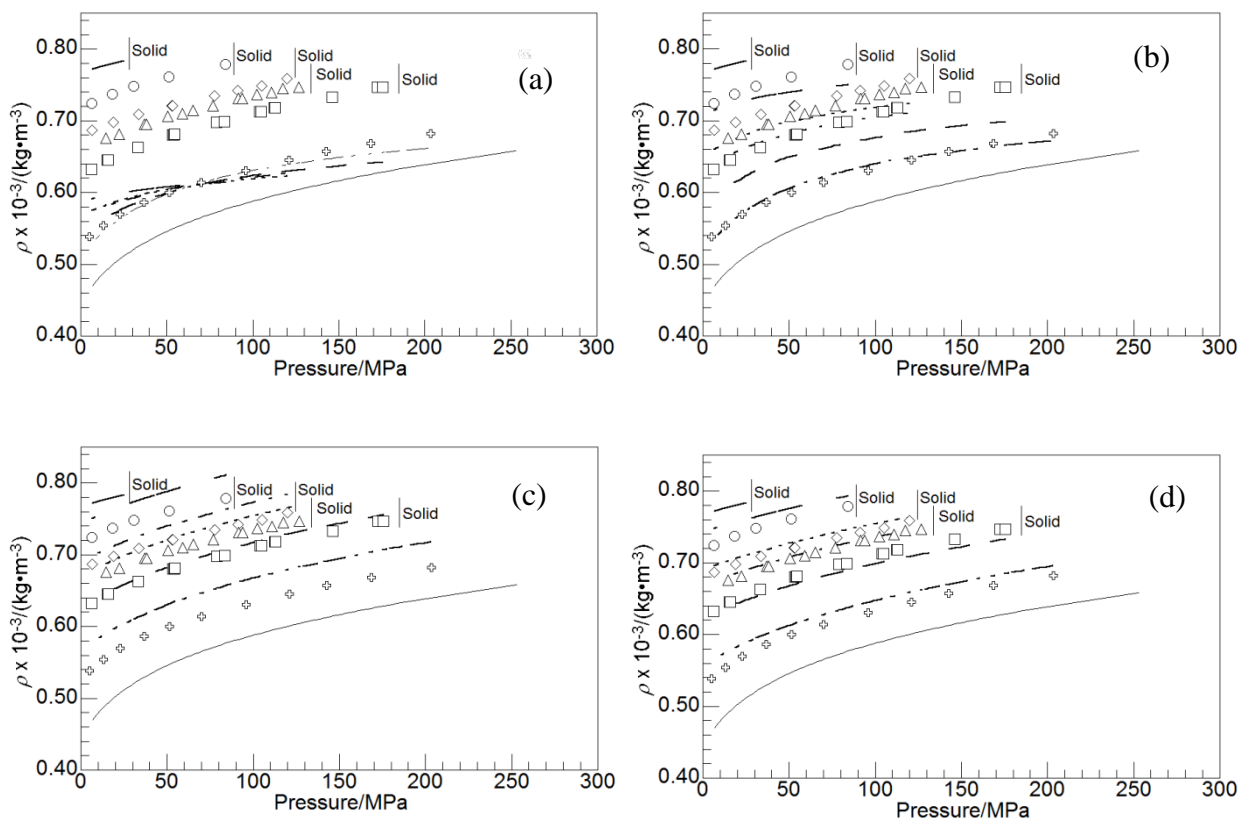
Figure 4.18. Comparison of the performance of (a) PREoS, (b) VT-PREoS, (c) Low-P PC-SAFT EoS, and (d) HTHP PC-SAFT EoS predictions (dashed lines) with the experimental density data (symbols) at ~323 K for the C_3-C_{20} mixture at 0.3025 (○) and (—— ——); 0.6483 (◊) and (- —— - —); 0.7375 (Δ) and (·········); 0.8367 (□) and (— — —); and 0.9310 (⚏) and (- —— -- ——) propane mole fraction. The solid lines represent pure eicosane density (top) and propane density data (bottom). Vertical solid lines represent the liquid-solid phase boundary encountered during the experiments.
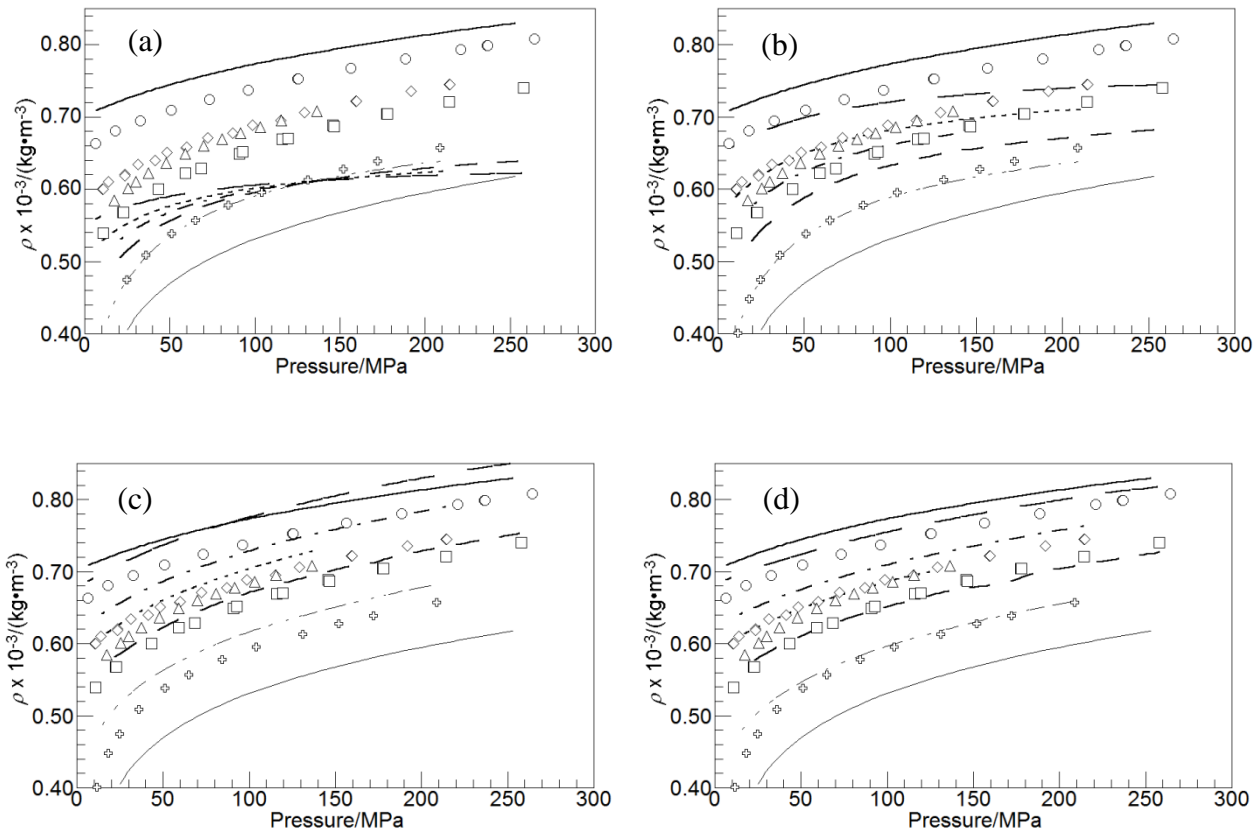
Figure 4.19. Comparison of the performance of (a) PREoS, (b) VT-PREoS, (c) Low-P PC-SAFT EoS, and (d) HTHP PC-SAFT EoS predictions (dashed lines) with the experimental density data (symbols) at ~423 K for the C_3-C_{20} mixture at 0.3025 (○) and (—— ——); 0.6483 (◊) and (- —— - —); 0.7375 (Δ) and (········); 0.8367 (□) and (— — —); and 0.9310 (⊞) and (- —— -- ——) propane mole fraction. The solid lines represent pure eicosane density (top) and propane density data (bottom).
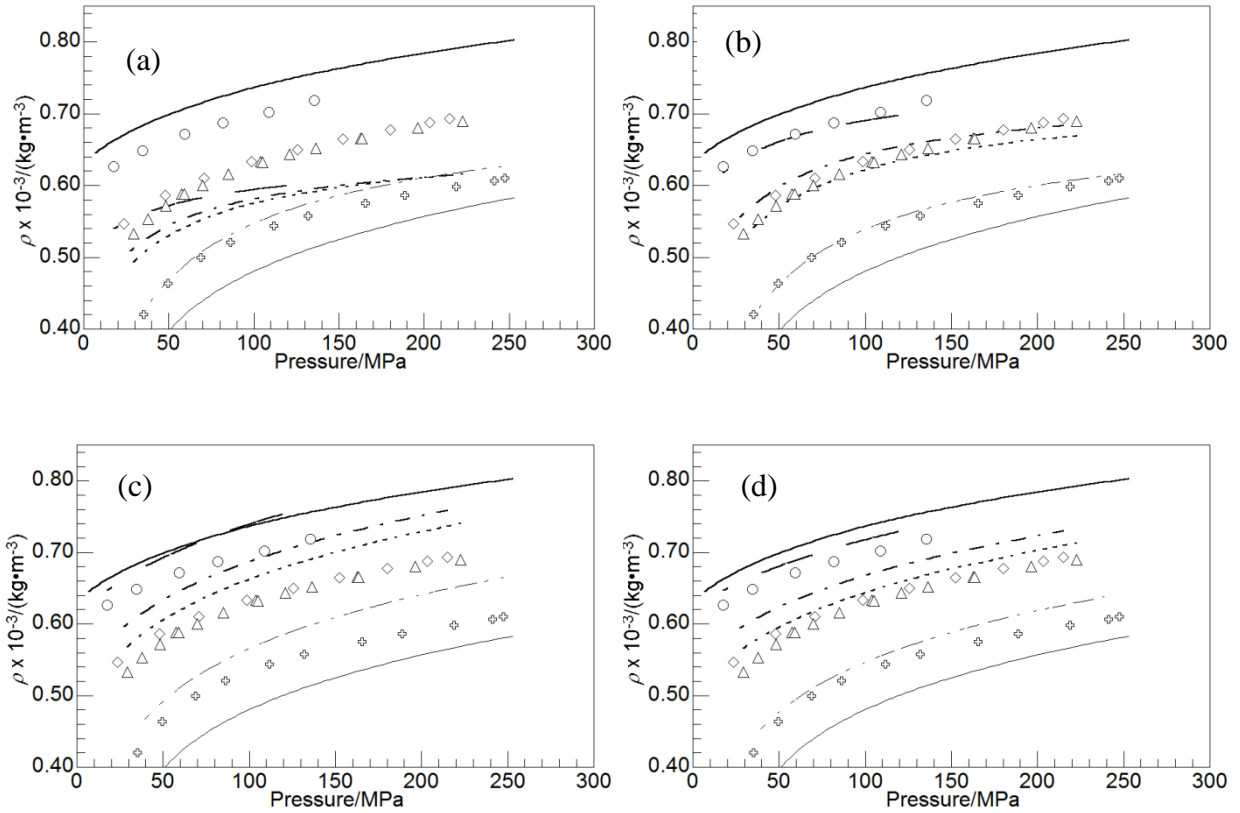
Figure 4.20. Comparison of the performance of (a) PREoS, (b) VT-PREoS, (c) Low-P PC-SAFT EoS, and (d) HTHP PC-SAFT EoS predictions (dashed lines) with the experimental density data (symbols) at ~520 K for the C_3-C_{20} mixture at 0.3025 (○) and (—— ——); 0.6483 (◊) and (- —— - —); 0.7375 (Δ) and (⋯⋯⋯); 0.8367 (□) and (— — —); and 0.9310 (⊹) and (- —— -- ——) propane mole fraction. The solid lines represent pure eicosane density (top) and propane density data (bottom).
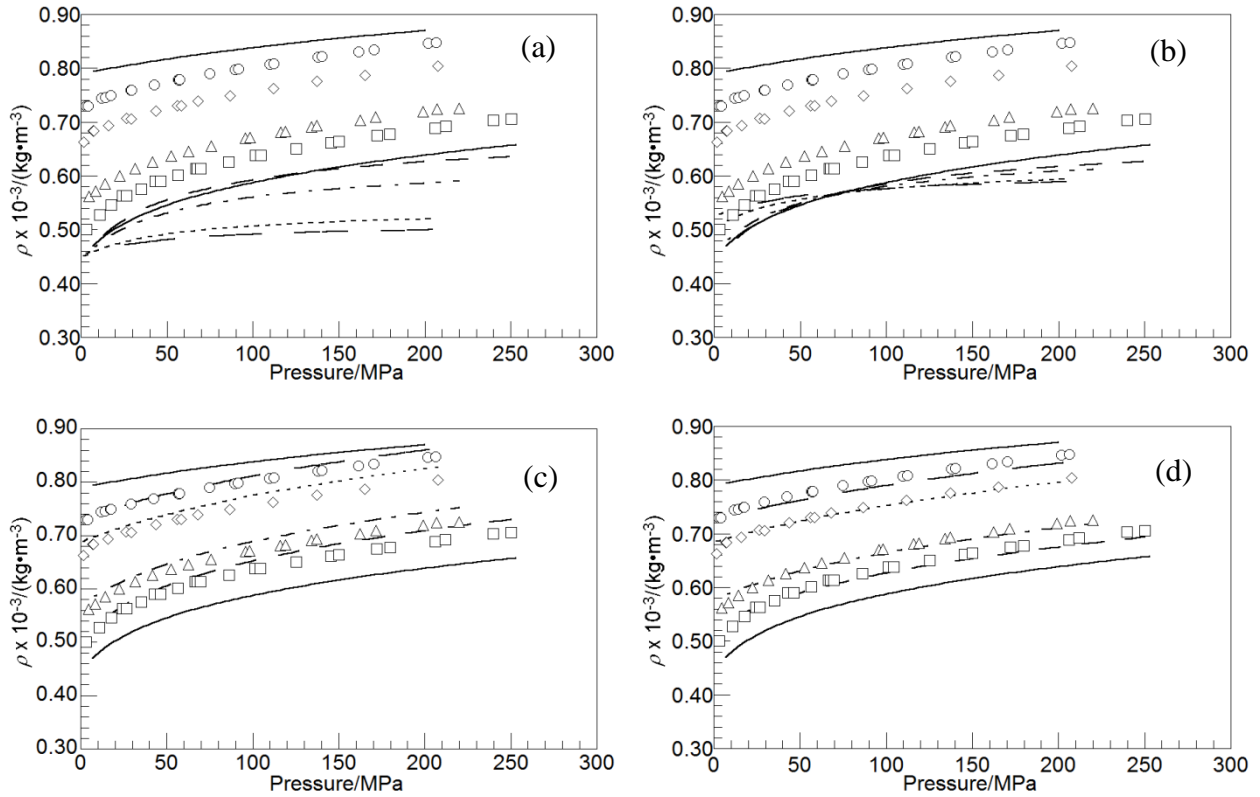
Figure 4.21. Comparison of the performance of (a) PREoS, (b) VT-PREoS, (c) Low-P PC-SAFT EoS, and (d) HTHP PC-SAFT EoS predictions (dashed lines) with the experimental density data (symbols) at ~323 K for the C_3-C_{30} mixture at 0.6550 (○) and (⎯⎯ ⎯⎯); 0.7960 (◊) and (- ⎯ - ⎯); 0.9439 (Δ) and (⋯⋯⋯);and 0.9752 (□) and (⎯ ⎯ ⎯) propane mole fraction. The solid lines represent pure squalane density (top) and propane density data (bottom).

105
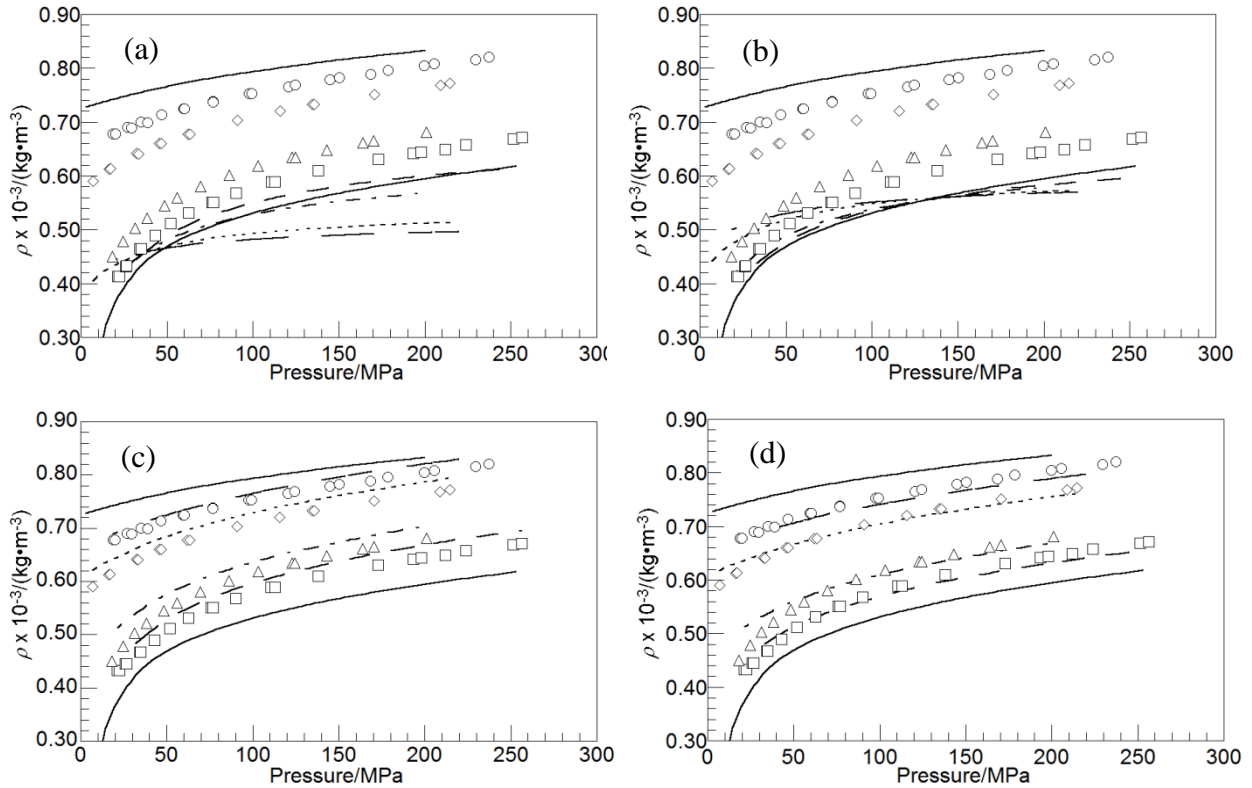
Figure 4.22. Comparison of the performance of (a) PREoS, (b) VT-PREoS, (c) Low-P PC-SAFT

EoS, and (d) HTHP PC-SAFT EoS predictions (dashed lines) with the experimental density data

(symbols) at ~423 K for the C_3-C_{30} mixture at 0.6550 (○) and (—— ——); 0.7960 (◊) and (- —

- —); 0.9439 (Δ) and (········);and 0.9752 (□) and (— — —) propane mole fraction. The solid

lines represent pure squalane density (top) and propane density data (bottom).
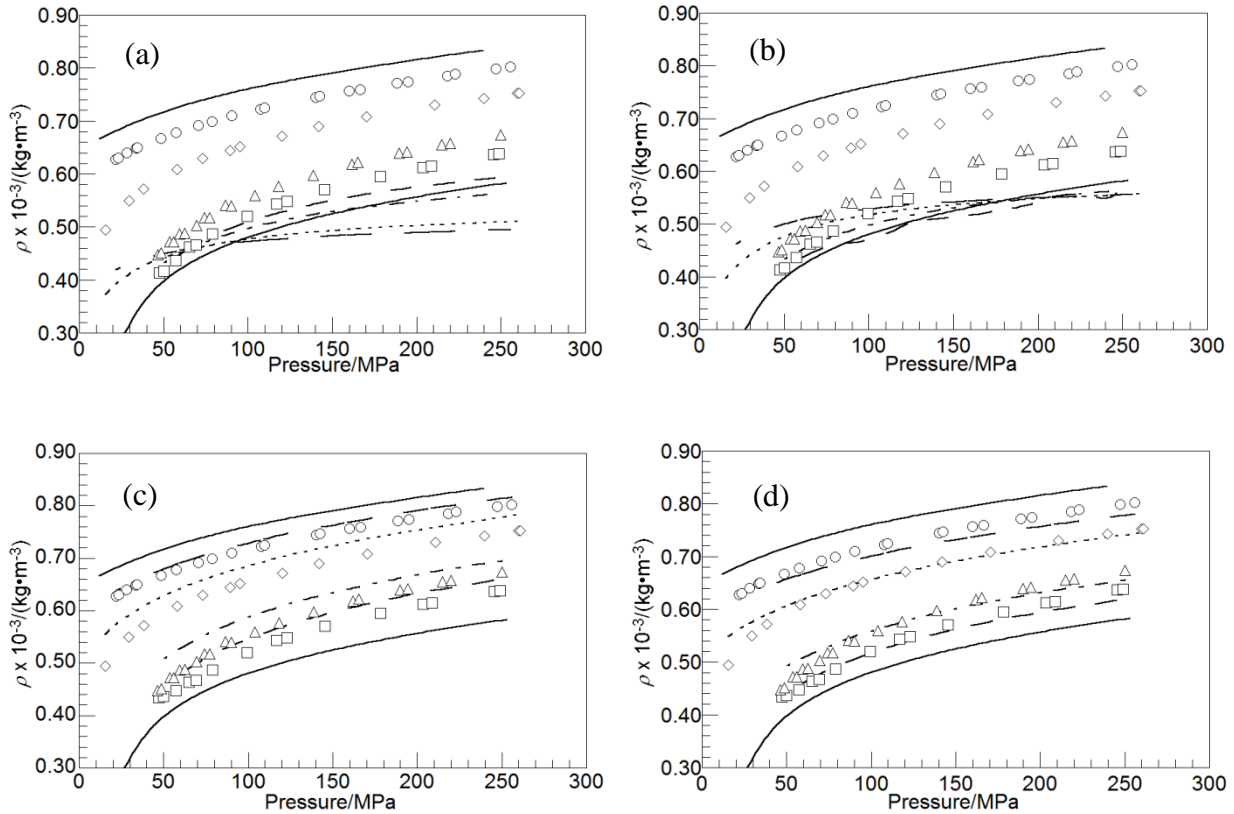
Figure 4.23. Comparison of the performance of (a) PREoS, (b) VT-PREoS, (c) Low-P PC-SAFT EoS, and (d) HTHP PC-SAFT EoS predictions (dashed lines) with the experimental density data (symbols) at ~520 K for the C_3-C_{30} mixture at 0.6550 (○) and (—— ——); 0.7960 (◊) and (- —- —); 0.9439 (Δ) and (········);and 0.9752 (□) and (— — —) propane mole fraction. The solid lines represent pure squalane density (top) and propane density data (bottom).

In the case of the PC-SAFT EoS, the predictions with the Low-P parameters overpredict virtually all of the mixture densities at all three isotherms, especially at high pressures. It is remarkable that the PC-SAFT EoS predictions with the Low-P parameters provide similar prediction performance to the HTHP correlated volume-translated version of the PREoS. This shows the superior performance of the PC-SAFT EoS over the cubic EoS in general for

predicting HTHP mixture density data in the sense that the cubic EoS with parameters correlated to HTHP data only provided similar predictions to the PC-SAFT EoS even with Low-P parameters. The inferior performance of the cubic EoS can be attributed to the semi-empirical nature of the equation unlike the PC-SAFT EoS that has a theoretical thermodynamic basis. Overall, the PC-SAFT EoS with the HTHP parameters provide the best predictions of all the models evaluated

4.3.4. Modeling Results for Propane-Eicosane (C_3-C_{20}) Phase Behavior

Experimental phase behavior data for the C_3-C_{20} mixture are also modeled with the cubic- and the SAFT-based EoS. For the cubic EoS, the results for the PREoS and the VT-PREoS are exactly the same since the volume-translation does not affect calculations for the phase equilibiria [34,117]. However, both the Low-P and the HTHP pure component parameters are tested with the PC-SAFT EoS for vapor-liquid equilibria predictions. Figure 4.24 shows the performance of the PREoS in modeling the experimental data for five isotherms. Figure 4.25 shows the modeling performance of the PC-SAFT with Low-P parameters and Figure 4.26 shows the performance with the HTHP parameters for the same experimental data. All the calculations are obtained with the binary interaction parameter, k_{ij}, set to zero to give a baseline comparison for all the equation of state models.
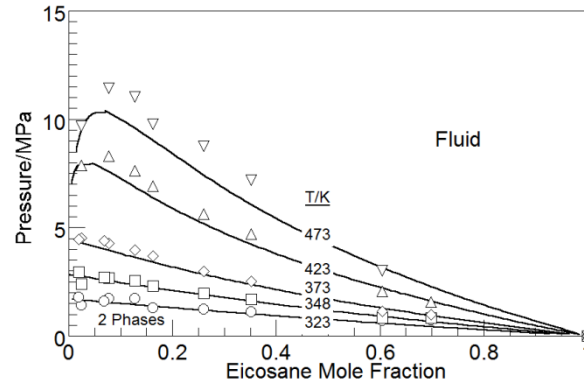
Figure 4.24. Comparison of the PREoS modeling predictions (lines) with the experimental data (symbols) for the C_3-C_{20} mixtures at five temperatures. Calculations are obtained with $k_{ij} = 0$.
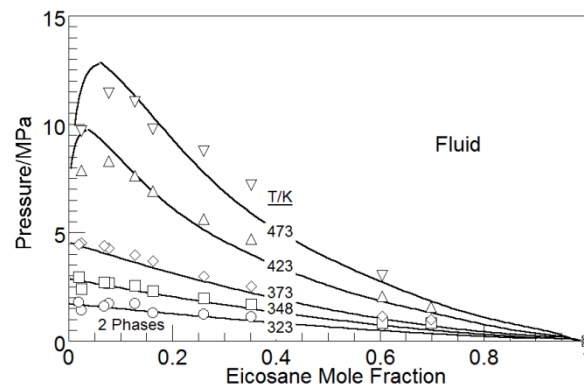
Figure 4.25. Comparison of the PC-SAFT EoS modeling predictions, using the Low-P pure component parameters (lines), with the experimental data (symbols) for the C_3-C_{20} mixtures at five temperatures. Calculations are obtained with $k_{ij} = 0$.

109
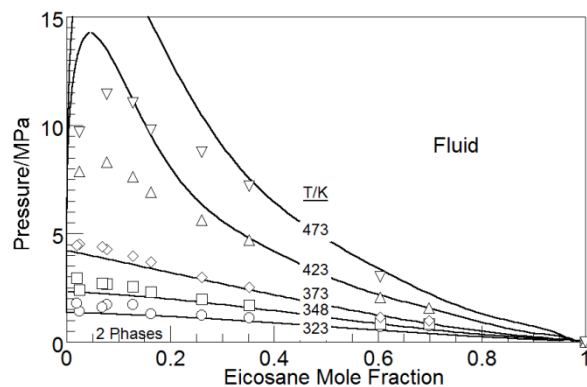
Figure 4.26. Comparison of the PC-SAFT EoS modeling predictions, using the HTHP pure component parameters (lines), with the experimental data (symbols) for the C_3-C_{20} mixtures at five temperatures. Calculations are obtained with $k_{ij} = 0$.

From the plots, it can be observed that all three models exhibit similar modeling characteristics for the the C_3-C_{20} mixtures at 323, 348, and 373 K. However, at 423 and 473 K, the PC-SAFT EoS with the HTHP parameters provided the worst predictions while also over estimating the mixture critical points. For the 423 K isotherm, the PREoS provided the best predictions, especially for the mixture critical point, while PC-SAFT with the Low-P parameters provided the best estimates of the mixture critical point for the 473 K isotherm. Clearly, the phase behavior prediction performance of these EoS is related to the genesis of their pure component parameters. The Low-P parameters for both the PREoS and the PC-SAFT EoS were obtained by fitting the vapor-pressure curves, while the HTHP parameters for the PC-SAFT are obtained by fitting only HTHP density data. Therefore, it is not surprising that the PC-SAFT with the HTHP parameters gave the worst performance among the models tested since the experimental phase behavior data are at moderately low pressures. A similar observation

www.manaraa.com

between the performances of the two sets of PC-SAFT pure component parameters for the C_3-C_{10} binary mixture is reported by Burgess *et al*. [54].

As with asymmetric binary mixtures, it is often necessary to use a small, nonzero k_{ij} value for modeling the phase behavior. For the C_3-C_{20} system, it is not possible to obtain a quantitative fit of the phase behavior data over the entire temperature and composition ranges with a single k_{ij} value [118]. Therefore, the value that yields the "best fit" of k_{ij} is chosen that provides the best vapor-liquid equilibria predictions for the 373 K isotherm. The k_{ij} value thus obtained is 0.02 for both the PREoS and the Low-P PC-SAFT EoS. The performance of the PREoS with Low-P parameters and with $k_{ij} = 0.02$ is shown in Figure 4.27 and the performance of the PC-SAFT EoS with Low-P parameters and with $k_{ij} = 0.02$ is shown in Figure 4.28. Note that the small k_{ij} value of 0.02, as obtained here, does not result in a significant change in the performance of the EoS for modeling mixture density data. It has been recently demonstrated for the PC-SAFT EoS that density calculations are more sensitive to the size parameter, σ, while phase behavior calculations are more sensitive to the energy parameter, ε. [119]. Therefore, the small change in ε caused by the k_{ij} does not significantly affect the performance of the PC-SAFT models for density calculations.
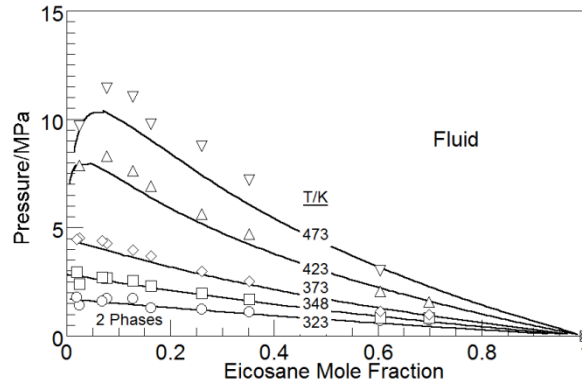
Figure 4.27. Comparison of the PREoS modeling predictions (lines) with the experimental data (symbols) for the C_3-C_{20} mixtures at five temperatures. Calculations are obtained with $k_{ij} = 0.02$.
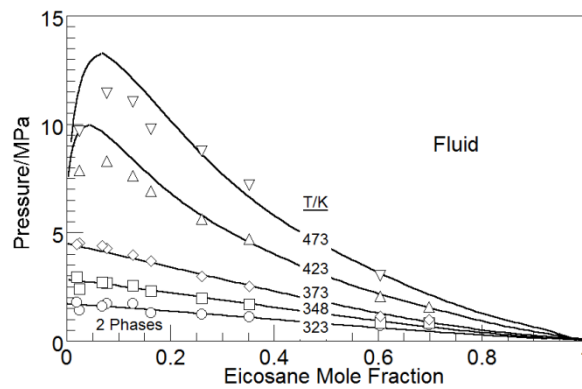
Figure 4.28. Comparison of the PC-SAFT EoS modeling predictions, using the Low-P pure component parameters (lines), with the experimental data (symbols) for the C_3-C_{20} mixtures at five temperatures. Calculations are obtained with $k_{ij} = 0.02$.

4.3.5. Concept of Hybrid PC-SAFT EoS

From the previous two sections, it can be concluded that the EoS models, especially the PC-SAFT EoS, have their various strengths at different temperature and pressure conditions. The Low-P parameters obtained by fitting the EoS to the vapor pressure curve tend to over-predict

the density in the HTHP region. In addition, the parameters obtained by fitting the EoS to HTHP density data do not adequately predict the phase behavior data. Therefore, a concept was proposed in the literature that provides a way to continuously hybridize the two sets of pure-component parameters for PC-SAFT EoS calculations [120] over a wide range of operating conditions. The "hybrid" parameters are expressed as a function of pressure and are defined in equations 4.9-4.12 for the three pure component parameters. In essence, this method favors the Low-P parameters at low pressure conditions and the HTHP parameters at the high pressure conditions. The disadvantage of this method is that the pure component parameters are now implicit in pressure. For practical purposes however, the concept of "hybridizing" the parameters can be a useful tool for reliably calculating themophysical properties of hydrocarbons and their mixtures over a wide range of conditions. However, the results for the hybrid PC-SAFT are not investigated in this study

$$m = m_{Low-P} + \left(m_{HTHP} - m_{Low-P} \right) \left(1 - e^{-\left(\frac{P}{100} \right)^2} \right) \tag{4.9}$$

$$\sigma_0 = \sigma_{Low-P} + \left(\sigma_{HTHP} - \sigma_{Low-P} \right) \left(1 - e^{-\left(\frac{P}{100} \right)^2} \right) \tag{4.10}$$

$$\sigma = \sigma_0 \left(1 - 0.12 \cdot \left| \left(\sigma_{HTHP} - \sigma_0 \right) \left(\sigma_{Low-P} - \sigma_0 \right) \right| \right) \tag{4.11}$$

$$\frac{\varepsilon}{k} = \left(\frac{\varepsilon}{k} \right)_{Low-P} + \left[\left(\frac{\varepsilon}{k} \right)_{HTHP} - \left(\frac{\varepsilon}{k} \right)_{Low-P} \right] \left(1 - e^{-\left(\frac{P}{100} \right)^2} \right) \tag{4.12}$$

113

4.4 Final Comments

Binary mixture density data are reported for propane mixtures at various compositions with decane, eicosane, and squalane at temperatures to 525 K and pressures to 265 MPa. Vapor-liquid equilibria phase behavior data are also reported for the C_3-C_{20} mixture for 10 isopleths at temperatures to 473 K. Mixture density data for C_3-C_{10} mixtures compare well to the limited available literature data [16,17] while phase behavior data for the C_3-C_{20} mixture are compared to the data of Gregorowicz *et al.* that was only reported to 358 K [115]. Therefore, this study has successfully extended the literature database for these mixtures to HTHP conditions related to formation in ultra-deep reservoirs as obtained in the Gulf of Mexico. Performance of cubic-based and SAFT-based EoS are compared against the reported experimental data. The PC-SAFT EoS especially with HTHP parameters provide the best density predictions for the three binary mixtures where the best results were obtained for the C_3-C_{10} mixture. However, the PC-SAFT with HTHP parameters provide the worst predictions for the C_3-C_{20} mixture phase behavior data and the PC-SAFT EoS with Low-P parameters provide reasonable predictions, which are also similar to predictions obtained with the PC-SAFT EoS.

Chapter 5 Experimental and Modeling Results for Two Crude Oil Samples

5.1. Introduction

To properly validate the suitability of the PC-SAFT EoS model previously shown to give a good representation of the properties of hydrocarbon mixtures, there is the need to test model predictions against the properties of real crude oil systems. In addition, the properties need to be obtained at high-temperature, high pressure (HTHP) conditions for the appropriate evaluation of the model for ultra-deep well reservoir applications. However, to our knowledge, no published data are available for crude oil systems at temperatures higher than ~ 400 K and 155 MPa [121]. In this study HTHP density data are measured for two Gulf of Mexico crude, stock-tank "dead" oil samples obtained from different companies that have operations in that region. The dead oil is the liquid fraction of the crude oil after it is flashed from reservoir temperature and pressure to ambient conditions and the gas contents of the live crude oil are liberated. The density measurements are reported for the two crude oil systems, as well as their mixtures with methane (to simulate a "live" crude oil) at temperatures to 523 K and pressures to 275 MPa.

For modeling calculations, it would be computationally expensive to account for each of the numerous components of crude oil. A useful method to overcome this is by suitable characterization of the crude oil as mixtures of well-defined fractions, which helps to greatly simplify the computation. Several characterization techniques, based on different properties of the oil, have been reported in the literature since the earliest studies reported by Katz and Firoozabadi [122-125]. These authors used boiling point temperatures to separate carbon number fractions by using the boiling points of *n*-paraffins to determine the cut points. The characterization procedure proposed by Whitson [125], widely used in upstream applications,

involves the subdivision of crude oil into single carbon number fractions. Other methods of crude oil characterization include the paraffins-naphathenes-aromatics (PNA) method based on refractive index data. All of these procedures utilize cubic EoS models, which have been demonstrated to be poor for modeling thermophysical properties of asymmetric mixtures. However, the PC-SAFT EoS [51], in conjunction with an appropriate characterization method, is a promising modeling prospect for predicting crude oil properties. The characterization method used in this study is based on the method used by Panuganti et al. [126], which is an extension of the work proposed by Ting et al. [127], used in the literature to model crude oil bubble points as well as asphaltene onset precipitation. The PC-SAFT EoS is used with correlations for the HTHP parameters published by Burgess *et al*. [54] and the Low-P parameters published by Gross and Sadowski [51].

5.2. Experimental Results and Correlations

5.2.1. Experimental Density Results

Density for dead crude oils A and B, presented in Tables 5.1 and 5.2, are measured from ambient conditions to 525 K and 270 MPa. In addition, density data are also obtained for simulated live oils containing ~5 wt% methane with dead oil A, presented in Table 5.3, and for simulated live oils containing ~10 wt% methane with dead oil B, presented in Table 5.4. The data are obtained using the experimental methods described in chapter 2. However, for these experiments the o-ring sealed floating piston is replaced with metal bellows to ensure there are no elastomeric o-rings in the experimental setup that can be degraded by any of the numerous components of the crude oil. Although the reported density are listed in the order increasing pressure for each isotherm, experimental pressures are chosen in a non-monotonous manner that

includes both increasing and decreasing order of pressure to minimize any experimental artifacts that might occur in the measurements and to verify the consistency of the experimental data.

Table 5.1. Experimental density data, ρ, at different temperatures, T, and pressures, P, for dead crude oil A, obtained in this study.

P /MPa	ρ /kg•m^{-3}	P /MPa	ρ /kg•m^{-3}	P /MPa	ρ /kg•m^{-3}
T/K =	325.2 ± 0.2		423.0 ± 0.1		522.5 ± 0.2
16.9	893	16.9	827		
34.1	904	34.1	842		
51.2	913	51.2	854	51.2	802
68.3	921	68.3	866	68.3	816
85.3	929	85.3	877	85.3	829
86.0	929	86.0	877	86.0	830
102.4	935	102.4	886	102.4	841
119.5	944	119.5	895	119.5	851
136.6	951	136.6	903	136.6	861
138.1	951	138.1	903	138.1	861
152.4	957	152.4	910	152.4	870
153.8	957	153.8	910	153.8	870
169.6	964	169.6	917	169.6	879
170.9	964	170.9	917	170.9	879
188.0	970	188.0	924	188.0	887
205.3	975	205.3	930	205.3	894
222.4	980	222.4	937	222.4	901
239.7	985	239.7	943	239.7	907
256.8	990	256.8	949	256.8	913
270.4	994	270.4	954	270.4	919

117

Table 5.2. Experimental density data, ρ, at different temperatures, T, and pressures, P, for dead crude oil B, obtained in this study.

P /MPa	ρ /kg•m^{-3}	P /MPa	ρ /kg•m^{-3}	P /MPa	ρ /kg•m^{-3}
T/K =	324.5 $\pm$ 0.1		424.0 $\pm$ 0.1		523.6 $\pm$ 0.2
3.1	882	3.1	815		
6.6	885	6.6	819	6.5	751
16.9	893	16.8	830	16.8	768
34.0	903	33.9	844	33.9	789
51.0	912	51.0	856	50.9	804
68.0	921	68.0	865	68.0	818
85.1	928	85.0	875	85.0	830
86.0	928	86.3	875	86.0	830
102.1	935	102.1	884	102.0	841
119.3	942	119.3	892	119.1	850
136.4	948	136.4	900	136.3	859
137.8	948	137.8	900	137.8	859
152.0	953	151.7	907	151.8	866
153.5	953	153.5	907	153.5	866
169.3	960	168.8	914	168.3	874
170.6	959	170.6	914	170.5	874
187.7	966	187.7	921	187.6	882
204.9	971	204.9	927	204.8	889
222.1	977	222.0	932	222.0	896
239.0	982	239.0	938	239.7	903
256.4	988	256.3	944	256.3	909
		269.9	949	269.9	914

Table 5.3. Experimental density data, ρ, at different temperatures, T, and pressures, P, for dead crude oil A mixture with 5 wt% methane obtained in this study.

P /MPa	ρ /kg•m^{-3}	P /MPa	ρ /kg•m^{-3}	P /MPa	ρ /kg•m^{-3}	P /MPa	ρ /kg•m^{-3}
T/K =	296.3 ± 0.1		324.5 ± 0.1		424.0 ± 0.5		520.6 ± 0.8
33.9	826	30.7	805	27.2	734		
47.8	840	34.1	808	34.0	743		
50.9	842	51.2	823	50.9	761	51.0	706
68.2	853	68.5	834	67.9	775	67.9	724
68.2	853	84.8	843	84.7	787	84.5	739
85.2	862	85.4	844	84.9	787	84.8	739
101.8	870	102.2	852	101.8	798	101.8	752
101.8	871	119.1	860	118.9	808	118.9	763
128.9	883	135.7	868	135.4	817	135.4	773
		136.2	868	135.8	817	135.7	773
		152.7	875	152.5	825	152.5	782
		153.2	875	152.9	826	153.0	782
		156.1	876	169.3	833	169.3	791
		159.5	878	169.9	833	169.8	791
		160.0	878	186.9	840	186.8	800
				203.4	846	203.4	807
				220.4	853	220.4	815
				237.4	860	237.4	822
				251.0	865	254.4	828
				253.8	866	270.0	834

Table 5.4. Experimental density data, ρ, at different temperatures, T, and pressures, P, for dead crude oil B mixture with 10 wt% methane obtained in this study.

P /MPa	ρ /kg·m^{-3}	P /MPa	ρ /kg·m^{-3}	P /MPa	ρ /kg·m^{-3}	P /MPa	ρ /kg·m^{-3}
T/K =	323.6 ± 0.1		364.2 ± 0.3		423.7 ± 0.3		523.7 ± 0.8
51.0	772	51.0	747	50.9	706	67.8	667
68.0	787	67.9	763	67.9	726	67.8	667
84.6	798	84.6	775	84.5	741	84.5	687
85.0	799	85.0	776	84.9	741	84.8	688
101.9	809	101.8	786	101.8	754	101.7	703
119.0	819	119.8	797	118.9	766	118.8	718
135.6	827	135.5	805	135.5	775	135.4	730
135.9	827	135.5	805	135.8	776	135.7	731
152.6	834	135.9	805	152.5	784	152.4	742
153.1	834	152.5	814	152.7	785	152.9	742
169.5	841	169.4	821	169.4	793	169.3	752
170.1	841	170.0	822	169.9	793	169.7	752
187.1	848	187.0	829	186.9	801	186.9	761
203.6	854	203.5	835	203.5	808	203.4	769
220.7	861	203.5	835	220.3	816	220.5	777
237.7	867	237.5	847	237.6	822	237.5	784
254.8	873	254.5	854	254.6	828	254.5	791
270.3	880	270.2	860	270.2	834	270.1	797

5.2.2. Modified Tait Equation Fit to Experimental Density Data

The modified Tait equation [20] is fitted to experimental data reported here for the crude oil samples. Equation 5.1 gives the Tait equation where ρ_0 is the density at P_0, which is chosen as 0.1 MPa, while B and C are adjustable parameters.

$$\frac{\rho - \rho_0}{\rho} = C \log_{10} \frac{P + B}{P_0 + B}$$

(5.1)

$$\delta = \frac{1}{n} \sum_{1}^{n} \left| \frac{\rho_{i,\text{Tait}} - \rho_{i,\text{experimental}}}{\rho_{i,\text{experimental}}} \right| \bullet 100$$

(5.2)

The Tait equation parameters are again optimized by minimizing the mean absolute percent deviation (δ, equation 5.2) while adjusting the parameters. A single value of C is used for each system while ρ_0 and B are quadratic functions of temperature as given in equations 5.3 and 5.4, respectively. Table 5.5 lists the parameters for each system along with the δ and the standard deviation, λ, for the fit. Note that the value of C obtained is the same for all the dead crude oils and their mixtures with methane. The C value is also similar to what was obtained for the well-characterized pure compounds and binary mixtures investigated in the earlier chapters.

$$\rho_0 / (kg \bullet m^{-3}) = \sum_{i-0}^{2} a_i (T / K)^i$$

(5.3)

$$B / MPa = \sum_{i-0}^{2} b_i (T / K)^i$$

(5.4)

121

Table 5.5. Tait equation parameter fits, mean absolute percent deviations, δ, and standard deviation values, λ, for δ, obtained for the crude oil samples A and B and their mixtures with methane.

Fluid	Crude A	Crude B	Crude A + 5 wt.% methane	Crude B + 10 wt.% methane
C	0.2275	0.2275	0.2275	0.2275
a_0	1133.0	1123.0	1055.3	891.76
a_1	-0.8284	-0.8258	-0.8772	-0.20445
a_2	$1.828 \cdot 10^{-4}$	$2.195 \cdot 10^{-4}$	$1.102 \cdot 10^{-4}$	$9.452 \cdot 10^{-4}$
b_0	375.00	370.00	307.06	243.17
b_1	-0.9805	$-1.091 \cdot 10^{-4}$	-0.9660	-0.7791
b_2	$6.956 \cdot 10^{-4}$	$8.526 \cdot 10^{-4}$	$8.128 \cdot 10^{-4}$	$6.321 \cdot 10^{-4}$
δ	0.15	0.14	0.16	0.14
λ	0.11	0.16	0.13	0.15

5.3. PC-SAFT EoS Modeling Methods for Crude Oil

In recent PC-SAFT modeling studies of crude oils, it has been established that dispersion forces and not polarity is the major intermolecular force that dominates phase behavior calculations [126,128-130]. It is therefore not necessary to account for intermolecular association in the PC-SAFT equation and only three adjustable parameters are required: the number of segments, m, the temperature-independent segment diameter, σ, and the segment-segment dispersion interaction energy, ε/k. The parameters are obtained for pure compounds by fitting the PC-SAFT EoS to experimental vapor pressure and density data and these parameters are reported

for methane by Gross and Sadowski [51]. However, crude oils contain numerous compounds and it is not feasible to account for the pure component parameters for all the compounds. Fortunately, PC-SAFT parameters have been demonstrated to be a smooth function of molecular weights for several chemical families [131]. Therefore, the crude oil must be divided into fractions including saturates, aromatics + resins, and asphaltenes. The PC-SAFT EoS parameters for each fraction are thus obtained from molecular weight correlations as described by Punnapala and Vargas [130] for a set of Low-P parameters and are listed in Table 5.6. A similar correlation scheme has been used to obtain HTHP parameters, which are listed in Table 5.7. In the tables, the aromaticity parameter, γ, is present in the correlations for both aromatic + resin and asphaltene fractions. A $\gamma = 0$ value means that the component in question has 100% of the character of a polynuclear aromatic (PNA) while a $\gamma = 1$ value means that the component only contains benzene derivatives, such as an alkyl benzene [127]. Gonzalez *et al.* [131] reversed this definition, setting $\gamma = 0$ for benzene derivatives and 1 for PNAs. In this work, we use the definition of Punnapala and Vargas [130], who defined $\gamma = 0$ for saturates, not benzene derivatives, and 1 for PNAs.

Table. 5.6. Low-P PC-SAFT pure component parameter correlations for each dead oil fraction. [130]

Correlations for saturates	Correlations for aromatics + resins and asphaltenes
$m = 0.0257 * M_w + 0.8444$	$m = (1-\gamma)(0.0257 * M_w + 0.8444) + \gamma(0.0101 * M_w + 1.7296)$

$$\sigma = 4.047 - 4.8013\frac{\ln\left(M_w\right)}{M_w}$$

$$\sigma = \left(1-\gamma\right)\left(4.047 - 4.8013\frac{\ln\left(M_w\right)}{M_w}\right)$$
$$+\gamma\left(4.6169 - \frac{93.98}{M_w}\right)$$

$$\varepsilon/k = \exp\left(5.5769 - \frac{9.523}{M_w}\right)$$

$$\varepsilon/k = \left(1-\gamma\right)\exp\left(5.5769 - \frac{9.523}{M_w}\right)$$
$$+\gamma\left(508 - \frac{234100}{M_w^{1.5}}\right)$$

Table. 5.7. HTHP PC-SAFT pure component parameter correlations for each dead oil fraction.

Correlations for saturates	Correlations for aromatics + resins, and asphaltenes
$m = 0.04117 * M_w + 0.8955$	$m = \left(1-\gamma\right)\left(0.04117 * M_w + 0.8955\right)$ $+\gamma\left(0.02617 * M_w + 1.7751\right)$
$\sigma = 0.1430 * M_w + 2.578$	$\sigma = \left(1-\gamma\right)\left(0.1430 * M_w + 2.578\right)$ $+\gamma\left(4.811 - 0.09209 * M_w\right)$
$\varepsilon/k = \exp\left(5.5443 - \frac{13.237}{M_w}\right)$	$\varepsilon/k = \left(1-\gamma\right)\exp\left(5.5443 - \frac{13.237}{M_w}\right)$ $+\gamma\left(-103.02 + 81.535 * \ln\left(M_w\right)\right)$

5.3.1. Characterization Results

The organic contents of crude oils are predominantly present as saturated and unsaturated hydrocarbons. Therefore, the dead oils used in this study can be characterized based on the amount of saturates, aromatics, resins, and asphaltenes (SARA) contents of the dead oil. The composition of the stock tank oil is thus simplified using the SARA method, which has been

124

applied on several occasions for PC-SAFT modeling of asphaltene precipitation in crude oil systems [126,130-132]. The saturate fraction contains linear, branched, and cyclic hydrocarbons. Aromatics comprise any molecule that contains one or more aromatic rings. Resins, or polar aromatics that contain at least one polar heteroatom such as oxygen, comprise the fraction of the stock tank oil that is insoluble in propane yet soluble in *n*-pentane, *n*-heptane, and toluene [130]. Asphaltenes are defined as the portion of the oil that is soluble in aromatic solvents such as toluene but insoluble in light alkane solvents such as *n*-pentane [126,130].

5.3.2. Asphaltene Precipitation and Solid Phase Extraction

Asphaltenes contents of the dead crude oil samples are first precipitated by mixing with pentane on a 1 g oil to 40 mL pentane basis, and recovered using Whatman 0.8 micron filter paper. Once the asphaltene components of the crude oil samples are removed, the SARA analysis is completed by running solid phase extraction (SPE) experiments. Briefly, 4 mL of the pentane-soluble fraction of the crude oil is injected onto an SPE column (Supelco Discovery® SPE DSC-Si Silica Tube with a 12 mL volume, and a 2 g packing mass). The saturate contents are extracted with pentane, followed by the extraction of the aromatic contents with toluene. Lastly, the resin fractions are obtained by extraction with ethyl acetate. Table 5.8 shows the SARA analysis results as relative mass distribution of saturates, aromatic and resin, and asphaltene fractions for the two dead crude oil samples. The saturates content of crude A is higher while crude B has a higher amount of the aromatic + resins as well as asphaltenes.

Table 5.8. Saturates, aromatics + resins, and asphaltenes compositional fraction of dead crudes A and B.

Chemical Fraction	Crude A	Crude B
Saturates	0.6687	0.5637
Aromatics + Resins	0.2824	0.3789
Asphaltenes	0.0489	0.0573

5.3.3. GC Analyses and Crude Oil Molecular Weight Determination

The molecular weight distribution of the crude oils are obtained from the results of gas chromatography (GC) analyses using an Agilent 6890 gas chromatograph. The mobile phase, helium, is set at a flow rate of 1.5 mL/minute and the stationary phase is a dimethyl polysiloxane film of thickness 0.10 μm. The GC column (0.53 mm inside diameter, 5 meters long, Restek Corporation, 70112) can be operated for sustained times at temperatures to 430° C (703 K) with minimal column bleed, *i.e.*, loss of the stationary phase as a result of high temperature. A flame ionization detector is used based on the proportionality of the response to the mass of species present. Crude oil samples are prepared in carbon disulfide (CS_2) at a 40:1 mass ratio of CS_2 to oil since all crude oil species, including asphaltenes, are soluble in CS_2. The relatively low concentration of oil is chosen in order to extend the lifetime of the column.

Molecular weight distributions are determined from the mass fraction results obtained from the GC chromatograms. For carbon number 6 through 9, the identity and quantity of the prevalent species are determined and a weighted average molecular weight is defined for each carbon number fraction. Molecular weights and specific gravities for each specific carbon number (SCN) fraction of carbon number 10 through 33 are defined in the manner put forth by

126

Katz and Firoozabadi [122]. The remaining components are lumped into one fraction that encompasses all components of carbon number 34 and above. The molecular weight of this component is determined from the overall molecular weight of the oil sample in question. The results for crude oil A are presented in Table 5.9 and the results for crude oil B are presented in Table 5.10.

Table 5.9. Whitson characterization representation for heavy Gulf of Mexico oil, crude A.

Component		Molecular Weight	Density	Stock Tank Oil		Simulated Res. Fluid	
(Symbol/Name)		g/mol	g/cc	mol%	wt%	mol%	wt%
CH_4	Methane	16.04		0.000	0.000	44.36	5.00
C_6	Hexanes	86.18	0.664	5.75	2.03	3.20	1.94
C_7	Heptanes	94.99	0.703	6.84	2.67	3.80	2.54
C_8	Octanes	109.19	0.725	7.33	3.29	4.08	3.13
C_9	Nonanes	121.14	0.758	6.50	3.23	3.62	3.07
C_{10}	Decanes	134.72	0.779	6.28	3.45	3.49	3.29
C_{11}	Undecanes	147.00	0.790	5.93	3.58	3.30	3.41
C_{12}	Dodecanes	161.00	0.801	5.54	3.66	3.08	3.49
C_{13}	Tridecanes	175.00	0.812	5.17	3.71	2.88	3.54
C_{14}	Tetradecanes	190.00	0.823	4.95	3.86	2.75	3.67
C_{15}	Pentadecanes	206.00	0.833	4.55	3.84	2.53	3.66
C_{16}	Hexadecanes	222.00	0.840	3.93	3.58	2.19	3.41
C_{17}	Heptadecanes	237.00	0.848	3.31	3.22	1.84	3.06
C_{18}	Octadecanes	251.00	0.853	2.69	2.77	1.50	2.64
C_{19}	Nonadecanes	263.00	0.858	2.29	2.47	1.27	2.35
C_{20}	Eicosanes	275.00	0.863	2.45	2.77	1.36	2.64
C_{21}	Heneicosanes	291.00	0.868	2.37	2.83	1.32	2.70
C_{22}	Docosanes	305.00	0.873	1.94	2.43	1.08	2.32
C_{23}	Triacosanes	318.00	0.878	1.72	2.24	0.96	2.14
C_{24}	Tetracosanes	331.00	0.882	1.64	2.23	0.91	2.12
C_{25}	Pentacosanes	345.00	0.886	1.56	2.21	0.87	2.10
C_{26}	Hexacosanes	359.00	0.890	1.48	2.17	0.82	2.07
C_{27}	Heptacosanes	374.00	0.894	1.35	2.07	0.75	1.97
C_{28}	Octacosanes	388.00	0.897	1.19	1.90	0.66	1.81
C_{29}	Nonacosanes	402.00	0.900	1.09	1.80	0.61	1.72
C_{30}	Triacontanes	416.00	0.903	1.00	1.71	0.56	1.63
C_{31}	Hentriacontanes	430.00	0.907	0.92	1.63	0.51	1.55

127

		Molecular Weight	Density	Stock Tank Oil		Simulated Res. Fluid	
C_{32}	Dotriacontanes	444.00	0.910	0.85	1.55	0.47	1.47
C_{33}	Tritriacontanes	458.00	0.913	0.78	1.47	0.43	1.40
C_{34+}	Tetratriacontanes+	718.00	0.915	8.61	25.39	4.79	24.18

Molecular Weight = 243

Table 5.10. Whitson characterization representation for heavy Gulf of Mexico oil, crude B.

Component		Molecular Weight	Density	Stock Tank Oil		Simulated Res. Fluid	
(Symbol/Name)		g/mol	g/cc	mol%	wt%	mol%	wt%
CH_4	Methane	16.04		0.000	0.000	63.85	10.00
C_6	Hexanes	86.18	0.664	2.97	1.01	1.07	0.90
C_7	Heptanes	94.99	0.703	4.82	1.80	1.74	1.62
C_8	Octanes	109.19	0.725	5.96	2.56	2.15	2.30
C_9	Nonanes	121.14	0.758	5.78	2.75	2.09	2.47
C_{10}	Decanes	134.72	0.779	5.94	3.13	2.15	2.81
C_{11}	Undecanes	147.00	0.790	5.88	3.40	2.13	3.05
C_{12}	Dodecanes	161.00	0.801	5.71	3.61	2.06	3.24
C_{13}	Tridecanes	175.00	0.812	5.49	3.78	1.98	3.39
C_{14}	Tetradecanes	190.00	0.823	5.39	4.02	1.95	3.61
C_{15}	Pentadecanes	206.00	0.833	5.05	4.09	1.83	3.67
C_{16}	Hexadecanes	222.00	0.840	4.44	3.87	1.60	3.48
C_{17}	Heptadecanes	237.00	0.848	3.78	3.52	1.37	3.16
C_{18}	Octadecanes	251.00	0.853	3.10	3.06	1.12	2.75
C_{19}	Nonadecanes	263.00	0.858	2.65	2.74	0.96	2.46
C_{20}	Eicosanes	275.00	0.863	2.86	3.09	1.03	2.77
C_{21}	Heneicosanes	291.00	0.868	2.78	3.18	1.00	2.85
C_{22}	Docosanes	305.00	0.873	2.28	2.74	0.83	2.46
C_{23}	Triacosanes	318.00	0.878	2.02	2.53	0.73	2.27
C_{24}	Tetracosanes	331.00	0.882	1.93	2.51	0.70	2.26
C_{25}	Pentacosanes	345.00	0.886	1.83	2.48	0.66	2.23
C_{26}	Hexacosanes	359.00	0.890	1.73	2.45	0.63	2.20
C_{27}	Heptacosanes	374.00	0.894	1.58	2.32	0.57	2.08
C_{28}	Octacosanes	388.00	0.897	1.39	2.12	0.50	1.91
C_{29}	Nonacosanes	402.00	0.900	1.27	2.01	0.46	1.81
C_{30}	Triacontanes	416.00	0.903	1.17	1.91	0.42	1.71
C_{31}	Hentriacontanes	430.00	0.907	1.07	1.80	0.39	1.62
C_{32}	Dotriacontanes	444.00	0.910	0.98	1.71	0.35	1.53
C_{33}	Tritriacontanes	458.00	0.913	0.90	1.61	0.32	1.45
C_{34+}	Tetratriacontanes+	672.00	0.915	9.24	24.43	3.34	21.93

Molecular Weight = 255

5.3.4. Elemental Analyses

Elemental analyses of the dead crude oils and their associated asphaltene fractions is obtained using a Perkin Elmer Series II CHNS/O Analyzer (model 2400). Prior to analysis, the asphaltene fractions are dried for 24 hours under vacuum (30 mm Hg) and ambient temperature to remove any volatile, non-asphaltene compounds left from the precipitation experiments. Both crude oil samples are run as is. The analyzer is calibrated using pure *n*-tetradecane as the standard reference material. From the results, the hydrogen-to-carbon ratios (H/C) are obtained and shown in Table 5.11 along with the aromaticity values, γ, for each crude oil as well as their asphaltene fractions.

Table 5.11. Values of H/C molecular ratio in dead crude oils and their associated asphaltene fractions. Aromaticity, γ, is calculated using the method of Huang and Radosz. [133]. The molecular weights of the crude oils are given in Tables 5.9 and 5.10 while that of the asphaltenes is set at 1700 g/mol as is done in the literature [126,127].

	H/C	Aromaticity γ
Crude A	1.69	0.269
Crude B	1.67	0.285
Asphaltenes A	0.716	0.506
Asphaltenes B	0.638	0.509

Typically, the value of γ for the aromatics + resins component is obtained from a fit to reservoir fluid bubble point data while the γ value for asphaltenes is obtained from a fit to

asphaltene onset pressure data at which point the asphaltene contents of a live crude oil are precipitated. However, in this work, the γ values are "experimentally estimated" from knowledge of the molecular H/C ratio of the crude oil as obtained from elemental analysis characterization results. The values for γ are calculated using the correlations proposed by Huang and Radosz [133]. Strictly speaking, the correlations are only defined for use with hydrocarbons only containing hydrogen and carbon atoms. However, crude oils do contain a small amount of sulfur, oxygen, nitrogen, and other heteroatoms. These heteroatoms are not deemed to be present in sufficient amount to significantly alter the γ calculations and are, thus, neglected. The γ values are calculated using equation 5.5 where CN, defined in equation 5.6 is the carbon number of the hydrocarbon in question. CN_p is the carbon number that a sample of that molecular weight would possess if it were 100% saturate character, and CN_{PNA} is the carbon number that it would possess if it had 100% PNA character. CN, CN_p, and CN_{PNA} are calculated as indicated by Huang and Radosz [133].

$$\gamma = \frac{CN - CN_p}{CN_{PNA} - CN_p} \tag{5.5}$$

$$CN = \frac{M_w}{12.011 + 1.0079\left(H/C\right)} \tag{5.6}$$

The aromaticity of the aromatic + resin fraction is calculated by taking a weighted average over the dead oil and using the values obtained for the dead oil and the asphaltene fraction according to equation 5.7. Note that in equation 5.7, the aromaticity value for the saturate fraction is already set to zero as previously defined and obtained from Punnapala and Vargas [130].

$$\gamma_{A+R} = \frac{\gamma_{oil} - w_{asph}\gamma_{asph}}{w_{A+R}} \tag{5.7}$$

5.4. PC-SAFT Density Predictions

Once the characterization results are obtained, the PC-SAFT EoS can now be employed to model the crude oil density reported in this study. The PC-SAFT EoS is used with correlations for both the Low-P and HTHP sets of parameters as defined in section 5.3. The PC-SAFT EoS HTHP density modeling results for crude A and its mixture with 5 wt% methane are presented in Table 5.12 using both the Low-P and the HTHP sets of parameters. It is obvious that the PC-SAFT EoS gives the best density predictions when using the HTHP parameters for the "simulated live" oil A. Surprisingly the model also gave the worst results when using HTHP parameters for the dead oil A, while the Low-P parameters improved the predictions for the dead oil HTHP density. Similar modeling results, presented in Table 5.13, are obtained with crude oil B for both the dead oil and the "simulated live" oil with 10 wt% methane added to the dead oil. The performance of each set of parameters with the PC-SAFT EoS for modeling crude oil B is parallel to the results obtained for crude oil A. Overall, the model gives slightly better predictions with either set of parameters for crude oil B than crude oil A.

131

Table 5.12. PC-SAFT EoS HTHP density modeling results for dead crude oil A and its mixture with 5 wt% methane (CH_4). The aromaticity, γ, is 0.867 for the aromatic + resin fraction and 0.506 for the asphaltene fraction.

Crude Oil	T/K	δ Low-P	λ Low-P	δ HTHP	λ HTHP
A	325.2	1.46	0.97	3.84	0.19
	423.0	1.43	0.79	4.20	0.11
	522.5	0.98	0.54	4.46	0.09
A + 5 wt% CH_4	296.3	0.28	0.23	0.84	0.29
	324.5	0.54	0.36	0.78	0.28
	424.0	1.39	0.54	0.76	0.19
	520.6	2.09	0.63	0.70	0.33

Table 5.13. PC-SAFT EoS HTHP density modeling results for dead crude oil B and its mixture with 10 wt% methane (CH_4). The aromaticity, γ, is 0.676 for the aromatic + resin fraction and 0.509 for the asphaltene fraction.

Crude Oil	T/K	δ Low-P	λ Low-P	δ HTHP	λ HTHP
B	324.5	0.91	0.77	2.37	0.20
	424.0	0.91	0.78	2.76	0.17
	523.6	0.74	0.53	2.96	0.29
B + 10 wt% CH_4	323.6	0.28	0.15	0.87	0.29
	364.2	0.31	0.24	0.89	0.28
	423.7	0.65	0.30	0.80	0.28
	523.7	1.23	0.27	0.75	0.29
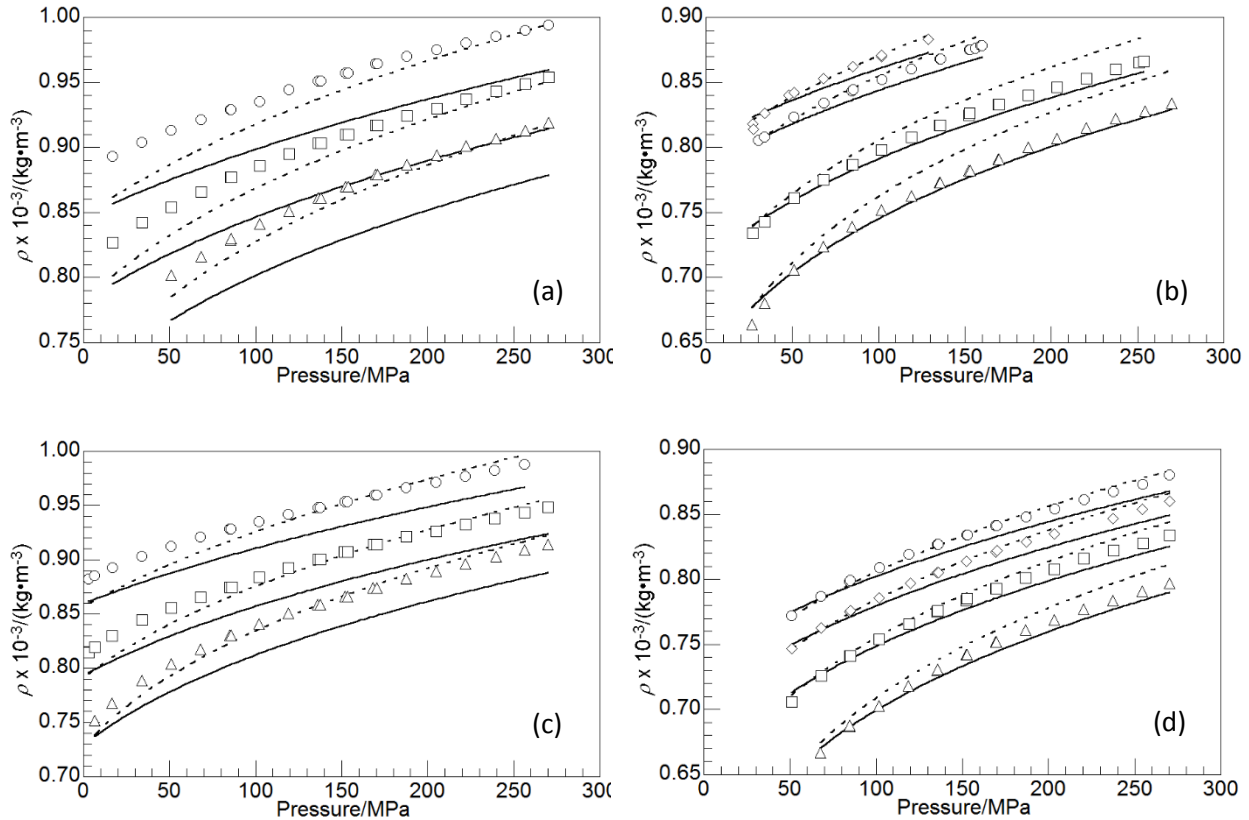
Figure 5.1. Comparison of the PC-SAFT EoS modeling performance for predicting HTHP density data for dead oil A (a), crude oil A mixture with 5 wt% methane (b), dead oil B (c), and crude oil B mixture with 10 wt% methane (d) using Low-P (·········) and the HTHP (——) parameters at 323 K (○), 423 K (□), and 523 K (Δ), while (◊) is 296 K in (b), and 364 K in (d).

It is not apparent why the PC-SAFT model with parameters fitted to vapor pressure and saturated liquid density data gives better density predictions than the PC-SAFT model with HTHP parameters fit to HTHP pure component density data. From the results for well-characterized binary mixtures obtained in chapter 4, the HTHP parameters gave better HTHP mixture density results. However, from the results presented in Figure 5.1, it can be observed that PC-SAFT density predictions for both dead oils are consistently lower than the experimental

المنارة للاستشارات

www.manaraa.com

results when using the HTHP parameters. In the case of the Low-P parameters, the PC-SAFT underpredicts the density at low pressures although the difference between calculated and experimental data decreases as the pressures increase. In fact, at high pressures, the model starts to overpredict the density data. For well-characterized systems, the PC-SAFT EoS with Low-P parameters typically overpredicts the density at high pressures by 5% or more [4,14,54,77,78]. The difference between predictions obtained with HTHP parameters and experimental data is essentially the same at every pressure, suggesting the slope for the predicted density is similar to the slope of the experimental data. As such, the PC-SAFT EoS predictions with HTHP parameters provides better predictions for second derivative properties than the Low-P parameters, despite the Low-P parameters providing the better density predictions.

PC-SAFT EoS predictions for the isothermal compressibility are compared with the isothermal compressibility calculated from the Tait equation fit to experimental data. The expression for the isothermal compressibility, β, is given in equation 5.8.

$$\beta = -\frac{1}{V}\left(\frac{\partial V}{\partial P}\right)_T \tag{5.8}$$

Table 5.14 presents the modeling results for the isothermal compressibility using both the Low-P and the HTHP parameters for crude oil A, while Table 5.15 presents similar results for crude B. Here the HTHP parameters give the best isothermal compressibility predictions as compared to the Low-P parameters for both the dead oils and their mixtures with methane.

Table 5.14. PC-SAFT EoS isothermal compressibility modeling results for dead crude oil A and its mixture with 5 wt% methane (CH_4). The aromaticity, γ, is 0.867 for the aromatic + resin fraction and 0.506 for the asphaltene fraction.

Crude Oil	T/K	δ Low-P	λ Low-P	δ HTHP	λ HTHP
	325.4	28.88	2.26	3.75	2.19
A	423.2	20.08	3.51	1.83	1.28
	522.5	14.99	2.85	0.99	0.50
	296.3	17.65	0.29	10.60	3.80
A + 5 wt%	323.8	15.82	0.36	7.67	4.45
CH_4	423.0	11.42	0.76	6.63	4.80
	520.6	14.54	4.89	1.40	2.01

Table 5.15. PC-SAFT EoS isothermal compressibility modeling results for dead crude oil B and its mixture with 10 wt% methane (CH_4). The aromaticity, γ, is 0.676 for the aromatic + resin fraction and 0.509 for the asphaltene fraction.

Crude Oil	T/K	δ Low-P	λ Low-P	δ HTHP	λ HTHP
	324.5	36.65	2.72	9.79	5.17
B	424.0	23.32	3.50	7.95	4.81
	523.6	18.87	3.36	7.74	4.75
	323.6	9.10	0.88	8.66	4.45
B + 10 wt%	364.2	7.72	0.21	8.87	3.97
CH_4	423.7	6.19	0.98	8.54	3.10
	523.6	3.98	3.17	8.55	0.58
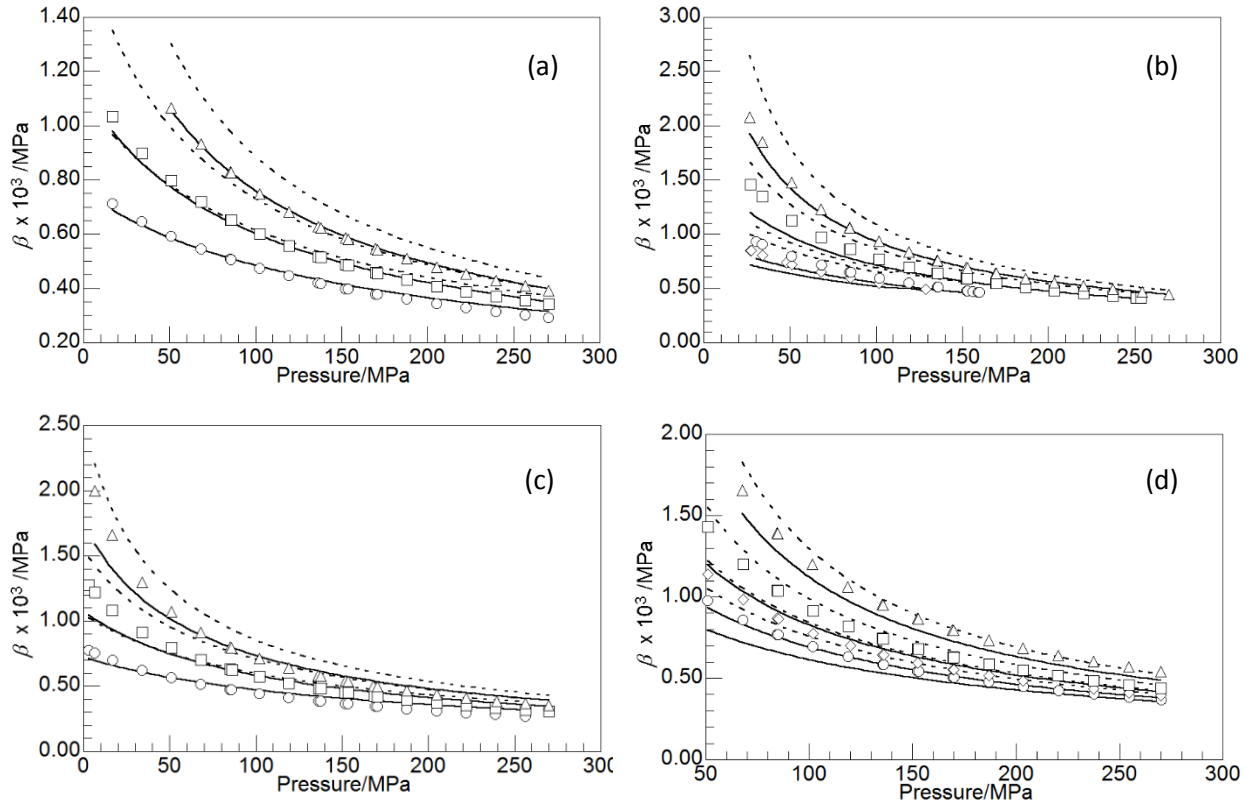
Figure 5.2. Comparing PC-SAFT EoS modeling performance using either the Low-P (········) or the HTHP (——) parameters for predicting isothermal compressibility for dead oil A (a), crude oil A mixture with 5 wt% methane (b), dead oil B (c), and crude oil B mixture with 10 wt% methane (d) at 323 K (○), 423 K (□), and 523 K (△), while (◊) is 296 K in (b), and 364 K in (d).

5.5 Final Comments

High-temperature, high-pressure densities are measured at temperatures to 523 K and pressures to 270 MPa for two dead crude oil samples supplied by two companies with operation in the Gulf of Mexico. This PhD study also reports densities at similar conditions for simulated live oils obtained by the addition of methane gas to the dead crude oils. PC-SAFT EoS modeling methodology obtained from the literature is applied to model the crude oil density reported here

136

without the use of any fitting parameter, as is required in the literature. The aromaticity parameters for both the aromatic + resin and the asphaltene fraction, γ, are estimated from the results of the elemental analysis of each oil. Fractional composition for the saturate, aromatic + resin, and asphlatene fractions are obtained from the SARA analysis of each dead oil. From these analyses results, the PC-SAFT EoS parameters are calculated from correlations to both the Low-P parameters and the HTHP parameters, which are then compared for modeling the HTHP crude oil density data obtained in this study.

The PC-SAFT EoS with either sets of parameters provided better fits for the simulated live crude oil data than for the dead crude oil data. Surprisingly though, the PC-SAFT EoS gave better density predictions when using the Low-P parameters as compared to the HTHP parameters. However, the Low-P parameters underpredict the density data at low pressures but overpredict the data at high pressures, which means the slope of the predicted density versus pressure curves are wrong. Furthermore, the performance of each set of parameters is evaluated to model the isothermal compressibility data obtained from a Tait equation correlation of the experimental density data. Here, the PC-SAFT EoS with the HTHP parameters provides the better fit of the isothermal compressibility data since the PC-SAFT EoS with the HTHP parameters more accurately represented the slope of the density versus pressure curves.

Chapter 6 Conclusion and Future Work

6.1. Conclusions

In order to meet the increasing world energy demand, search for newer sources for petroleum has led to the necessity of pursuing and recovering petroleum from ultra-deep reservoirs that are several miles beneath the earth's surface. These reservoirs exist at high-temperature, high-pressure conditions with temperatures that can be in excess of 500 K and/or pressures up to 200 MPa such as those found in the Gulf of Mexico. These conditions are projected to continue to rise as newer wells are explored. Knowledge of the thermophysical properties of petroleum constituents at these conditions is therefore crucial for safe and effective production of petroleum from these reservoirs. Hence, this PhD study covers a significant gap found in the literature by extending the thermophysical database of hydrocarbons and their mixtures to HTHP conditions with temperatures to 523 K and 275 MPa.

Experimental HTHP density data are reported for propane, squalane, and *bis* (2-ethylhexyl phthalate) as representative pure compounds. For the mixtures, HTHP densities are reported for propane binary mixtures with decane, eicosane, and squalane. Furthermore, density data are also reported for two dead crude oils delivered from the Gulf of Mexico along with densities for their mixtures with methane. Experimental data are measured with a variable-volume high-pressure view cell that is coupled to a linear variable differential transformer. The reported density data compare well, within the experimental uncertainty, to the limited available data in the literature.

The performance of the Peng-Robinson (PR), the HTHP volume-translated (VT) PR, and the Perturbed-Chain Associating Fluid Theory (PC-SAFT) equations of state (EoS). Parameters

138

needed for each equation are obtained from the literature from correlations to either vapor pressure and saturated density data or single-fluid phase HTHP density data. The PREoS gave the worst HTHP density predictions for the well-characterized systems but gives reasonable predictions for the vapor-liquid equilibria (VLE) of the propane-eicosane mixture. The HTHP VT-PREoS provided improved HTHP density predictions over the PREoS but the density predictions for low-volatility, high molecular weight compounds are poor. Both cubic EoS are semi-empirically based and require critical properties that are not readily available for high molecular weight compounds and must be inferred from indirect methods such as group contribution methods. The best HTHP density predictions were obtained with the PC-SAFT EoS especially when using HTHP pure component parameters, which however, gave the worst VLE predictions. The PC-SAFT EoS with Low-P parameters gave good predictions for the VLE data that are comparable to the PREoS results, although the density predictions are not as good as what was obtained with the HTHP parameters.

For the crude oils investigated here, the PC-SAFT EoS gave a good representation of the HTHP density data for both the dead crude oils and their mixtures with methane. Specifically, the PC-SAFT EoS with the Low-P parameters provided better density predictions within 1.5%, as compared to 4% obtained with the HTHP parameters, for the dead crude oils. The HTHP parameters provided marginally better density predictions for the dead oil mixtures with methane that are within 1%. Interestingly though, the PC-SAFT EoS with the HTHP parameters provided the better predictions for the isothermal compressibility, a second-derivative property, for both the dead crude oils and their mixtures with methane. The deviations from experimental data are within 10 % as compared to deviations, up to 37%, obtained with the Low-P parameters. This is because the HTHP parameters provided a closer match of the slope of the density versus pressure

curve for all the crude oil systems than the Low-P parameters, despite the fact that the Low-P parameters yielded better density predictions for the dead crude oils.

6.2. Future Work

The experimental data presented in this study extends the database for the hydrocarbon compounds and dead crude oils studied here to HTHP conditions. The study also attempted to simulate a live crude oil by the addition of methane. However experimental density and phase behavior data should be measured for real live reservoir oils. It will also be interesting to observe how the aromaticity parameter translate to systems of well-characterized systems. Additionally, live oil mixtures with brine and other processing fluids should also be experimentally studied at HTHP conditions to gain further understanding and ensure safe and efficient production from ultra-deep wells. The sapphire window in the setup of the high-pressure view cell allows for visual observation of the view cell and phase behavior data can thus be obtained. However, the opaque nature of crude oil renders the visualization useless in the measurement of phase behavior data. Therefore, other methods must be employed in order to obtain experimental phase behavior data for crude oil systems.

The experimental data reported in this study are modeled with the cubic- and the SAFT-based EoS with varying degree of success. Overall, the PC-SAFT EoS provided the best predictions especially with the right sets of pure component parameters. However, none of the models provided reliable predictions for both the VLE data and the HTHP density data and by extension the HTHP isothermal compressibility data. Therefore, further work is required in the developments and improvements of EoS models that can accurately capture the thermophysical properties of crude oil and its constituents at various conditions.

140

Literature Cited

[1] T. Baird, T. Fields, R. Drummond, D. Mathison, B. Langseth, A. Martin, L. Silipigno, Oilfield Rev. 10 (1998) 50-67.

[2] C. Avant, S. Daungcauw, B. Behera, S. Danpanich, W. Laprabang, I. De Santo, G. Heath, K. Osman, Z. Kahn, J. Russell, Oilfield Review 24 (2012) 4-19.

[3] G. DeBruijn, C. Skeates, R. Greenaway, D. Harrison, M. Parris, S. James, F. Mueller, S. Ray, M. Riding, L. Temple, Oilfield Rev 20 (2008).

[4] K. Liu, Y. Wu, M.A. McHugh, H. Baled, R.M. Enick, B.D. Morreale, Journal of Supercritical Fluids 55 (2010) 701-711.

[5] G. Deng, J. Doane, A. Ruffo, G.-D. Shyu, S. Collins, Design Verification, Optimization and Validation of Ultra-HPHT Completion and Production Tools, Society of Petroleum Engineers, 2014.

[6] I.K. Gamwo, W.A. Burgess, D. Tapriyal, H.O. Baled, B.D. Morreale, Y. Soong, R.M. Enick, B.A. Bamgbade, Y. Wu, M.A. McHugh, Status of Equation of State Project at the NETL, Offshore Technology Conference, 2014.

[7] A. Allal, C. Boned, A. Baylaucq, Physical Review E 64 (2001).

[8] H.O. Baled, Density and viscosity of hydrocarbons at extreme conditions associated with ultra-deep reservoirs-measurements and modeling, University of Pittsburgh, Ann Arbor, 2012, 125.

[9] H.O. Baled, D. Tapriyal, B.D. Morreale, Y. Soong, I. Gamwo, V. Krukonis, B.A. Bamgbade, Y. Wu, M.A. McHugh, W.A. Burgess, R.M. Enick, International Journal of Thermophysics 34 (2013) 1845-1864.

[10] S. Brelvi, Saudi Aramco Journal of Technology (1998) 30-34.

[11] W.E. Ramage, L.M. Castanier, H. Ramey Jr, The comparative economics of thermal recovery projects, Stanford Univ., CA (USA). Petroleum Research Inst., 1987.

[12] F. Dauber, R. Span, Applied Energy 97 (2012) 822-827.

[13] O. Kunz, W. Wagner, Journal of chemical & engineering data 57 (2012) 3032-3091.

[14] Y. Wu, B. Bamgbade, K. Liu, M.A. McHugh, H. Baled, R.M. Enick, W.A. Burgess, D. Tapriyal, B.D. Morreale, Fluid Phase Equilibria 311 (2011) 17-24.

[15] J.M. Milanesio, J.C. Hassler, E. Kiran, Industrial & Engineering Chemistry Research 52 (2013) 6592-6609.

[16] F. Saryazdi, H. Motahhari, F. Schoeggl, S. Taylor, H. Yarranton, Energy & Fuels 27 (2013) 3666-3678.

[17] H. Reamer, B. Sage, Journal of Chemical and Engineering Data 11 (1966) 17-24.

[18] D.E. Nanu, W. Poot, D. Geană, T.W. de Loos, Journal of Chemical & Engineering Data 48 (2003) 571-575.

[19] M. Aalto, S. Liukkonen, Journal of Chemical & Engineering Data 41 (1996) 79-83.

[20] J. Dymond, R. Malhotra, International journal of thermophysics 9 (1988) 941-951.

[21] D.R. Caudwell, J.P.M. Trusler, V. Vesovic, W.A. Wakeham, Journal of Chemical and Engineering Data 54 (2009) 359-366.

[22] W.G. Cutler, R.H. McMickle, W. Webb, R.W. Schiessler, Journal of Chemical Physics 29 (1958) 727-740.

141

[23] H. Eduljee, D. Newitt, K. Weale, Journal of the Chemical Society (Resumed) (1951) 3086-3091.

[24] D.-Y. Peng, D.B. Robinson, Industrial & Engineering Chemistry Fundamentals 15 (1976) 59-64.

[25] G. Soave, Chemical Engineering Science 27 (1972) 1197-1203.

[26] C.H. Twu, J.E. Coon, J.R. Cunningham, Fluid Phase Equilibria 105 (1995) 49-59.

[27] H. Baled, R.M. Enick, Y. Wu, M.A. McHugh, W. Burgess, D. Tapriyal, B.D. Morreale, Fluid Phase Equilibria 317 (2012) 65-76.

[28] J.-C. de Hemptinne, P. Ungerer, Fluid Phase Equilibria 106 (1995) 81-109.

[29] H. De Sant'ana, P. Ungerer, C. Batut, G. Moracchini, J. Sanchez, J. Carrier, D. Jensen, Oil & Gas Science and Technology 53 (1998) 265-281.

[30] H.B. de Sant'Ana, P. Ungerer, J.C. de Hemptinne, Fluid Phase Equilibria 154 (1999) 193-204.

[31] K. Frey, Improving thermodynamic property estimation through volume translation, Massachusetts Institute of Technology, Ann Arbor, 2010.

[32] K. Frey, C. Augustine, R.P. Ciccolini, S. Paap, M. Modell, J. Tester, Fluid Phase Equilibria 260 (2007) 316-325.

[33] K. Frey, M. Modell, J. Tester, Fluid Phase Equilibria 279 (2009) 56-63.

[34] W.-R. Ji, D. Lempe, Fluid Phase Equilibria 130 (1997) 49-63.

[35] K. Magoulas, D. Tassios, Fluid Phase Equilibria 56 (1990) 119-140.

[36] P.M. Mathias, T. Naheiri, E.M. Oh, Fluid Phase Equilibria 47 (1989) 77-87.

[37] A. Péneloux, E. Rauzy, R. Fréze, Fluid Phase Equilibria 8 (1982) 7-23.

[38] P. Ungerer, C. Batut, Oil & Gas Science and Technology 52 (1997) 609-623.

[39] L.-S. Wang, J. Gmehling, Chemical engineering science 54 (1999) 3885-3892.

[40] M.S. Wertheim, J Stat Phys 35 (1984) 19-34.

[41] M.S. Wertheim, J Stat Phys 35 (1984) 35-47.

[42] M.S. Wertheim, J Stat Phys 42 (1986) 459-476.

[43] M.S. Wertheim, J Stat Phys 42 (1986) 477-492.

[44] W.G. Chapman, K.E. Gubbins, G. Jackson, M. Radosz, Industrial & Engineering Chemistry Research 29 (1990) 1709-1721.

[45] W.G. Chapman, G. Jackson, K.E. Gubbins, Molecular Physics 65 (1988) 1057-1079.

[46] S.H. Huang, M. Radosz, Industrial & Engineering Chemistry Research 29 (1990) 2284-2294.

[47] S.H. Huang, M. Radosz, Industrial & Engineering Chemistry Research 30 (1991) 1994-2005.

[48] B. Alder, D. Young, M. Mark, The Journal of Chemical Physics 56 (1972) 3013-3029.

[49] S.S. Chen, A. Kreglewski, Berichte Der Bunsen-Gesellschaft-Physical Chemistry Chemical Physics 81 (1977) 1048-1052.

[50] N.F. Carnahan, K.E. Starling, Journal of Chemical Physics 51 (1969) 635-&.

[51] J. Gross, G. Sadowski, Industrial & engineering chemistry research 40 (2001) 1244-1260.

[52] J.M. Lasarte, L. Martin, E. Langa, J.S. Urieta, A.M. Mainar, Journal of Chemical and Engineering Data 53 (2008) 1393-1400.

[53] P.D. Ting, P.C. Joyce, P.K. Jog, W.G. Chapman, M.C. Thies, Fluid phase equilibria 206 (2003) 267-286.

[54] W.A. Burgess, D. Tapriyal, B.D. Morreale, Y. Wu, M.A. McHugh, H. Baled, R.M. Enick, Fluid Phase Equilibria 319 (2012) 55-66.

[55] W.A. Burgess, D. Tapriyal, I.K. Gamwo, Y. Wu, M.A. McHugh, R.M. Enick, Industrial & Engineering Chemistry Research 53 (2014) 2520-2528.

[56] J.A. Amorim, O. Chiavone-Filho, M.L.L. Paredes, K. Rajagopal, Journal of Chemical and Engineering Data 52 (2007) 613-618.

[57] F. Audonnet, A.A.H. Padua, Fluid Phase Equilibria 181 (2001) 147-161.

[58] T.S. Banipal, S.K. Garg, J.C. Ahluwalia, Journal of Chemical Thermodynamics 23 (1991) 923-931.

[59] D.R. Caudwell, J.P.M. Trusler, V. Vesovic, W.A. Wakeham, International Journal of Thermophysics 25 (2004) 1339-1352.

[60] A. Ettahir, C. Boned, B. Lagourette, P. Xans, International Journal of Thermophysics 16 (1995) 1309-1334.

[61] S. Outcalt, A. Laesecke, T.J. Fortin, Journal of Chemical Thermodynamics 42 (2010) 700-706.

[62] S.L. Outcalt, A. Laesecke, T.J. Fortin, Journal of Molecular Liquids 151 (2010) 50-59.

[63] A.A.H. Padua, J. Fareleira, J.C.G. Calado, W.A. Wakeham, International Journal of Thermophysics 15 (1994) 229-243.

[64] A.A.H. Padua, J. Fareleira, J.C.G. Calado, W.A. Wakeham, International Journal of Thermophysics 17 (1996) 781-802.

[65] A.A.H. Padua, J. Fareleira, J.C.G. Calado, W.A. Wakeham, Journal of Chemical and Engineering Data 41 (1996) 731-735.

[66] D.R. Caudwell, Viscosity of dense fluid mixtures, Chemical Engineering, Imperial College, London, 2004.

[67] P.W. Bridgman, Proceedings of the American Academy of Arts and Sciences 61 (1926) 57-99.

[68] P.W. Bridgman, Proceedings of the American Academy of Arts and Sciences 66 (1931) 185-233.

[69] P.W. Bridgman, Proceedings of the American Academy of Arts and Sciences 74 (1942) 399-424.

[70] P.W. Bridgman, Proceedings of the American Academy of Arts and Sciences 77 (1949) 129-146.

[71] T. Ito, Y. Nagata, H. Miyamoto, Int. J. Thermophys. 35 (2014) 1636-1646.

[72] S. Muromachi, H. Miyamoto, M. Uematsu, Journal of Chemical Thermodynamics 40 (2008) 1594-1599.

[73] E.W. Lemmon, M.O. McLinden, D.G. Friend, Thermophysical properties of fluid systems. in: P.J. Lindstrom, W.G. Mallard, (Eds.), NIST Chemistry Webbook, NIST Standard Reference Database Number 69, Gathersburg MD, 20899, retrieved 2012.

[74] B.A. Bamgbade, Y. Wu, H.O. Baled, R.M. Enick, W.A. Burgess, D. Tapriyal, M.A. McHugh, Journal of Chemical Thermodynamics 63 (2013) 102-107.

[75] Y. Wu, B.A. Bamgbade, H. Baled, R.M. Enick, W.A. Burgess, D. Tapriyal, M.A. McHugh, Industrial & Engineering Chemistry Research 52 (2013) 11732-11740.

[76] Y. Wu, B.A. Bamgbade, W.A. Burgess, D. Tapriyal, H.O. Baled, R.M. Enick, M.A. McHugh, Journal of Physical Chemistry B 117 (2013) 8821-8830.

[77] B.A. Bamgbade, Y. Wu, W.A. Burgess, D. Tapriyal, I.K. Gamwo, H.O. Baled, R.M. Enick, M.A. McHugh, Journal of Chemical Thermodynamics 84 (2015) 108-117.

[78] B.A. Bamgbade, Y. Wu, W.A. Burgess, D. Tapriyal, I.K. Gamwo, H.O. Baled, R.M. Enick, M.A. McHugh, Industrial & Engineering Chemistry Research 54 (2015) 6804-6811.

[79] B.A. Bamgbade, Y. Wu, W.A. Burgess, M.A. McHugh, Fluid Phase Equilibria 332 (2012) 159-164.

[80] Y. Wu, S.T. Dudek, B.A. Bamgbade, M.A. McHugh, Fluid Phase Equilibria 382 (2014) 180-186.

[81] Y. Wu, K. Liu, B.A. Bamgbade, M.A. McHugh, Fuel 111 (2013) 75-80.

[82] E.W. Lemmon, M.O. McLinden, W. Wagner, Journal of Chemical & Engineering Data 54 (2009) 3141-3180.

[83] G.P. Dubey, M. Sharma, Journal of Chemical and Engineering Data 53 (2008) 1032-1038.

[84] M. Fermeglia, G. Torriano, Journal of Chemical and Engineering Data 44 (1999) 965-969.

[85] G.H. Graaf, H.J. Smit, E.J. Stamhuls, A. Beenackers, Journal of Chemical and Engineering Data 37 (1992) 146-158.

[86] K.R. Harris, Journal of Chemical and Engineering Data 54 (2009) 2729-2738.

[87] G. Korosi, E.S. Kovats, Journal of Chemical and Engineering Data 26 (1981) 323-332.

[88] V.I. Korotkovskii, A.V. Lebedev, O.S. Ryshkova, M.F. Bolotnikov, Y.E. Shevchenko, Y.A. Neruchev, High Temperature 50 (2012) 471-474.

[89] A. Kumagai, S. Takahashi, International Journal of Thermophysics 16 (1995) 773-779.

[90] K. Lal, N. Tripathi, G.P. Dubey, Journal of Chemical & Engineering Data 45 (2000) 961-964.

[91] S.K. Mylona, M.J. Assael, M.J.P. Comunas, X. Paredes, F.M. Gacino, J. Fernandez, J.P. Bazile, C. Boned, J.L. Daridon, G. Galliero, J. Pauly, K.R. Harris, Journal of Physical and Chemical Reference Data 43 (2014).

[92] K.J. Sax, F.H. Stross, Analytical Chemistry 29 (1957) 1700-1702.

[93] N. Tripathi, International Journal of Thermophysics 26 (2005) 693-703.

[94] K.A.G. Schmidt, D. Pagnutti, M.D. Curran, A. Singh, J.P.M. Trusler, G.C. Maitland, M. McBride-Wright, Journal of Chemical & Engineering Data 60 (2014) 137-150.

[95] O. Fandino, L. Lugo, M.J.P. Comunas, E.R. Lopez, J. Fernandez, Journal of Chemical Thermodynamics 42 (2010) 84-89.

[96] F. Ciotta, G. Maitland, M. Smietana, J.P.M. Trusler, V. Vesovic, Journal of Chemical & Engineering Data 54 (2009) 2436-2443.

[97] D. Tomida, A. Kumagai, C. Yokoyama, International Journal of Thermophysics 28 (2007) 133-145.

[98] A. Kumagai, D. Tomida, C. Yokoyama, International Journal of Thermophysics 27 (2006) 376-393.

[99] O. Fandino, A.S. Pensado, L. Lugo, M.J.P. Comunas, J. Fernandez, Journal of Chemical and Engineering Data 50 (2005) 939-946.

[100] E. Kuss, M. Taslimi, Chemie Ingenieur Technik 42 (1970) 1073-1120.

[101] N. Agaev, A. Kerimov, Z. Nuriddinov, I. Vyssh, U. Zaved, Neft Gaz 19 (1976) 72-74.

[102] R. C. Reid, J. M. Prausnitz, B.E. Poling, The Properties of Gases and Liquids, Fourth ed., MaGraw-Hill Inc, New York, 1987.

[103] D.M. VonNiederhausern, G.M. Wilson, N.F. Giles, Journal of Chemical & Engineering Data 45 (2000) 157-160.

[104] E.D. Nikitin, A.P. Popov, Y.G. Yatluk, Journal of Chemical and Engineering Data 51 (2006) 1326-1330.

[105] K. Saido, T. Kuroki, T. Ikemura, M. Kirisawa, Journal of the American Oil Chemists Society 61 (1984) 945-949.

[106] L. Constantinou, R. Gani, Aiche Journal 40 (1994) 1697-1710.

[107] J. Marrero, R. Gani, Fluid Phase Equilibria 183 (2001) 183-208.

[108] R.L. Brown, S.E. Stein, Boiling Point Data. in: P.J. Lindstrom, W.G. Mallard, (Eds.), NIST Chemistry Webbook, NIST Standard Reference Database Number 69, Gathersburg MD, 20899, retrieved 2012.

[109] J. Garcia, X. Paredes, J. Fernandez, Journal of Supercritical Fluids 45 (2008) 261-271.

[110] A. Tihic, G.M. Kontogeorgis, N. von Solms, M.L. Michelsen, L. Constantinou, Industrial & Engineering Chemistry Research 47 (2008) 5092-5101.

[111] J. Gross, G. Sadowski, Industrial & Engineering Chemistry Research 41 (2002) 1084-1093.

[112] C. Peters, H. Van Der Kooi, J. De Roo, J.D.S. Arons, J. Gallagher, J.L. Sengers, Fluid Phase Equilibria 51 (1989) 339-351.

[113] J.S. Rowlinson, F. Swinton, Liquids and Liquid Mixtures: Butterworths Monographs in Chemistry, Butterworth-Heinemann, 1982.

[114] R.L. Scott, P.H. van Konynenburg, Discussions of the Faraday society 49 (1970) 87-97.

[115] J. Gregorowicz, T.W. De Loos, J. De Swaan Arons, Journal of Chemical and Engineering Data 37 (1992) 356-358.

[116] D. Pecar, V. Dolecek, Acta Chimica Slovenica 54 (2007) 538-544.

[117] M. Zabaloy, E. Brignole, Fluid phase equilibria 140 (1997) 87-95.

[118] J. Liu, Y. Kim, M.A. McHugh, Fluid phase equilibria 248 (2006) 44-49.

[119] Y. Wu, Experimental Determination and Equation of State Modeling of High-Pressure Fluid Behavior, 2013.

[120] W.A. Burgess, D. Tapriyal, B.D. Morreale, Y. Soong, H.O. Baled, R.M. Enick, Y. Wu, B.A. Bamgbade, M.A. McHugh, Fluid Phase Equilibria 359 (2013) 38-44.

[121] J. Larsen, H. Sorensen, T. Yang, K. Schou Pedersen, EOS and viscosity modeling for highly undersaturated Gulf of Mexico reservoir fluids, SPE Annual Technical Conference and Exhibition, Society of Petroleum Engineers, 2011.

[122] D.L. Katz, A. Firoozabadi, Journal of Petroleum Technology 30 (1978) 1649-1655.

[123] P. Leelavanichkul, M.D. Deo, F.V. Hanson, Petroleum Science and Technology 22 (2004) 973-990.

[124] M.R. Riazi, Industrial & engineering chemistry research 36 (1997) 4299-4307.

[125] C.H. Whitson, Society of Petroleum Engineers Journal 23 (1983) 683-694.

[126] S.R. Panuganti, F.M. Vargas, D.L. Gonzalez, A.S. Kurup, W.G. Chapman, Fuel 93 (2012) 658-669.

[127] P.D. Ting, G.J. Hirasaki, W.G. Chapman, Petroleum Science and Technology 21 (2003) 647-661.

[128] J.S. Buckley, Energy & Fuels 13 (1999) 328-332.

[129] J.S. Buckley, G.J. Hirasaki, Y. Liu, S. Von Drasek, J.X. Wang, B.S. Gil, Petroleum Science and Technology 16 (1998) 251-285.

[130] S. Punnapala, F.M. Vargas, Fuel 108 (2013) 417-429.

[131] D.L. Gonzalez, G.J. Hirasaki, J. Creek, W.G. Chapman, Energy & fuels 21 (2007) 1231-1242.

[132] D.L. Gonzalez, P.D. Ting, G.J. Hirasaki, W.G. Chapman, Energy & fuels 19 (2005) 1230-1234.

[133] S. Huang, M. Radosz, Fluid phase equilibria 70 (1991) 33-54.

Vita

Babatunde Bamgbade was born in April 1987 in Ibadan, Oyo state Nigeria. He graduated high school in 2002 from Loyola College Ibadan. He then proceeded to the Obafemi Awolowo University in Ile-Ife, Nigeria, for his Bachelor's degree in Biochemistry, where he met his wife, Gbemisola. He started his Graduate School studies at the Virginia Commonwealth University in 2009, where he received his Master of Science in Engineering in August 2012.